UNIVERSITY OF SOUTHAMPTON

FACULTY OF ENGINEERING, SCIENCE AND MATHEMATICS

School of Chemistry

Sol-Gel Preparation of Silicon Nitride Materials

by

Shereen Hassan Mohamed Gaber Hassan

Thesis for the degree of Doctor of Philosophy

November 2009

UNIVERSITY OF SOUTHANPTON

ABSTRACT

FACULTY OF EGNINEERING, SCIENCE & MATHEMATICS

SCHOOL OF CHEMISTRY

Doctor of Philosophy

SOL-GEL PREPARATION OF SILICON NITRIDE MATERIALS

By Shereen Hassan Mohamed Gaber Hassan

Sol-gel techniques are mainly used for oxides but are of growing interest for non-oxide materials. They allow formation of solid materials through gelation of precursor solutions and can be used to control composition and to produce a large number of useful morphologies such as films, monoliths, aerogels, foams and materials with ordered pores on various length scales. Often the synthesis of non-oxide materials using sol-gel methods has focused on producing powders for applications such as catalysis, where controlled porosity and basic catalytic sites are the point of interest.

In this thesis, formation of silicon nitride based materials as thin films, aerogels, inverse opal films and phosphor powders have been synthesised using non-oxide sol-gel methods. For thin films formation of amorphous silicon nitride, [$Si(NHMe)_4$] solution in tetrahydrofuran (THF) with ammonia in the presence of a triflic acid catalyst was used. The sols formed from this mixture were used to make films using a simple dip coating technique. A number of coating and pyrolysis regimes have been compared. Aerogels were prepared through a small change in the sol preparation conditions leading to bulk gelation, supercritical drying was then applied to these gels. For templated films, the precursor was dissolved in hexane and polystyrene array tiles were coated with that solution using dip, drop or capillary techniques. The effects of several coating techniques and different pyrolysis temperatures on film morphologies have been studied.

In addition, the sol-gel process offers an effective and controllable means of adding elements into Si-N matrix with the aim of combining the low reactivity of silicon nitride materials with other functional properties. Co-ammonolysis of a rare-earth amide with a silicon amide is shown to be an effective route to phosphor materials. Amorphous $Tb:SiN_x$ composition show strong photoluminescence and the variation in PL intensity with composition has been probed.

TABLE OF CONTENTS

TABLE OF FIGURES

TABLE OF TABLES

DECLARATION OF AUTHORSHIP

I, Shereen Hassan Mohamed Gaber Hassan, declare that the thesis entitled:

'Sol-Gel Preparation of Silicon Nitride Materials' and the work presented in this thesis are both my own and have been generated by me as the result of my own original research.

I confirm that:

- This work was done wholly while in candidature for a research degree at this University;
- Where any part of this thesis has previously been submitted for a degree or any other qualification at this University or any other institution, this has been clearly stated;
- Where I have consulted the published work of others, this is always clearly attributed;
- Where I have quoted from the work of others, the source is always given. With the exception of such quotations, this thesis is entirely my own work;
- I have acknowledged all main sources of help;
- Where the thesis is based on work done by myself jointly with others, I have made clear exactly what was done by others and what I have contributed myself;
- Parts of this work have been published as :

- *A non-oxide sol–gel route to synthesise silicon imidonitride monolithic gels and high surface area aerogels.* S. Hassan, A. L. Hector, J. R. Hyde, A. Kalaji, *Chem. Commun.,* 2008, 5304.

- *Template Infiltration Routes to Ordered Macroporous TiN and SiNx Films.* B. M. Grey, S. Hassan, A. L. Hector, A. Kalaji, B. Mazumder, *Chem. Mater.,* **21,** 2009, 4210.
- *Non-oxide sol-gel synthesis of terbium doped silicon nitride phosphors,* S. Hassan, M. Carravetta, A. L. Hector, L. A. Stebbings, in press

AKNOWLEDGEMENTS

I would like to thank my Egyptian government for financing my research. I would also like to thank Hector group, Dr Baishakhi Mazumder for her assistance when it was required, Andrew Jackson and Pietro (for comedy value), Dr Fei Cheng for his help, Dr Barbara Cressey for her help when I had problem at the microscopy centre; Dr James Hyde for his effort for running supercritical drying technique and Dr Marina Carravetta for running solid state NMR experiment.

I would also like to reserve a special thank you for my supervisor Dr Andrew L Hector for his excellent guidance, support, patience and friendship which without it I surely would not have managed to get here.

Finally and most importantly, I would like to thank the people who mean the most to me, my family, Mum, Dad, sister and brother for their limitless love, assistance and support all the time. Special thank must go to my lover husband Hassan, my sweetie daughters Lojayn and Lenah for their encouragement, love, support and providing me with the opportunities to get her. I really couldn't do it without them.

LIST OF ABBREVIATIONS

THF	Tetrahydrofuran.
CVD	Chemical vapour deposition.
MCVD	Modified chemical vapour deposition.
TEOS	Tetraethylorthosilicate.
3DOM	Three-dimension ordered macroporous.
LED	Light emitting-diode.
SEM	Scanning electron microscopy.
XRD	X-ray diffraction.
XPS	X-ray photoelectron spectroscopy.
IR	Infrared spectroscopy.
TEM	Transmission electron microscopy.
MAS-NMR	Magic angle spinning- nuclear magnetic resonance spectroscopy.
TGA	Thermogravimetric analysis.
PL	Photoluminescence.
EVA	Diffract evaluation programme.
EM	Electron microscopy.
EDX	Energy dispersive x-ray.
NNNC	Nottingham nanotechnology and nanoscience centre.
NCESS	National centre for electron spectroscopy and surface analysis.
BDDT	Brunauer, Deming, Deming and Teller.
BET	Brunauer, Emmett and Teller.
LPCVD	Low pressure chemical vapour deposition.
APCVD	Atmospheric pressure chemical vapour deposition.
ECR-PECVD	Electron cyclotron resonance plasma-enhanced chemical vapour deposition.

PVA	Polyvinyl alcohol.
TDMAT	Tetrakis(dimethylamino)titanium.
Triflic	Trifluoromethanesulfonic.
TMAS	Tetramethylaminosilane.
ALD	Atomic layer deposition.
PS	Polystyrene.
DSC	Differential scanning calorimetry.
PECVD	Plasma enhanced chemical vapour deposition.
PVD	Physical vapour deposition.
HWCVD	Hot wire chemical vapour deposition.

INTRODUCTION

1.1 The Sol-Gel Method

Sol-gel techniques have attracted considerable attention because of their ability to produce different morphologies such as dense monoliths, fibres, films, mesoporous structures and nanostructured materials. These products have potential uses for optical, magnetic, catalytic and structural applications.[1] Sol-gel processing takes place through a series of steps: hydrolysis, condensation, gelation, ageing and drying. It is based on the generation of a stable suspension of colloidal particles (amorphous or crystalline) or polymer in a liquid, a **sol.** This is subsequently linked up to immobilise the liquid phase in a porous, three dimensional solid network, this is referred to as a **gel.**[2]

Taking silica formation as an example, a sequence of hydrolysis reactions followed by condensation results in sol formation, Fig.1.1 Precursor molecules such as $[Si(OR)_4]$ (R = Me, Et or Pr) are linked together to form polymeric particles containing Si-O-Si linkages. The reactions are usually catalysed by acidic or basic conditions which promote the rates of reactions dramatically and provide a certain degree of control over the structural properties of the sols and final products, Fig. 1.2.[3]

Hydrolysis: $Si(OR)_4 + nH_2O \rightarrow Si(OR)_{4-n}(OH)_n + nROH$

Condensation: $X_3SiOH + HOSiX_3 \rightarrow X_3Si\text{-}O\text{-}SiX_3 + H_2O$

$X_3SiOR + HOSiX_3 \rightarrow X_3Si\text{-}O\text{-}SiX_3 + ROH$

(X may be any of OR, OH or $OSiX_3$; X=Me, Et)

Fig. 1.1 Hydrolysis and condensation of silicon tetra-alkoxides.

Under acid catalysis the initial hydrolysis step removes one of the electron donating alkoxy groups forming trialkoxy silanol $(RO)_3Si\text{-}OH$.[3] The mechanism of acid catalysis is shown in Fig. 1.3. It depends on decreasing the high electronegativity of Si atom by induce a negative charge (H^+ from acid). Hence, enhance the low nucleophilicity nature of water for nucleophilic substitution giving trialkoxy silanol. The protonation of this silanol species

becomes less favorable and hence the second hydrolysis step is slower. Due to the high reactivity of terminal Si-OR groups, hydrolysis catalysed with acid will result in chain elongation initially and formation of a linear polymer. Cross-linking then takes place by interlinking of chains after hydrolysis of Si-OR side groups. Finally a homogenous dense gel with small pores will be formed.

On the other hand, with base catalysis, hydrolysis reactions are slower, but once the electron donating-OR groups are removed, large highly cross-linked sol particles are formed. Furthermore, growth of particles continues throughout condensation and the interlinking of the highly cross-linked polymer leads to porous gel formation with large pores.

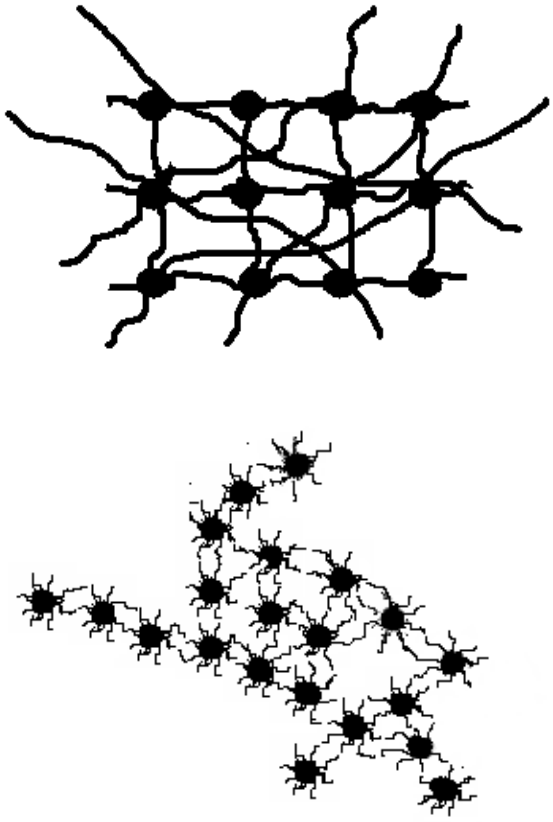

Fig. 1.2 The products of acid-catalysed (top) and base-catalysed (bottom) condensation.

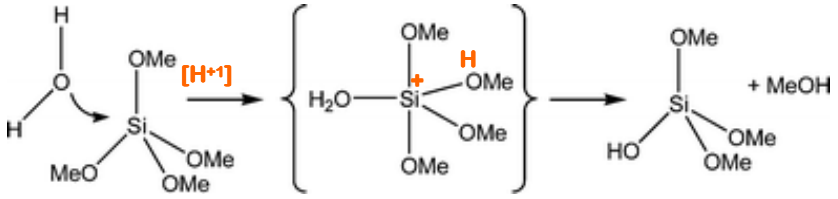

Fig. 1. 3 Nucleophilic substitution of $Si(OMe)_4$ by water using acid catalysis.

Generally, more linkages form to give a gradual increase of viscosity until the gelation point.[3] This point is distinguished by a high viscosity gel that spans the vessel supporting the solvent within it. At gelation, continuous chemical and physical changes take place due to further increases in cross-linking via trans-pore condensation reactions of pore surface hydroxide groups. The gelled sample becomes more robust due to additional associated cross-linking during this ageing process. Typically gels are then dried and different stages can be distinguished during the liquid evaporation.

The loss of the solvent during ageing (water, alcohol, co-solvents etc.) occurs by expulsion of the liquid from the gel (syneresis). Once no further cross-linking occurs to drive syneresis, solvent loss can only occur through evaporation from within the pore structure. If the gel is still very flexible, it will shrink by an amount equal to the volume of the solvent that evaporates. Eventually through ageing and drying the gel structure becomes rigid enough to resist further shrinkage. At this stage the surface tension of the solvent and the small pore size of the gel can generate a high pressure across liquid menisci in the pores and this capillary stress can cause cracking of the gel network. Powders or monolithic xerogel materials can be formed by careful conventional evaporative drying while highly porous, low density aerogel monoliths with maintainance of network structure can be produced using supercritical drying processes. Finally, densification takes place in which heat treatment (pyrolysis) is required for the production of dense glasses and ceramic materials.[3]

1.1.1 Oxide Sol-Gel Method

Sol-gel methods have been extensively used to produce oxide materials with controlled shapes and sizes on all length scales. Furthermore, micro- and meso-porous materials with high effective surface areas and small pore sizes with a narrow size distribution can be obtained.[4]

The manner in which different processing routes are applied to sol and gel to produce a variety of materials is illustrated in Fig. 1.4.[2] From the sol, powders can be obtained by spray-drying, fibres spun or drawn and coating techniques such as spin- or dip- coating can be used to produce films. During gelation processing, several drying techniques can be applied such as supercritical solvent extraction and solvent evaporation to produce different morphologies e.g. aerogel and xerogel respectively. Furthermore, other useful nanostructures such as tubes, fibres and membranes can be designed using a templating agent which will be removed after drying leaving porous materials depending on the selected template. Different oxide morphologies have been fabricated such as thin films, fibres, aerogels, templated materials, etc.

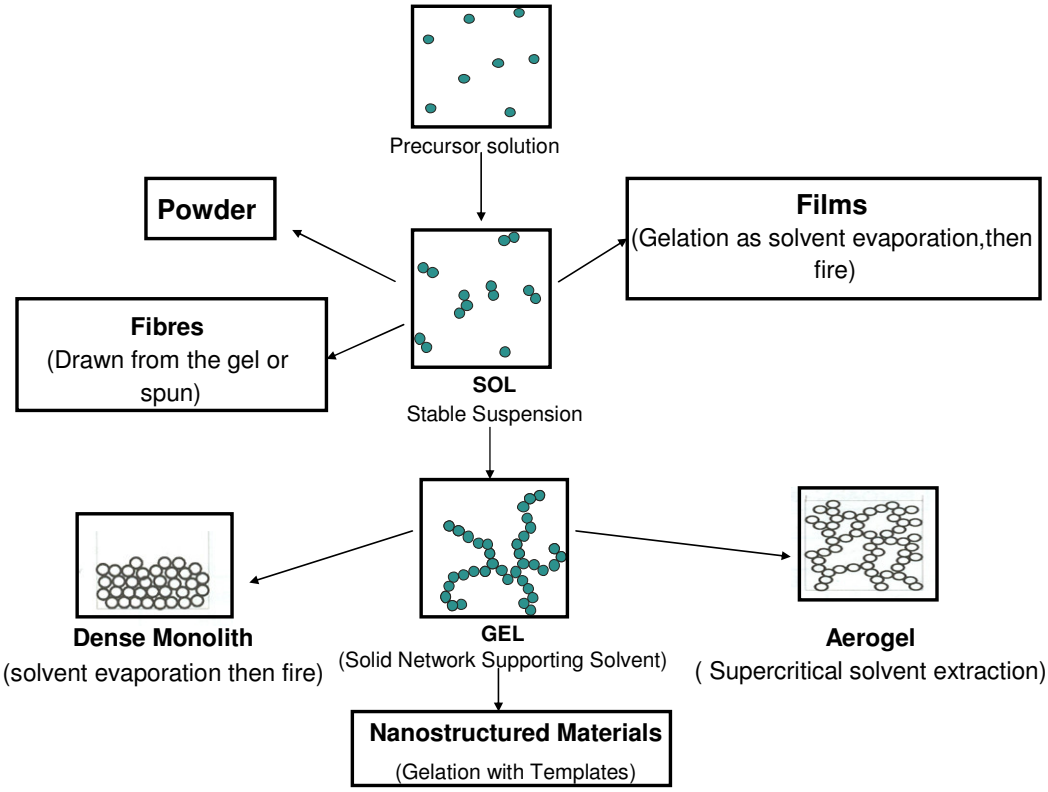

Fig.1.4 Processing route to materials using sol-gel methods.

1.1.1.a Thin Films

Metal oxide thin films have attracted considerable attention over the last two decades. A wide range of research efforts are underway to prepare of oxide thin films with properties such as high chemical stability, high transparency, large band gap, good conductivity and photoelectric properties that make them candidates for industrial applications including gas sensors, solar cells, transparent electrodes and membranes.[5,6,7,8]

Chemical vapour deposition (CVD) has been used for thin film preparation and coating of inorganic materials of various compositions.[2] It is based on exposing a hot substrate to one or more volatile precursors which react and/or decompose on the substrate surface producing the desired deposit. The volatile by-product is removed by vacuum or flowing gas through the chamber. This method had been heavily used in applications such as microelectronics, coatings for catalysis, membranes and optical layers in waveguides.

Sol- gel processing is one of the most useful fabrication methods for oxide thin films. Coating techniques such as dip and spin-coating have been applied to coat sols onto substrates, before gelation takes place during solvent evaporation. Samples are typically left to dry at room temperature before firing to the required temperatures.

Using the dip-coating approach, TiO_2 films, with significant interest as a photocatalyst were prepared by dipping titanium plate of 0.25 mm thickness in titanium oxide solution and pulling it up at 0.15 mm s^{-1}. Different heat treatments were applied at 400, 600 and 700 ^oC, for 10 min. each producing different titanium oxide films.[9] At 400 ^oC TiO_2 of anatase structure was formed, while the rutile structure was formed at 700 ^oC. A mixture of both structures was obtained at 600 ^oC. Mixed Ce/Ti/Zr oxide thin films for use as transparent electrodes have been reported from a similar route.[5]

Spin-coating has also been employed to produce films.[10,11] For example, SnO_2, WO_2 and In_2O_3 thin films were prepared by spin coating a sol containing these metals at 2000 rpm onto a silicon substrate, leaving to dry in air at 60-70 ^oC for 5 mins. and then heating for 1 h in air at temperatures ranging from 150-500 ^oC, for SnO_2 and WO_2, or at 500 ^oC for In_2O_3.[12]

1.1.1.b Fibres

Several techniques have been applied for fibre fabrication. Modified chemical vapour deposition (MCVD) is commonly used for producing active fibres.[13] Since complicated apparatus is required for MCVD, sol-gel techniques are an attractive alternative.[14] A number of oxide fibre compositions have been prepared using sol-gel methods.

Alumina fibres are of growing interest because of their properties that make them versatile in applications such as catalyst supports in high temperature reactions, highly insulating material in the form of a blanket and for reinforcement of polymers and ceramics.[15] Different approaches have been used including sol-gel extrusion and spinning. For example, a prepared alumina sol[16] is thickened to form a paste appropriate for extrusion, then placed in extruder chamber under pressure from which fibres are expelled. The fibres are dried at room temperature and consequently calcined at high temperature.[17] Sol-gel based extrusion can produce a variety of shapes with constant cross-section such as fibres, tubes, rods, honey comb structures and channels.[18,19,20] On the other hand, a syringe can be used for spinning in which a sol of appropriate viscosity is taken in the syringe and a fibre drawn in a rectangular glass tray. The gelled fibres are dried at room temperature then fired at 1600 ^{o}C for 2 hrs.[15]

Silica fibres have also been synthesised. Hwang *et al* used tetraethyl orthosilicate (TEOS), ethanol, water and hydrochloric acid stirring for 1 hr as the precursor becomes viscous. Once the required sol viscosity had been reached, the fibre was pulled from the sol using a glass bar and then was dried in an oven at 80 ^{o}C. Finally the gelled fibre was fired at 1000 ^{o}C for 1 hr.[21] In addition, silicon-based non-oxide ceramic fibres (Si-Zr-C) as important reinforcement materials for several types of composite, have been prepared using inorganic-organic hybrid fibres that have previously been synthesized by sol-gel methods.[22]

1.1.1.c Templated Structures

Porous materials are classified into three types, according to the pore size: microporous, mesoporous and macroporous. Microporous structures have pore size diameter smaller than 2 nm, while in mesoporous materials the diameter is between 2 and 50 nm and in macroporous materials larger than 50 nm, Fig.1.5. Several templates have been used for

fabricating different nanocrystalline materials in which gelation occurs between the spaces of the template, then it is removed at a later stage. For example, mesoporous structures can be produced using surfactants or block copolymers while silica or polystyrene templates can be utilised to fabricate macroporous materials. Not all pores are the same but it can be distinguished into: closed pores where the pores are perfectly insulated from their neighbours and open pores with pores opened to the external solid surface.[2]

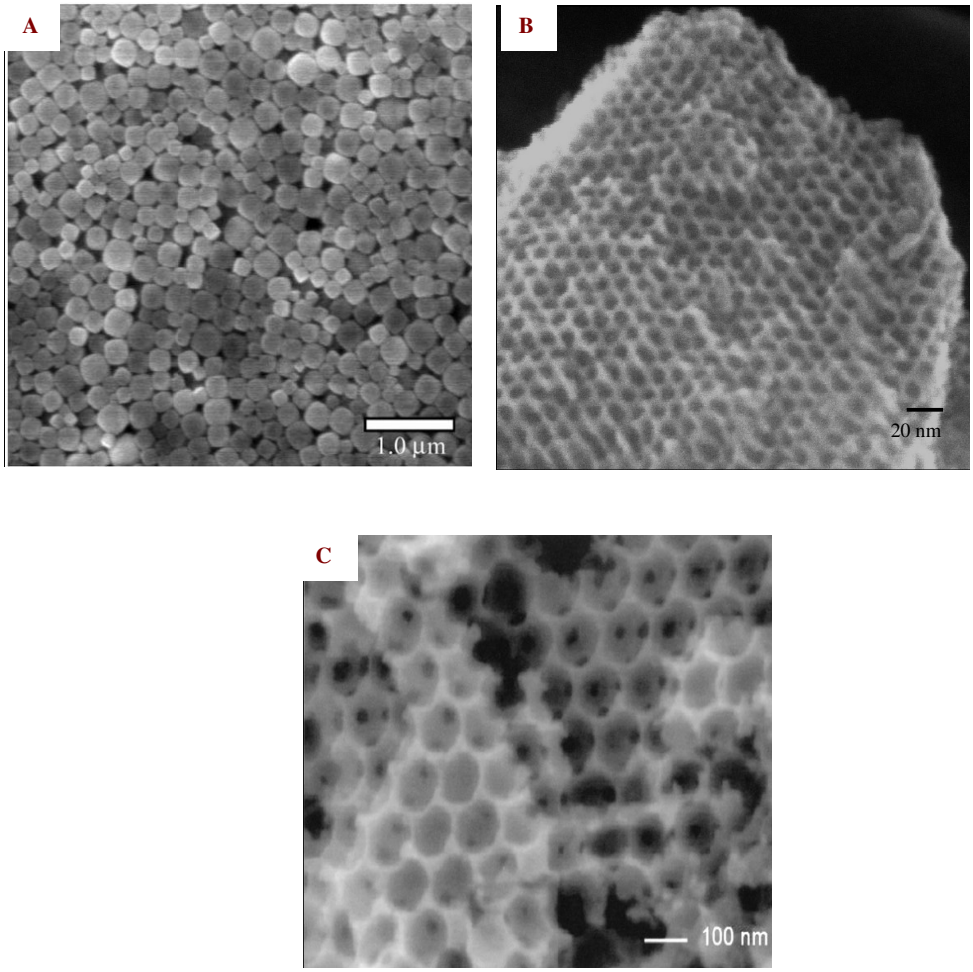

Fig.1. 5 SEM of a, close packing of microporous zeolite crystals, b, mesoporous Ta_2O_5, c, inverse opal SiO_2 (macroporous). Reprinted with permission from A. Walcarius, *Electroanal.,* 20, 2008, 711; K. Nakajima, *Chem. Lett.,* 34, *2005*, 394 and B. Holland, *J. Porous Mater.,* 10, 2003, 17 respectively.

Macroporous structures have been fabricated in oxides,[23,24,25] semiconductors[26] and organic polymers.[27] Macroporous materials with wide pore size distributions, such as Al_2O_3, SiC and TiO_2, have been prepared using techniques such as partial sintering,[28] using pore formers or foaming agents.[29]

Recently, the use of close-packed arrays of monodisperse spheres (especially silica or polystyrene) as templates have been the most promising simple and effective approaches used for ordered macroporous materials preparation. Ordered macroporous ceramic oxides consisting of SiO_2, TiO_2 and ZrO_2 have been produced using template-processing technique (polystyrene) by infiltration of the void space between spheres with a mixed solution of alkoxide precursors. The resulting inorganic-organic composite is then calcinated at an appropriate temperature.[30]

Furthermore, the quality of the colloidal crystal template used has a significant effect on the microstructure of fabricated macroporous metal oxides.[31] Using well ordered templates metal oxides are grown following the structure of the template forming three-dimension ordered macroporous (3DOM) structures. With less order templates, metal oxides sometimes do not grow in the desired morphology, for example cubic or sheetlike structures were formed in Cu_2O or ZnO. Selective crystals, cube or sheet, with less- ordered porous structure mirrored the fact that polystyrene spheres formed a less-ordered array in the template. The diffusion rate of the solution are different at different places and the growth rate of crystalline oxide is faster in these defects area which promotes the oxide growth following its own capital structure. The 3DOM structure materials received potential interest in which their unique properties, e.g. large accessible surface, highly ordered pore structure and identical submicrometer scale, candidate them to potential applications such as gas sensors,[32,33] photonic band gap crystal[34] and battery electrodes.[35]

Although the sol-gel process has been used for fabricating many of macroporous oxides,[25] there are few examples of templating processes to yield nitrides.[36] Also non-templated silicon nitride structures have been produced using sol-gel method such as aerogels , membranes[37] and mesoporous powders.[38]

1.1.1.d Aerogel

Aerogels are 3D porous network structures in which the typical structure and network of pores in a wet gel are largely maintained after replacing pore liquid by air. Silicon dioxide aerogels are the most studied aerogels and are useful thermal insulators, optical materials, radiation detectors, sensors and catalyst supports.[39] These are usually produced by using a supercritical fluid to exchange the solvent, then depressurising above the critical temperature of the fluid directly to the gas phase, thus avoiding any destructive surface tension effects.[40,41] Synthesis of SiO_2 aerogels dried at ambient pressure (subcritical drying) has also been reported by Smith *et al.*[42]

Incorporating metals into the aerogel framework has been investigated with the goal of modifying the structure and the catalytic activity. For example, a Co- SiO_2 aerogel has been grown on the walls of a ceramic monolith channel giving structured catalytic materials. This aerogel-coated monolith showed good catalytic performance for the generation of hydrogen from ethanol steam. The perfect homogeneity, high dispersity of cobalt particles in the aerogel and high porosity with larger pore size enhance the cobalt activation at lower temperature (580-590 K) and increase resistance to oxidation (563-613 K) compared to a Co- SiO_2 xerogel coating.[43]

There is also an extensive work on aerogels made from other oxides, carbon and recently II-VI semiconductor materials.[44]

The principle of SiO_2 gel formation has been expanded to non-silicate inorganic gels. The reactivity of metal alkoxides [$M(OR)_4$, M= Ti, Zr, Sn or Al] towards water is much higher than alkoxysilanes.[45] The formed aerogels have important potential in catalysis, such as the photocatalytic decomposition of methanol, hydrogenation of benzophenone to benzhydrol and CO_2 reformation of CH_4. Also mixed oxide aerogels (binary and ternary) consisting of SiO_2, TiO_2, ZrO_2 or Al_2O_3 combined with NiO, CuO, ThO_2, PbO or Fe_2O_3 have been prepared and their catalytic applications summarized by Pajonk and Baiker.[46,47]

Carbon aerogels have also received considerable attention. Since the surface area, pore volume and pore size distribution can be tuned, depending on the synthesis and preparation conditions, different forms with unique properties can be produced such as monoliths, beads, powders or thin films. Hence, carbon aerogels are promising materials for application in adsorption and catalysis. The preparation of these aerogels has been

reported.[48,49] Generally, a resorcinol- formaldehyde mixture undergoes polycondensation reactions using acid catalysis. After gelation, the wet gel was dried using supercritical drying to form an organic polymer aerogel. Carbonization was carried out by heating the aerogels to temperatures between 500 and 2500 ^{o}C under flowing of N_2 or Ar. During this process, the aerogel loses hydrogen and oxygen containing functionalities giving a highly pure carbon structure. In addition, several metals have been doped into carbon aerogels. Three different main strategies have been applied to introduce metal species into the carbon framework: dissolving metal precursors into the initial resorcinol-formaldehyde mixture sol, enhancing the ion exchange character of the organic aerogel by using a resorcinol derivative with appropriate functional groups instead of resorcinol or by deposition of metal precursors on the organic or carbon aerogel. For example, Ce-, Zr-doped carbon aerogels were produced by adding their nitrate to a resorcinol-formaldehyde mixture at different pH. The aerogels were carbonized at 1050^{o}C. Doping with Ce yielded materials with very low microporosity while synthesis of Zr-doped resulted in microporous materials.[50,51]

1.1.2 Non-Oxide Sol-Gel Method

Though sol-gel methods have traditionally been used for the synthesis of oxides, they have to a limited extent been successfully expanded to nitrides and chalcogenides, especially for highly porous materials. Silicon nitride and its metal doped derivatives have received a great deal of attention due to properties such as good resistance to thermal and chemical attack, good thermal conductivity, good hydrothermal and mechanical stability, good dielectric properties, toughness, hardness and corrosion resistance.[52,53] They are dielectric materials for microelectronic applications,[54,55] and have been used for protective coatings, diffusion masks[56] and structural applications at high temperature.[57] Its structure is quite different from that of silica. The Si-N-Si structure is rigid according to the necessity of nitrogen forming three bonds rather than two. The nitrogen atoms are arranged tetrahedrally around the silicon while the silicon neighbours are planer triangle arranged with respect to nitrogen, Fig. 1.6.

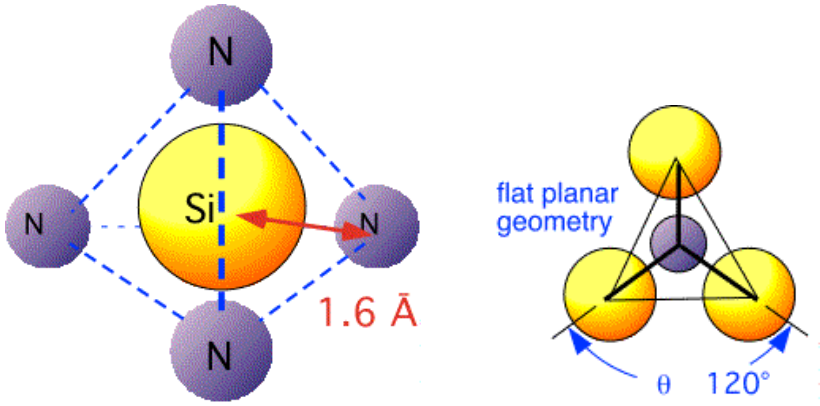

Fig. 1.6 Silicon nitride structure.

When produced via precursor routes, such materials are typically imidonitride compositions with significant numbers of NH and NH_2 groups that are responsible for base catalyst activity.[58,59,60] This important property can be utilised in catalytic reactions in which basicity is required to reinforce reaction such as methane oxidation, the Knoevenagel condensation reaction and dehydrogenation of lower alkanes (propane, iso-butane).

1.1.2.1 Porous Silicon Nitrides

The sol-gel literature concerned with nitride materials has been largely developed with silicon. Different porosity forms of silicon nitride have been fabricated and studied largely for their catalytic applications.

1.1.2.1. 1 Forms and Compositions

Bradley *et al*[36] synthesized microporous silicon imido nitride $[Si(N)_x(NH)_{y-n}]$ by reacting $[Si(Me_2N)_3(NH_2)]$ with ammonia in a hot concentrated solution of a long chain amine which was used as a template. The templated gel was pyrolysed carefully under a flow of ammonia yielding a microporous silicon imido nitride material with a narrow pore size distribution that can be tuned according to the choice of amine template.

Synthesis of mesoporous silicon nitride membranes has been reported.[37] Macroporous Al_2O_3 disks were dip coated from a $[Si(Me_2N)_3NH_2]$-based sol, which was prepared and stable for 6 hrs. The formed gel was fired to 1000 ^oC in NH_3. The membranes were found to be effective gas filters. Carbon monoxide, hydrogen and propane passed readily through the membrane to the sensor surface, while nitrogen dioxide did not pass through. This was suggested for use as a selective gas sensor system.

Metals have also been doped into silicon nitride for the purpose of modifying its properties. Two groups have reported separately the synthesis of high surface area Si-Al-N xerogels. Kaskel *et al*[61] synthesised high-surface area silicon aluminium nitride based xerogel. A solution of $[RAl(\mu\text{-}NHEt)(\mu\text{-}NEt)_2Si(NHEt)]_2$ (R = Et) precursor in pentane was placed in a 100 mL autoclave and ammonia condensed onto it. The mixture was heated to 413 K (*P* = 170 bar) for 12 hrs. The resulting solid has a high surface area (795 m^2g^{-1}) and was mesoporous with an average pore diameter of 5.8 nm. Cheng *et al*[62] produced mesoporous Si-Al-N xerogel by ammonolyis of the alanate $[(C_4H_8O)Al[HNSi(NMe_2)_3]_3]$ in the presence of triflic acid as a catalyst. The formed inorganic gel was dried and pyrolysed in NH_3 to different temperatures 200, 600 and 1000 ^oC. This procedure did not improve the basicity as intended but did provide an easy way of incorporating another element into silicon nitride.

Cheng *et al*[38] synthesized Pd nanoparticles supported on mesoporous Si_3N_4 which was used in the oxidation of methane and the selective hydrogenation of butadiene to butane. It was produced by reaction of $PdCl_2$ with a preformed silicon diimide gel,[36] followed by ammonia pyrolysis.

Transition metals [M= Ti, Ta and Zr] has incorporated into silicon nitride using a sol-gel approach with the aim of improving fracture strength and resistance to oxidation or thermal shock. [63] Metal amides $[Ti(NMe_2)_4$, $Zr(NMe_2)_4$ or $Ta(NMe_2)_5]$ were mixed with a silicon amide $[Si(NHMe)_4]$. The mixed solution was exposed to a flow of ammonia, forming a gel, then was pumped to dryness and pyrolysed to 1000 or 1500 ^oC under NH_3. At 1000 ^oC, the Ti/Si and Zr/Si nitrides were amorphous, but TaN had begun to crystallize from the Ta/Si gel at that temperature. At higher temperature, 1500 ^oC, all three products were composites of MN nanocrystals within an amorphous M/Si/N matrix.

1.1.2.1.2 Catalysis

Production of porous silicon nitride using sol-gel routes has been focussed mainly on the catalysis application area. It provides a useful support for catalytically active phases especially for gas-phase and liquid phase reactions due to its high thermal conductivity and stability at high temperatures compared with metal oxides.[64,38] Silicon nitride is of great interest as heterogeneous catalyst.[65]

Micro- and mesoporous silicon imido nitrides, described previously,[36] have been compared as catalysts to determine whether shape selectivity can be achieved. The solid base catalyst properties have been demonstrated through the Knoevanagel reaction as condensation of benzaldehyde with malonitrile at 50°C that give 1,1-dicyanophenylethylene with 94%-100% selectivity, Fig.1.7.

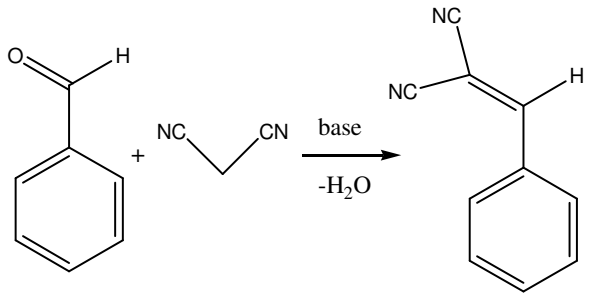

Fig.1.7 The Knoevanagel condensation reaction between benzaldehyde and malononitrile.

Similar to the material previously discussed for gas sensors in section 1.1.2.1.1, silicon carbonitride membranes that can be used as catalyst supports in high temperature membrane reactors were synthesized, [66,67] Fig.1.8. Methyltrichlorosilane [$MeSiCl_3$] was mixed with 10 equivalents of [Me_2SiCl_2] and the mixture crosslinked with [$(SiMe_3)_2NCN$]. The formed viscous material was spin coated on macroporous Si_3N_4 substrate and pyrolysed at 1000°C in Ar giving silicon carbonitride with 7-10 nm pore size.

Fig.1.8 Carbodiimide-based sol-gel route for silicon nitride.

Furthermore, macroporous SiCN has been formed by infiltration of 1.5 and 0.5 μm silica spheres with a preceramic precursor, polysilazane, followed by curing steps and pyrolysis at 1200 ^{o}C under Ar atmosphere for 2 h. The resultant porous monolith SiCN is promising as a catalyst support for high-temperature fuel reforming due to its high geometric surface area and good stability up to 1200 ^{o}C.[68]

High surface area Si/Al/N composition, which was effective at catalyzing the Michael addition of malonitrile to acrylonitrile with 96% conversion, was reported by Kaskel *et al.*[61] Tetra(ethyleamino)silane [$Si(NHEt)_4$] was reacted with trimethyl or triethyl aluminium and the product ammonolysed in supercritical ammonia at 150 ^{o}C.

1.1.2.2. Metal Nitride Materials

Sol gel techniques have also been expanded beyond silicon nitride and some metal nitride materials have been fabricated. The syntheses are much more difficult due to the less electronegative properties of the precursors, compared with those of silicon, which results in precipitation at the ammonolysis step. Nitrides of heavier group 13 elements, such as gallium, aluminium and indium, are very important semiconductor especially for light emission. Porous GaN with and without an amine templating agent was synthesised.[69] [$Ga_2(NMe_2)_6$] was reacted with ammonia and the product powder was dried and heated to 400 ^{o}C and above. The non-templated structure consisted of micron-sized crystallites, whereas nonylamine- templated GaN was nanocrystalline with an average pore diameter of 9 nm. Unlike with the silicon imido nitride system described earlier, changing the chain length of the templating amine did not tune GaN pore size and the diameters of the pores varied much more with the synthesis temperature. Photonic crystals of GaN have been synthesized using 3D-ordered synthetic opal-SiO_2 which was infiltrated with Ga_2O_3 followed by annealing at 1000 ^{o}C for 30 hrs in a mixture of nitrogen hydrides.[70]

Hexagonal boron nitride (h-BN) is an important ceramic material and high surface area BN is an effective ceramic support for catalysts. Narula and Paine synthesized h-BN films and aerogels using a sol-gel method.[71] First, a cyclic borazine [$[(BCl)(NH)]_3$] was cross-linked with hexamethyldisilazane [$(Me_3Si)_2NH$]. For film deposition, a coating was deposited before gelation and pyrolysed under NH_3 giving h-BN. Aerogels with surface areas of 200-400 $m^2\ g^{-1}$ were also produced using supercritical drying in CO_2 solvent followed by pyrolysis at 1000 ^oC. In addition, BN fibres could be produced. A $[(BCl)(NH)]_3/(Me_3Si)_2NH$-derived xerogel was dissolved in liquid ammonia, then fibres were drawn from the resulting solution.

Several reports have discussed synthesis of different nanocrystaline TiN forms. Jackson and Hector synthesized a stable sol that acted as a precursor to TiN.[72] Good quality films of nanocrystalline TiN were produced from these sols. Stoichiometric amounts of primary amine cross-linking agent such as propyl amine were reacted with [$Ti(NMe_2)_4$] to minimize precipitation. The dip-coated substrates were then heated under a flow of ammonia. Also, TiN xerogels with particle sizes from 2 to 60 nm depending on pyrolysis conditions were obtained by drying the bulk sol and pyrolysing under the same conditions.

Kim and Kumta[73] synthesized nanocrystalline TiN (10-20 nm) with low oxygen content using the "hydrazide sol-gel" method in which titantium isopropoxide was reacted with hydrazine and the alkoxy hydrazide product fired above 800 ^oC under a flow of Ar. There are indications that TiN has catalytic properties in hydrogen transfer reactions in which one isomer of stilbene can be synthesized in a stereoselective manner.[74]

1.2 Luminescence

Luminescence is the emission of electromagnetic radiation, light, that occurs from electronically excited states. This radiation can be emitted via various physical or chemical mechanisms. These mechanisms put the atoms into an excited state that has much higher energy than that of the ground state. Emission of a photon is the result of a transition from an excited to a ground state.[75] However, not all transitions yield photons. The emission is restricted by the electronic state of the excited electrons. Luminescence has been classified into two main categories- fluorescence (primary luminescence) and

phosphorescence (afterglow component) depending on the nature of the excited state and duration of the emission after the removal of excitation. In fluorescence, the electron in the excited singlet state is paired by opposite spin to the second electron in the ground state orbital. Consequently, the emission of a photon occurs spontaneously and its rate is typically 10^8 s^{-1}. For phosphorescence, the emission takes place from the lowest triplet excited state in which the electron has the same spin orientation as the ground state. So the transition to the ground state is forbidden and the emission has a slow rate (10^3 s^{-1}). This phenomenon is due to the presence of trapping centres which delay radiative recombination.[76]

The fundamental excitation and emission processes in a hypothetical material are illustrated in Fig.1.9. When excitation processes take place, the material is raised from the ground state, E_0, to excited states, E_1 - E_5. If the gap between an excited level, E_2, and the adjacent lower level, E_1, is small, non-radiative decay will take place producing phonon emission as heat to the material.

The emission of light depends on the energy gap between adjacent energy levels. If the material has a reasonably large energy gap, it will luminescence.[77] Luminescent inorganic materials are either large band gap semiconductors or insulators. Luminescence may occur in solids (crystals or glasses) as well as in liquids or gases.

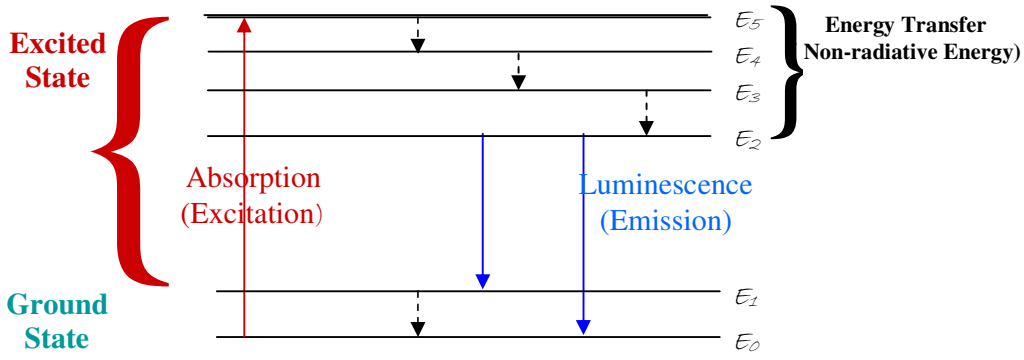

Fig.1.9 The excitation and emission process in a hypothetical material.

1.2.1 Luminescence Properties of Lanthanides

Lanthanide elements have unique luminescence properties that attract a great deal of interest for various applications as phosphors. These properties are due to their electronic structure. The emission of most trivalent lanthanide ions, Ln(III), is related to $4f^{n*} \rightarrow 4f^{n}$ transitions in the visible and near-infrared regions. For instance, the Eu^{3+} ion produces red luminescence and the Tb^{3+} ion gives green luminescence. These two ions act as activators in various kinds of practical phosphors.[78]

The electronic core nature of the 4*f* orbitals, which are shielded from the coordination environment, the crystal field and solvent influence, result in little vibrational coupling with the surrounding host material into which the ions are doped and narrow emission bands. All these lead to the production of pure colour and potentially high emission quantum efficiencies with long luminescence lifetimes.

Lanthanide-doped luminescent materials have various applications. The fields of these applications depend on the emitting wavelength. The ions that emit in the visible range are utilized in flat-panel televisions, cell phones, light emitting-diode devices (LEDs),[79,80,81]in biophysical assays[82,83] as well as in liquid crystals[84,85] while those that emit in the near-IR can be used in telecommunications,[86] laser applications and optical amplifiers.[87,88]

White-light LEDs are based on blue or UV emission from a GaN-based LED, and have much higher efficiency than that of incandescent lamps. They have a long life-time and at the same time save energy, are compact and are mercury-free which is very important for environmental reasons.

Phosphor materials play a key role in white light LEDs by converting the high energy light to a mixture of wavelengths. The phosphor materials used in LEDs should display specific properties such as:

- High thermal and chemical stability.
- High absorption in the near-UV.
- Low degradation and keeping up the high efficiency in a polymer matrix.
- Low thermal quenching.

Not all the applied phosphors have the above mentioned properties. Unfortunately some phosphors are less efficient due to thermal quenching. Some life times are reduced due to phosphor deterioration. An example of an unstable phosphor system is sulphide – based phosphors, these suffer from large thermal quenching.[89] Hence, improvements in the properties of phosphors are an area of great interest.

1.2.2 Influences on the Luminescence Properties

1.2.2.1 Concentration Quenching

One might expect that the efficiency of luminescence will be increased when the concentration of the phosphor ions increases. This is true to a certain limit of concentration. Reduction, quenching, of the luminescence takes place when the dopant ion concentration exceeds a critical value. This is called concentration quenching. At high concentration, the transfer of energy between ions is preferred. So the probability of energy transfer to another ion is much greater than the probability of radiative decay. As a result, the excitation energy will transfer other ions instead of being emitted as radiation.

There is another effect that influences the visible luminescence, related to the existence of centres called sinks or quenching traps. Perfect crystals are not obtained even under the most careful growth conditions. There are still defects, or traces of other ions, present. Hence excitation energy may transfer to these centres. These excited centres cannot transfer this excitation into the emission of radiation. So the quantum efficiency of the luminescence is decreased, since these centres withdraw the excitation from the regular dopant ions.[90] The effect of high and low concentration on the luminescence of materials is shown in Fig.1.10.

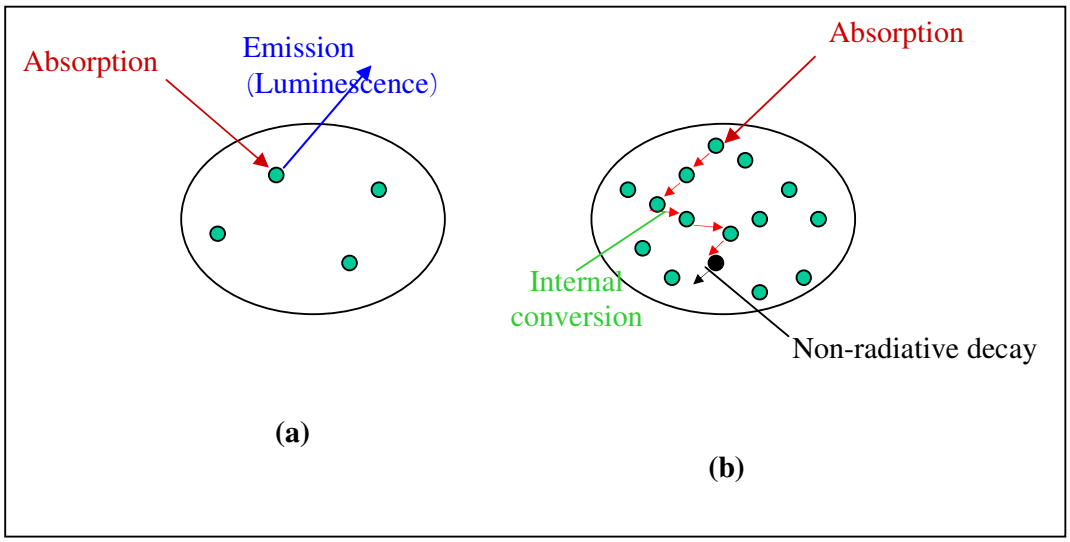

Fig.1.10 Concentration effect on Luminescence property, (a) low concentration results in luminescent emission, (b) high concentration leads to non-radiative decay.

1.2.2.2 Content of OH^- - Groups

The presence of OH^- group in oxide materials also quenches the excited energy state population. At high concentration of ions, energy transfer occurs and the effect of hydroxyl groups becomes applicable.

Once the material is excited, this excitation energy is spread through it and reaches the dopant ions (rare earth ions). If these ions are connected to hydroxyl groups, the phonon activity is increased and phonon- assisted non-radiative processes are enhanced. This process entails decreasing the efficiency of the luminescence due to considerable energy loss. At the contrary site in which the ions are not coordinated to hydroxyl group, the phonon activity decreases.

Consequently, materials having high concentration of hydroxyl groups will have excited states of short lifetimes. The same effect can occur when non-oxidic materials have been used since the tetrahedral SiO_4 units in materials such as silicate, aluminosilicate and aluminium phosphate have analogues in the structure chemistry of silicon nitride. Silicon imidonitride materials, usually referred to as amorphous silicon nitride, have

imidonitride composition with significant NH and NH_2 groups which in turn have the same effect as OH^- groups.

1.2.3 Lanthanide Doped Oxide Materials via Sol- Gel Processing

Different lanthanides have been doped in several oxide materials such as silica and binary mixed oxide materials using sol-gel methods.

1.2. 3. 1 Silica Gels

Sol-gel methods are the cheapest and simplest way to synthesise silica glasses doped with lanthanide compounds.[91] Synthesis of silica glasses doped with Er^{3+}, Yb^{3+} and Nd^{3+} compounds have attracted attention due to their use in signal amplifiers for telecommunications and fibre lasers.[92,93] However, concentration quenching of their luminescence is a problem due to continuous clusterisation of lanthanide compounds during synthesis. Phosphate complexes of lanthanide elements have been used for doping in the silica system. It enhances the uniform distribution of lanthanides in the matrix of silica glass and at the same time provides a chemical bonding between the organic and inorganic components at the gel formation stage.[94,95]

Dong *et a*l [96] incorporated novel binary complexes of $Er^{3+}$and Tb^{3+} with N-propyl-4-carboxy phthalimide into silica gels using the sol-gel method. The produced composite showed strong red or green emission but with slightly lower intensities compared with original complexes. Moreover, spin-on Er-doped silica gel films on porous Al_2O_3 have been fabricated.[97] First, a porous Al_2O_3 film on a Si wafer substrate was formed.[98] The preparation steps of spin-on Er-doped silica gel films are illustrated in Fig.1.11. These films exhibited sharp photoluminescence features.

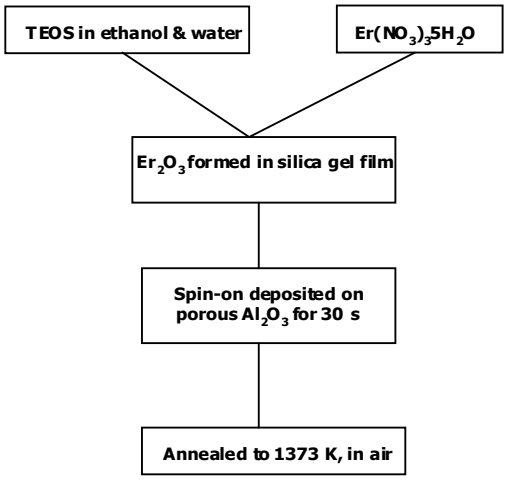

Fig.1.11 Process steps of spin-on Er-doped silica gel film.

1.2.3.2 Binary Mixed Oxide Material

Sol-gel techniques have been widely applied for preparation of binary mixed oxides.[99,100,101] SiO_2/TiO_2 mixed oxides are of interest for several optical applications such as optical filters, antireflective coatings and planar optical waveguides since their refractive index can be adjusted over a wide range of 1.2-2.1.[102] Europium-doped silica-titania thin films have been prepared using a sol-gel method.[103] Europium nitrate, tetraethoxy silane and ethanol were mixed together for 1 hr at room temperature followed by acidic hydrolysis. Separately titanium n-butoxide, acetylacetone and ethanol were stirred together for 1/2 hr at room temperature. The two solutions were mixed with stirring for 1 hr at room temperature and the obtained sol was spin-coated (3000 rpm) on a quartz glass support. The resultant thin film was pyrolysed at 500, 600, 700, 800 or 900 ^oC.

Further, lanthanide doped SiO_2-Al_2O_3 aerogels were reported.[104] Silicon and aluminium alkoxide precursors were hydrolysed separately and then mixed together. The ethyl and isobutyl alcohols have been removed from resultant sol by vacuum distillation at 35 ^oC to avoid gelation at this temperature. Then, 0.001 mole of lanthanide salt [$Pr(NO_3)_3.5H_2O$, $Sm(NO_3)_3.6H_2O$ or $EuCl_3.6H_2O$] were added and gelation was started

by raising the pH. Finally, the gel was dried under supercritical conditions (250 ^{o}C and 8.5 MPa of argon pressure). The alumina was proposed as a co-dopant[105,106] to overcome a non-uniform dispersion of lanthanide ions in the silica framework by surrounding each lanthanide ion with three AlO_4 tetrahedra which enhance the stability of the lanthanides.

Summary

Sol-gel techniques receive considerable attention. They provide useful means of producing many morphologies of high purity products such as films, fibres, monolith powders, aerogels and nanostructured materials. Historically this is mainly a method used for oxides, but sol gel processes for non-oxide, including nitride, materials are of growing interest. Often the non-oxide work has focused on producing powders for applications such as catalysis, where controlled porosity and basic catalytic sites are the point of interest. However, some groups have begun to produce other forms of material such as mesoporous silicon nitride membranes and semiconductor aerogels. We aimed to use this method to fabricate different silicon nitride material forms such as thin films, templated structures and aerogels. Furthermore, this technique will be extended to fabricate silicon nitride materials doped with lanthanide elements since sol-gel methods offer an effective means of adding elements into the Si-N matrix. The general aim of combining the low reactivity of these materials with other functional properties by doping in different elements has great potential.

1.3 References

[1] A.L.Hector, *Chem. Soc. Rev.,* **36,** 2007*,* , 1745.

[2] U.Schubert, N. Hüsing, *Synthetic of Inorganic Materials*, 2nd edition, WILEY-VCH Vverlag GmbH & Co. KGaA, Weinheim, 2004.

[3] J.D. Wright, N.A.J.M. Sommerdijk, *Sol-Gel Materials: Chemistry and Applications*, Taylor & Francis Books Ltd, London, 2001.

[4] F. Cheng, S. Clark, S.M. Kelly, J. S. Bradley, *J. Am. Ceram. Soc.,* **87**, 2004, 1413.

[5] F. E. Ghodsi, F. Z. Tepehan, G. G. Tepehan, *Optic. Mater.,* **31**, 2008, 63.

[6] S. Karuppuchamy, N. Suzuki, S. Ito, T. Endo, *Current applied Physics,* **9**, 2009, 243.

[7] Z. Wang, J. Li, H. Zhang, *J. Non-Crytal. Solids*, **354**, 2008, 3072.

[8] K. R. Murali, *J. Phys. Chem. Solids,* **68***,* 2007, 2293.

[9] Y. Hamasaki, S. Ohkubo, K. Murakami, H. Sei, G. Nogami, *J. Electrochem. Soc.,* **141,** 1994, 660.

[10] S. B. Yahia, L. Znaidi, A. Kanaev, J. P. Petitet, *Spectrochimica Acta Part A,* **71**, 2008, 1234.

[11] C. –J. Liu, P. K. Nayak, Z.-R. Lin, K.-Y. Jeng., *Thin Solid Films*, **516**, 2008, 8564.

[12] L. Francioso, M. Russo, A. M. Taurino, P. Siciliano, *Sensors and Actuators B,* **119**, 2006, 159.

[13] P. A. Tick, P.L. Bocko, *Optical Materials, Optical Fiber Materials*, M. Dekker, New York, Basel, 1990.

[14] R. Renner-Erny, L. D. Labio, *Optic. Mater.*, **29**, 2007, 919.

[15] J. Chandradass, M. Balasubramanian, *J. Mater. Process. Technol.*, **173**, 2006, 275.

[16] B. E. Yoldas, *Amer. Ceram. Soc. Bull*, **54**, 1974, 289.

[17] J. Chandradass, M. Balasubramanian, *Materials and Manufacturing Processes*, **21**, 2006, 319.

[18] C. Sunilkumar, US. Hareesh, BC. Pai, AD. Damodaran, KGK. Warrier, *Ceram. Int.*, **24**, 1988, 583.

[19] S. Ananthakumar, ARR. Menon, K. Prabhakaran, KGK. Warrier*, Ceram. Int.,* **27,** 2001, 231.

[20] S. Ananthakumar, KGK. Warrier, *J Euro Ceram Soc*, **21**, 2001, 71.

[21] K-S Hwang, J-T Kwon, J-S Oh, J-H An, B-H Kim, *J. Mater. Sci.*, **39,** 2004, 1683.

[22] I. Hasegawa, Y. Fukuda, M. Kajiwara, *Ceram. Inter.,* **25,** 1999, 523.

[23] M. Abdullah, F. Iskandar, S. Shibamoto, T. Ogi, K. Okuyama, *Acta. Mater.,* **52,** 2004, 5151; M. A. Carreon, V. V. Guliants, *Eur. J. Inorg. Chem.*, **27,** 2005.

[24] M. C. Carbajio; A. Gómez, M. J. Torralvo, E. Enciso, *J. Mater. Chem.,* **12,** 2002, 2740.

[25] S. Madhavi, S. Ferraris, T. White, *J. Solid State Chem.,* **179,** 2006, 866.

[26] F. Meseguer, A. Blanco, H. Míguez, F. García-Santamaria, M. Ibisate, C. López, *Colloids Surf. A.,* **202,** 2002, 281.

[27] B. Gates, Y. Yin, Y Xia, *Chem. Mater.,* **11,** 1999, 2827.

[28] J. F. Yang, G. J. Zhang, T. Ohji, *J. Mater. Res.,***16**, 2001, 1916.

[29] N. O. Engin, A. C. Tas,*J. Eur. Ceram. Soc.*,**19**, 1999, 2569.

[30] F. Tang, T. Uchikoshi, Y. Sakka, *Mater. Res. Bull.*, **41,** 2006, 268.

[31] X. Li, Y. Jiang, Z.Shi, Z. Xu, *Chem. Mater.*, **19**, 2007, 5424.

[32] R. W. J. Scott, S. M. Yang, G. Chabanis, N. Coombs, D. E. Williams, G. A. Ozin, *Adv. Mater.*, **13**, 2001, 1468.

[33] M. Acciarri, R. Barberini, C. Canevali, M. Mattoni, C. M. Mari, F Morazzoni, L. Nodari, S. Polizzi, R. Ruffo, U. Russo, M. Sala, R. Scotti, *Chem. Mater.*, **17,** 2005, 6167.

[34] Y. A. Vlasov, X. Z. BO, J. C. Sturm, D. J. Norris, *Nature*, **414**, 2001, 289.

[35] K. T. Lee, J. C. Lytle, N. S. Ergang, S. M. Oh, A. Stein, *Adv. Funct. Mater.*, **15**, 2005, 547.

[36] D. Farruseng, K. Schlichte, B. Spliethoff, A. Wingen, S. Kaskel, J. S. Bradley, F. Schüth, *Angew. Chem., Int. Ed.,* **40**, 2001, 4204.

[37] F. Cheng, S. M. Kelly, S. Clark, J. S. Bradley, M. Baumbzch, A. Schütze, *J. Membr. Sci.,* **280**, 2006, 530.

[38] F. Cheng, S. Clark, M. G. Fransconi, N. A. Young, C. Hope, S. M. Kelly, J. S. Bradley, *Chem. Mater.* **18**, 2006, 5996.

[39] N. Hüsing, U. Schubert, *Angew. Chem. Int. Ed.,* **37,** 1998, 22.

[40] J. B. Peri, *J. Phys. Chem.,* **70**, 1966, 2937.

[41] G. A. Nicolaon, S. J. Teicher, *Bull. Soc. Chem. Fr.,* 1968, 1900.

[42] D. M. Smith, R. deshpande, C. J. Brinker, " Better Ceramics Through Chemistry", *Mater. Res. Soc. Symp. Proc.,* **32**, 1992, 567.

[43] M. Domĭnguez, E. Taboada, E. Molins, J. Llorca, *Catal. Today,***138,** 2008, 193.

[44] S. L. Brock, I. U. Arachchige, K. K. Kalebaila, *Comments Inorg. Chem.,* **27,** 2006, 103; Y. P. Geo, C. N. Sisk, L. J. Hope-Weeks, *Chem. Mater.,* **19,** 2007, 6007.

[45] J. Choi, D. J. Suh, *Catal. Surv. Asia.,* **11**, 2007, 123.

[46] G. M. Pajonk, *Appl. Catal.***72**, 1991, 217; *Catal. Today,* **35**, 1997, 319.

[47] M. Schneider, A. Baiker, *Catal. Rev. Sci. Eng.* **37**, 1995, 515; *Catal. Today,* **35**, 1997, 339.

[48] RW. Pekala. US patent 4873218, 1989.

[49] RW. Pekala, CT. Alviso, FM. Kong, SS. Hulsey. *J. Non-Cryst Solids.,* **145,** 1992, 90.

[50] E. Beyarova, K. Kaneko. *Langmuir.* **15**, 1999, 7119.

[51] E. Beyarova, K. Kaneko, *Adv. Mater.* **12**, 2000, 1625.

[52] A. Liu, M. Cohen, *Phys. Rev.,* **B 41**, 1990, 727.

[53] J. Kim, K. Chung, *J. Appl. Phys.,* **83**, 1998, 5831.

[54] M. Arienzo, W. A. Orrarienzo, *Preparation and Properties of Silicon Nitride Based Materials,* Materials Science Forum Vol.**47**, Eds. D. A. Bonnell, T. Y. Tien (Trans Tech Publications, Zürich, 1989).

[55] T. P. Ma, IEEE Trans. Electron Devices, **45**, 1998, 680.

[56] J. V. Dalton, J. Electrochem. Soc: solid state science, **113**, 1966, 165C.

[57] L. Mingqi, S. Nemat-Nasser, *Mater. Sci. Engin.,* **A254,** 1998, 242.

[58] D. Hullmann, G. Wendt, U. Singliar, G. Ziegenbalg, *Appl. Catal. A: Gen.* **225**, 2002, 261.

[59] G. Garcia, F. J. Cadete Santos Aires, J. C. Bertolini, *J. Catalysis*, **214**, 2003, 26.

[60] Y. Xia, R. Mokaya, *J. Mater. Chem.* **14**, 2004, 2507.

[61] S. Kaskel, G. Chplais, K. Schlichte, *Chem. Mater.,***17**, 2005, 181.

[62] F. Cheng, S. M. Kelly, F. Lefebvre, S. Clark, R. Supplit, J. S. Bradley, *J. Mater. Chem.*, **15**, 2005, 772.

[63] J. Engering, M. Jansen, *Z. Anorg. Allg. Chem.,* **629**, 2003, 913.

[64] F. Cheng, S. M. Kelly, N. A. Young, S. Clark, S. M. A. Fransconi, J. S. Bradley, F. Lefebvre, *Chem. Commun***.** 2005, 5662.

[65] S. Kaskel, K. Schlichte, B. Zibrowius, *Phys. Chem. Chem. Phys.,* **4**, 2002, 1675.

[66] C. Balan, K. W. Völger, E. Kroke, R. Riedel, *Macromolecules*, **33**, 2000, 3304.

[67] K. W. Völger, R. Hauser, E. Kroke, R. Riedel, Y. H. Ikuhara, Y. Iwamoto, *J. Ceram. Soc. Jpn.,* **114**, 2006, 567.

[68] I.-K. Sung, M. M. Christian, D.-P. Kim, P. J. A. Kenis, *Adv. Funct. Mater.,* **15,** 2005, 1336.

[69] G. Chaplais, S. Kaskel, *J. Mater. Chem.*, **14**, 2004, 1017.

[70] V. G. Golubev, D. A. Kurdyukov, A. V. Medvedev, A. B. Pevtsov, L. M. Sorokin, J. L. Hutchison, *Semiconductors,* **35**, 2001, 1320.

[71] R. T. Paine, C. K. Narula, *Chem. Rev.,* **90**, 1990, 73.

[72] A. W. Jackson, A. L. Hector, *J. Mater. Chem.,* **17**, 2007, 1016.

[73] I. S. Kim, P. N. Kumta, *J. Mater. Chem.,* **13**, 2003, 2028.

[74] S. Kaskel, K. Schlichte, T. Kratzke, *J. Mol. Catal. A. Chemical,* **208**, 2004, 291.

[75] H. S. Nalwa, *Handbook of Luminescence, Display Material and Devices*, American Scientific Publishers, 2003, **1**.

[76] M. D. Lumb, *Luminescence Spectroscopy*, Academic Press Inc. (London) Ltd, 1978.

[77] M. D. Lumb, *Luminescence Spectroscopy*, Academic Press Inc.(London) Ltd., 1978.

[78] D. R. Vij, *Luminescence of Solids*, New York: Plenum Press, 1998.

[79] J. Kido, Y. Okamoto, *Chem. Rev.,* **102,** 2002**,** 2357**.**

[80] J.-C. G. Bűnzli, G. R. Choppin , *Lanthanide Probes in Life, Chemical and Earth Sciences- theory and Practice***,** Ed**.**, Elsevier, Amsterdam, 1989.

[81] G. Blasse, in *Handbook of Physics and Chemistry of Rare Earths,* Ed. J. K. A. Gschneidner, L. Eyring, North-Holland Publishing Company, Amsterdam, 1979, vol. 4.

[82] P. R. Selvin, *Annu. Rev. Biophys. Biomol. Struct.,***31**, 2002, 275.

[83] A. Mondry, R. Janicki, *Dalton Trans.,* 2006, 4702.

[84] K. Binnemans, *Chem. Rev.,***105**, 2005, 4148.

[85] K. Binnemans, C. Goerller-Walrand, *Chem. Rev.,* **102,** 2002, 2303.

[86] L. Gu, Z. Xiong, G. Chen, Z. Xiao, D. Gong, X. Hou, X. Wang, *Adv. Mater.*, **13**, 2001, 1402.

[87] W. J. Miniscalco, *J. Lightwave Technol.,* **9,** 1991, 234.

[88] P. G. Kik, A. Polman, *MRS Bull.,* **23,** 1998, 48.

[89] J. Y. Taso, *Light Emitting Diods (LEDs) for General Illumination Update*, *Optoelctronics ndustry Development Association*, Washington, DC, 2002.

[90] M. J. F. Digonnet, *Rare-Earth- Doped Fiber Lasers and Amplifiers*, 2nd. Ed., Marcel Dekker, New York, Basel, 2001.

[91] S, Gutzov, G. Ahmed, N. Petkova, E. Füglein, I. Petkov, *J. Non-Crystal. Solids,* **354,** 2008, 3438.

[92] E. Desurvire, *Erbium-Doped Fiber Amplifiers: Principles and Application*, New-York: John Wiley and Sons, 1994.

[93] W. Strek, P. J. Deren, K. Maruszewski, *et al*., *J. Alloys Comp.,* **275-277,** 1998, 420.

[94] Q.-M. Wang, B. Yan, *Inorg. Chem. Commun.,* **7**, 2004, 747.

[95] K. Binnemans, P. Lenaerts, K. Driesen, C. Görllen-Walrand, *J. Mater. Chem.,* **14,** 2004,191.

[96] D. Dong, Y. Men, S. Jiang, X. Ji, B. Jiang, *Mater. Chem. Phys.,* **70**, 2001, 249.

[97] N. V. Gaponenko, V. M. Parkun, O. S. Katernoga, V. E. Borisenko, A. V. Mudryi, E. A. Stepanova, A. I. Rat'ko, M. Cavanagh, B. O'Kelly, J. F. McGilp, *Thin Solid Films ,* **297**, 1997, 202.

[98] A. N. Vorobjeva, V. M. Parkun, *Microelectronika ,* **22**, 1993, 62.

[99] Q. Fang, M. Meier, J. J. Yu, Z. M. Wang, J.-Y. Zhang, J. X. Wu, A. Kenyon, P. Hoffmann, I. Boyd, *Mater. Sci. Eng. B,* **105**, 2003, 209.

[100] L. Wicikowski, B. Kusz, L. Murawski, K. Szaniawska, B. Susla, *Vacuum,* **54,** 1999, 221.

[101] A. Lukowiak, R. Dylewicz, S. Patela, W. Stręk, K. Maruszewski, *Optic. Mater.,* **27**, 2005, 1501.

[102] S. Lisinski, J. Krause, D. Schaniel, L. Ratkea, Th. Woikeb, *Scripta Materialia*, **58,** 2008, 553.

[103] I. Zaręba-Grodź, R. Pazik, W. Tylus, W. Mielcarek, K. Hermanowicz, W. Strek, K. Maruszewski, *Optic. Mater.,* **29**, 2007, 1103.

[104] S. Grandi, L. Costa, *J. Non-Cryst. Solids,* **225**, 1998, 141.

[105] M. J. Lochhead, K. L. Bray, *Mater. Res. Soc. Symp. Proc.,* **346**, 1994, 754.

[106] T. Fujiyama, M. Hori, M. Sasaki, *J. Non-Cryst. Solids,* **121**, 1990, 273.

EXPERIMENTAL TECHNIQUES

2.1 Introduction

This chapter describes the techniques used for the characterisation of films, aerogels, monolith xerogel and terbium doped silicon nitride powders which were produced throughout this thesis. For films scanning electron microscopy (SEM), x-ray diffraction (XRD) and x-ray photoelectron spectroscopy (XPS) techniques were used to characterise morphology, thickness and composition. For aerogels and xerogels the techniques included infrared spectroscopy (IR), SEM, transmission electron microscopy (TEM), magic angle spinning- nuclear magnetic resonance spectroscopy (MAS-NMR), thermogravimetric analysis (TGA) and XRD. These techniques focussed on the characterisation of chemical composition and their topographies. The surface area and pore size distribution measurements for aerogels were performed using nitrogen adsorption isotherms. Additionally the terbium silicon nitride material was characterised using photoluminescence spectroscopy (PL).

2.2 Thermogravimetric Analysis (TGA)

Themogravimetric analysis is a type of thermal analysis technique in which change in sample weight can be followed over a period of time during heating under an inert or reactive gas. It was used herein to determine the thermal stability of the material and the fraction of the volatile components. TGA was performed using a Mettler Toledo TGA/ SDTA851, Fig.2.1.

Due to the high air sensitivity of samples under study, the equipment was mounted inside a glovebox filled with nitrogen to minimise the risk of partial oxidation of the sample during handling which may result in inaccuracies during analysis.

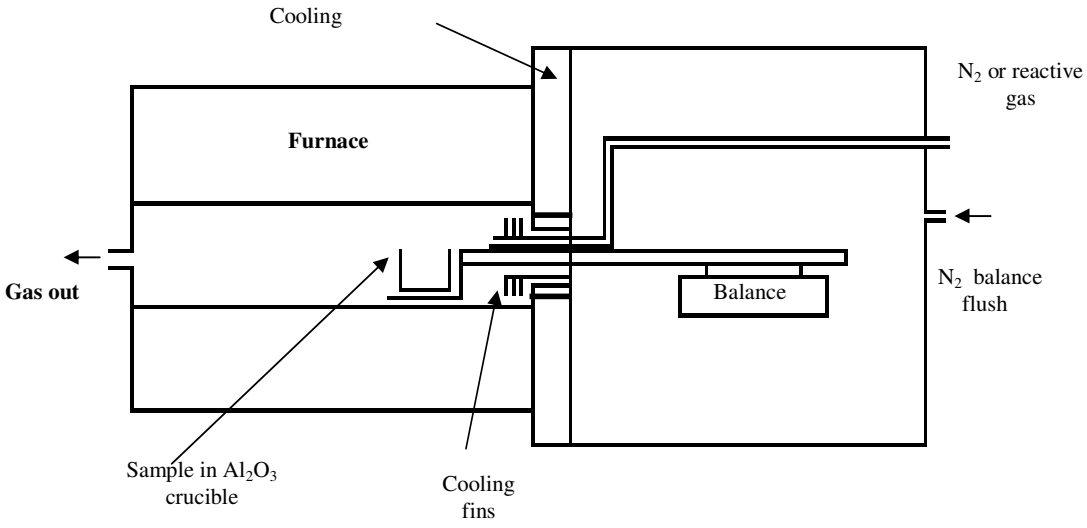

Fig. 2.1 A schematic diagram of Mettler Toledo TGA851e.

Pre- programmed heating regimes were adopted for the TGA samples heated under a flow of very high purity nitrogen (Air Products BiP grade, <10 ppb O_2 and <20 ppb H_2O). The sample (between 20–40 mg) was loaded in a dry alumina crucible (vol: 150 μL) and then placed onto the balance arm within the analyser. It was held at 25 °C for 10 minutes before gradually heating to 900 °C at a heating rate of 5 °/minute under a flow of gas (50 mL/min.) for the whole procedure. At 900 °C the sample was then held for one hour before allowing it to cool back to 25 °C. The balance assembly measures the initial sample weight and then continuously monitors any change in weight as a function of temperature and time throughout the procedure.

For low density samples, it is difficult to place more than 2-4 mg of material into 75 μL alumina sample pan. This quantity still gave acceptable results, but was the absolute minimum of sample mass required for the instrument in the glove box. Samples of at least 10 mg are prefered.

2.3 X- Ray Diffraction.

X-ray diffraction (XRD) is a versatile, non-destructive technique that reveals detailed information about the chemical composition and crystallographic structure of natural and manufactured materials. Since no two chemical substances have exactly the same crystalline structure, the diffraction pattern can be used as a fingerprint of the sample. Hence unknown materials can be identified from their powder pattern that will be indexed against known reflections and consequently identified.[1]

X-ray photons are generated when a high-speed beam of electrons bombards a metal plate. Electrons from the metal atom core are ejected and the holes are filled by electrons from higher energy orbitals with resultant emission of radiation. Copper is usually used due to its high thermal conductivity and ability to produce a strong flux of K_α X-rays at a useful wavelength to interact with the powdered sample.

Since a single X-ray wavelength is desired for diffraction experiments a crystal monochromator is used which is placed in series between the radiation source and the sample. This crystal monochromator is mounted in the correct orientation to diffract only X-ray photons of the desired wavelength (Cu $K_{\alpha 1}$ at 1.5406 Å in this case). The monochromated beam is collimated by aperture slits before striking the sample.

As X-ray photons impinge on the sample, some are scattered and others pass through to be scattered from other planes, as shown in Fig. 2.2, according to Bragg's Law. For the two scattered X-rays (waves) to be in phase, ABC must be equal to an integral number of wavelengths ($n\lambda$). If d is the distance between the planes,

$$AB = BC = 2d \sin\theta$$

Since $$ABC = 2AB = n\lambda$$

$$n\lambda = 2d \sin\theta \quad \text{[Bragg's Law]}$$

Where n: is integer λ : X-ray wavelength θ : Bragg's angle.

The scattered photons are then collected at the detector. The output is the intensity of X-rays (y-axis) detected as function of the diffraction angle 2θ (x-axis).

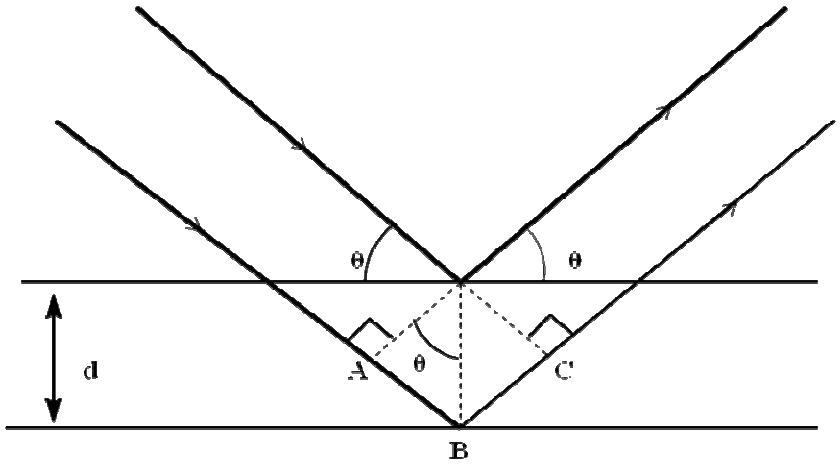

Fig. 2.2 Schematic diagram of X-ray diffraction.

Powder X-ray difraction data (PXD) was collcted using a Siemen D5000 diffractometer, in Bragg-Brentano geometry, Fig. 2.3, and a Bruker D8 advance C2 diffractometer, as in Fig. 2.4, both using Cu- $K_{\alpha 1}$ radiation.

The majority of routine X-ray characterisation work was carried out using the D5000. Samples were ground to an homogeneous particle size inside a nitrogen filled glove box and the resultant powder was mounted in a suitable air-sensitive sample holder and sealed. The sample holder was attached to the diffractometer and a range of 20 to 80 degrees (D5000) was collected.

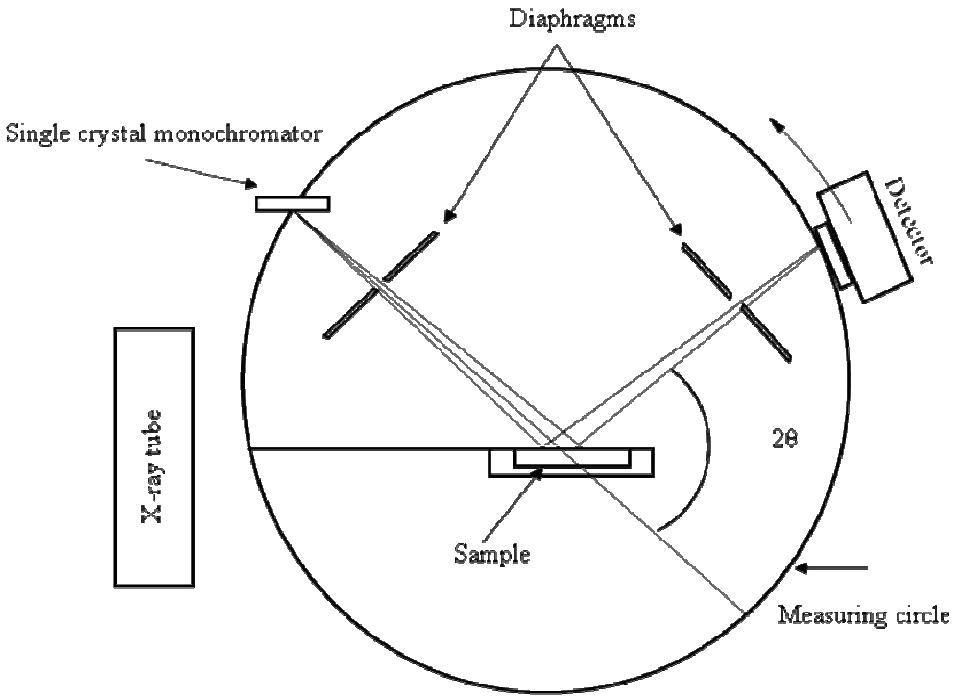

Fig. 2.3 A schematic diagram of the D5000 powder diffractometer (Bragg-Brentano geometry).

The C2 diffractometer can be applied for both samples and films *in situ*. The small spot size facility of C2 can be used in which very small quantities of sample can be analysed. Furthermore, it can be configured to a low incident X-ray angle to increase the effective thickness of a surface coating and hence record data on thin film samples with reduced contribution from the substrate, Fig. 2.4.

Throughout this thesis the C2 diffractometer was used to analyse films via low angle (5^{o} incident angle) diffraction. The data collected from both instruments was analysed using the Diffract Evaluation Programme (EVA).

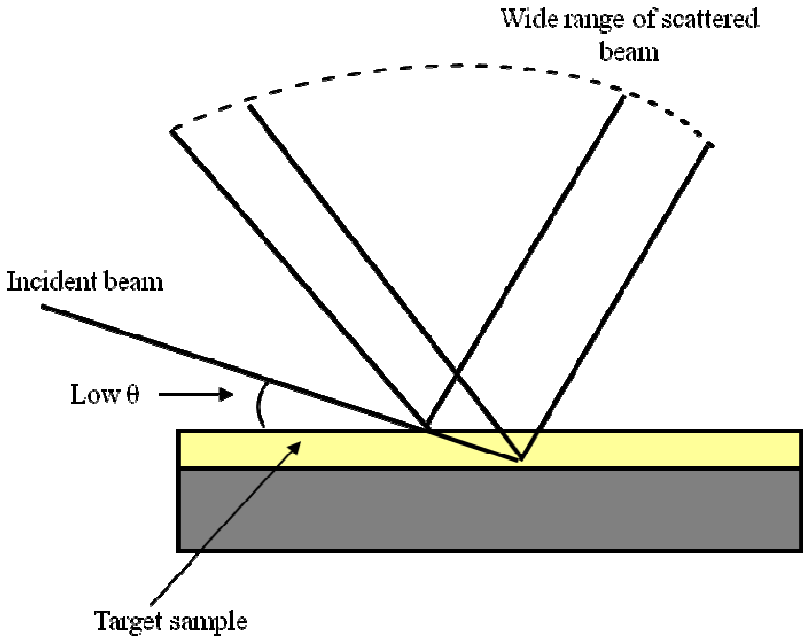

Fig. 2.4 Low angle diffraction used on the C2.

2.4 Combustion Microanalysis

Microanalysis was carried out on precursor materials and annealed nitrides. Information of the quantities of carbon, hydrogen and nitrogen were collected. This information can be used as a guide to sample stoichiometry compared to calculated percentage from ideal materials. Around 10–15 mg of samples were sealed inside glovebox and sent to MEDAC Ltd., Egham, Surrey. Different precursors as well as the annealed products had been microanalysed to compare the C, H and N concentration.

Due to the air sensitivity of both precursors and produced silicon nitride products, samples were handled and sealed under an argon atmosphere in a glove box. Hence C, H, N and halogen (Cl) could be analysed without sample degradation.

C, H & N analysis were carried out by combustion analysis using one a Thermo 1112 Flash elemental analyser. A standard sample was analysed eight times using different treatment conditions, Table 2.1.

Table 2.1 Different treatments of sample analysis.

Sample Identification
Weighed into tin capsule
Weighed into tin capsule with V_2O_5
Weighed into tin capsule with WO_3
Weighed into tin capsule with powdered Sn
Weighed into Al capsule
Weighed into Al capsule with V_2O_5
Weighed into Al capsule with WO_3
Weighed into Al capsule with powdered Sn

The results of the sample analyses showed that for silicon nitride samples, which are difficult to fully combust, the best treatment condition is a tin capsule with tungstic oxide or powdered tin added as a combustion aid. The use of Al capsules was detrimental since the N present remained uncombusted in the reactor. Hence tin capsules and a WO_3 additive were used for sample analyses. For chlorine analysis a Schöniger flask combustion followed by titration method is applied.

2.5 Infrared Spectroscopy

Infrared spectroscopy is a straightforward method for identification of chemical bonds (functional groups) within molecules. It is concerned with changes in the dipole moment that are produced from vibration or rotation. The absorption of IR radiation depends on increasing the energy of vibration or rotation associated with a covalent bond. This increase results in a change in the dipole moment of the molecule or solid. Nearly all materials containing covalent bonds will show absorption in the IR. The only exceptions are homonuclear diatomic molecules because no mode of vibration or rotation produces a change in the electric dipole of the molecules. Generally, the absorption of IR photons may be due to either change in the bond length (stretching) or alteration of the bond angles (bending). The former one is usually denoted by the symbolism ν. It is divided into two types: symmetric and asymmetric stretching modes.

IR experiments are typically based on passing IR radiation through a thin sample of compound and measuring which energies of the applied IR radiation are transmitted by the sample. IR spectra can be recorded for solids, liquids and gases using different sample arrangements. The absorption by a specific group occurs in a characteristic region of the spectrum. These absorptions appear as a series of peaks and are referenced by simply comparing them with tables of known compounds.[2] Similar frequencies occur in different molecules, therefore a vibration is considered as reflecting the atoms involved and the strength of bond holding them together.

Infrared spectroscopy was performed using a PerkinElmer spectrum One FT-IR spectrometer in conjunction with PerkinElmer's analytical software Spectrum v3.05.

Solid samples were prepared by incorporating them into a pressed pellet of cesium iodide for analysis. Due to the sensitivity of the precursor, the samples had to be prepared inside a nitrogen filled glovebox. A weighed portion of sample, approximately 3 mg, was mixed with 300 mg, of highly purified CsI using a pestle and mortar. The sample and CsI were ground well to reduce the particle size; otherwise the large particles would scatter the infrared beam causing a sloping profile in the baseline of the spectrum. Cesium iodide does not absorb in the region studied peaks so will not interfere with the spectrum. The mixture was placed in an evacuable die and subjected to a pressure of 10 M Pa for two minutes. Then the sample was placed between CsI disks in an IR cell with a Teflon spacer, see Fig.2.5.

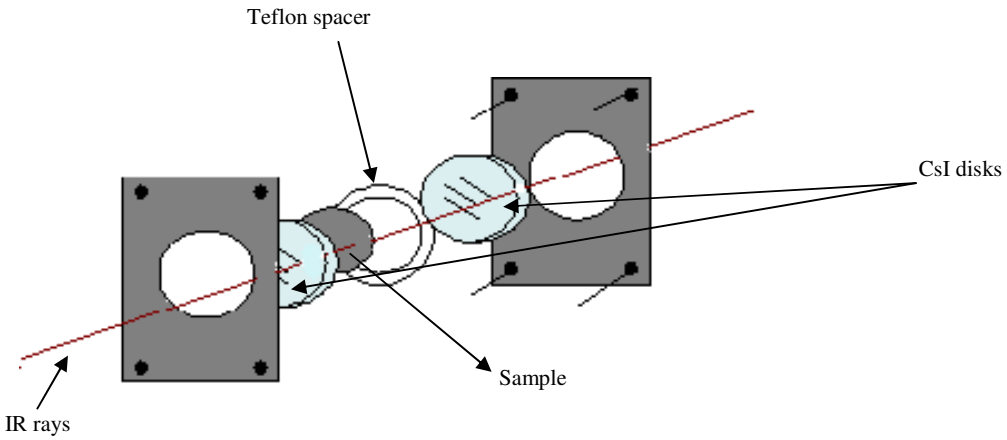

Fig. 2.5 A diagram of an IR sample holder cell.

2.6 Electron Microscopy (EM)

Electron microscopes use electrons to create an image of the sample. Smaller objects and details can be detected using EM rather than a light microscope since it offers a resolution capability thousands of times better than a light microscope. Furthermore it has much higher magnification that reaches up to two million times which can be used to examine metals and crystalline structures and the characteristics morphologies of the various surfaces.

There are different types of electron microscope. Scanning electron microscopy (SEM) and transmission electron microscopy (TEM) have been utilised throughout the study for this thesis. These two types are similar in that both of them employ a beam of electrons which are directed to the specimen. Therefore certain characters in both instruments such as the electron gun, condenser lenses and vacuum system are similar.

2.6.1 Scanning Electron Microscopy (SEM)

SEM is principally used to study the surface or near surface morphology of the specimen. SEM functions are generally explained as follow:

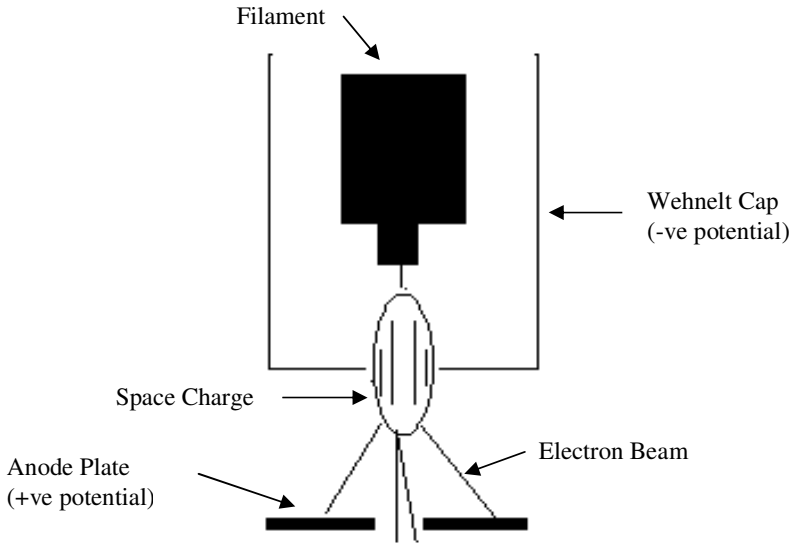

Fig.2.6 The electron gun.

The thermoionic gun, as shown in Fig.2.6, is the most widespread system. The filament (F), acts as a cathode, is heated and the electrons emitted from it are accelerated by a positive potential applied down the gun column toward the anode (A) and a beam of electrons is generated. A negative potential is applied to the ' Wehnelt Cap'(W) so that any emitted electron from the filament is repelled by that cap toward the horizontal centre. The electrons are collected in the space between filament tip and Wehnelt Cap, called a space charge. Those electrons at the bottom of the space charge nearest to the anode can exit the gun area through a small hole moving down the column to be used in imaging.

Once the stream of electrons departs the gun, it is condensed through the first condenser lens that used to form the beam and limit the amount of current in the beam. The beam is constricted by condenser aperture which used to eliminate the high-angle electrons from the beam. The second condenser lens forms the electrons into thin, coherent beam and the objective lens focuses the scanning beam onto the desired part of specimen to be analysed, Fig.2.7.

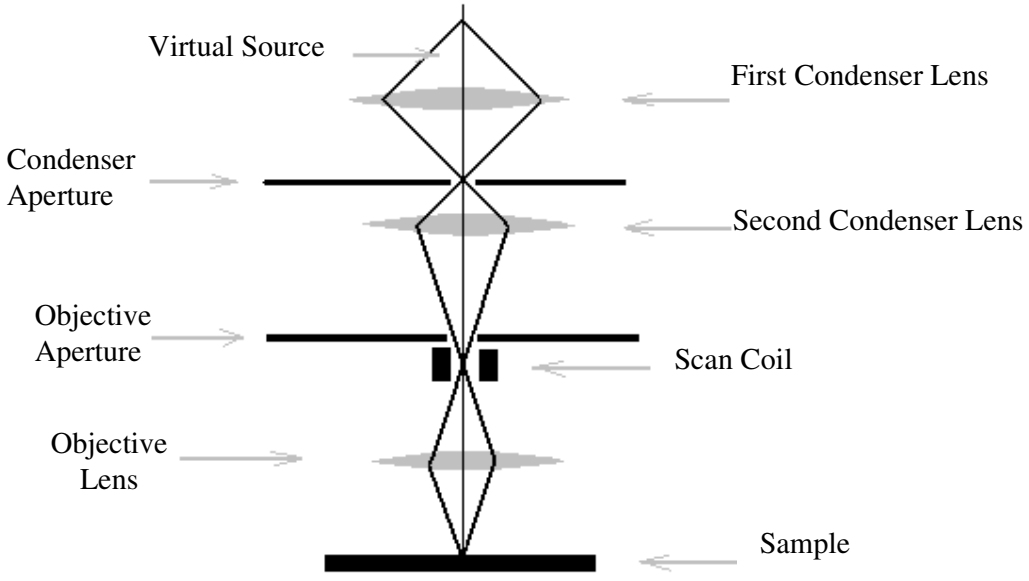

Fig. 2.7 A schematic representation of the SEM focussing process.

SEM images are produced by detecting the secondary electrons which are emitted from the sample surface due to the excitation by the primary electron beam. The electrons are detected using a scintillator-photomultiplier. The resulting signal is amplified into

two-dimension intensity distribution whose brightness depends on the number of secondary electrons reaching the detector. Then the image can be viewed and saved as digital image.

Scanning electron microscopy was carried out at the University Southampton Microscopy Centre using a JEOL JSM-5910 microscope to give surface structures of films and powders produced throughout the course of research. Due to the air-sensitivity of the samples, SEM samples were prepared inside a nitrogen filled glovebox, then quickly coated with carbon or gold and introduced to the analysis chamber. In order to analyse the film thicknesses, the tiles were cleaved and mounted perpendicular to the aluminium stub surface.

2.6.2 Transmission Electron Microscopy (TEM)

In a transmission electron microscope, an electron beam of uniform current density is transmitted through a thin specimen. Electrons are emitted from the electron gun and pass through two or three stage condenser lens system before illuminating the specimen. The objective lens provides the formation of either an image or a diffraction pattern of the specimen. A three or four stage lens system is used to magnify the electron intensity distribution behind the specimen and the image is viewed on a fluorescent screen recorded using a CCD camera.

Transmission electron microscopy was carried out using a JEOL JEM-3010 microscope. The samples were prepared also inside the glovebox. A small amount was suspended in dry toluene using ultrasound for 30 mins. A droplet of solution was deposited onto a carbon/copper grid using a pasteur pipette then allowed to dry.

TEM provides information about the internal surfaces of a material under examination and the images are viewed after passing the electrons through the specimen (transmitted) so a thin specimen is required. At SEM only surface or near surface morphology can be detected and the images viewed are a result of electrons scattered from the specimen.
TEM provides much higher resolution than SEM so can be used to image much smaller

features. However sampling can be difficult and it is harder to be certain that a representative sample is being imaged.

2.6.3 EDX

Energy dispersive X-ray analysis is an analytical technique used to identify the elemental composition of a specimen. This technique is used in conjunction with SEM and TEM instruments where the image capility of the microscope is used to select the region of interest.

When the electron beam impinges on the sample surface electron in an inner shell of one of the constituent atoms may be excited by the incident beam. Ejection from its shell creates an electron hole and an electron from an outer, higher energy shell will fill that hole. The difference in energy between the higher -energy shell and the lower one is released in the form of an X-ray photon. The energy of these photons is measured in the EDX detector. Since these energies are characteristic of the atomic structure of the element from which they were emitted elemental composition of the sample can be analysed.

EDX is not as surface sensitive technique as a XPS, since the X-rays, generated from a region about 2 microns in depth. A Lithium drifted Silicon (SiLi) detector is used in EDX and operated at liquid nitrogen temperature. The X-ray photon strikes the detector and will generate a photoelectron within the body of the Si. Electron-hole pairs are generated through the photoelectron travelling through the Si and are attracted to opposite ends of the detector with the aid of a strong electric field. Hence a current pulse is generated and its size depend on the number of electron-hole pairs created, which in turn depends on the energy of the incoming X-ray photon.

The SiLi detector was protected by a boron nitride window so N was difficult to detect and any nitrogen contained within the samples was rendered invisible. Furthermore, the ability to quantify the presence of any carbon in the sample itself is also removed since carbon coating is required to enhance the conductivity of the sample under examination prior to analysis so that the surface does not charge in the electron beam.

2.7 X-ray Photoelectron Spectroscopy (XPS)

XPS is one of several electron spectroscopy techniques that measure the kinetic energy of electrons that are emitted from matter as a consequence of bombarding it with ionising radiation of high-energy particles. It results from the ionisation of an electron from an inner shell. The kinetic energy, E, of the ionised electron is equal to the difference between the energy, hν, of the incident radiation and the binding energy, E_b, of the electron ($E = h\nu - E_b$). The detected elements are characterised by their binding energy.

Binding energy is defined as the attraction energy between the electron and the atomic nucleus. Hence, to eject an electron from an atom, enough energy must be applied to overcome its binding energy. For a given atom, a range of E_b values is possible, corresponding to the ionisation of electrons from different inner shells and these E_b values are characteristic for each element. The unique binding energy of each element in a sample depends on their electronic and chemical environment and that can be identified against an index of known elemental binding energy values.

XPS is essentially a surface sensitive tool as the electrons have a very little chance of escape with penetrating depth of 5 nm below the sample surface. This surface can be etched away using different materials; herein we used bombardment with argon ions for etching. This process is applied in order to remove the surface contamination that had either been deposited through handling or occurred due to oxidation, resulting from the high sensitivity of the materials, so that accurate determination of the samples composition just below the surface could be gained.

XPS of films was performed at Nottingham Nanotechnology and Nanoscience Centre (NNNC), University of Nottingham, and at National Centre for Electron Spectroscopy & Surface Analysis (NCESS), Daresbury Laboratory. At NNNC, a Kratos Axis Ultra XPS spectrometer equipped with a mono-chromated Al K-alpha X-ray source was used while a Scienta ESCA300 photoelectron spectrometer, equipped with a high power rotating anode monochromatised Al K alpha (hν = 1486.6 eV) X-ray source was used at NCESS.

2.8 Nuclear Magnetic Resonance Spectroscopy (NMR)

Basic Principle

NMR spectroscopy depends on the spin quantum number, I, of a nucleus. Nuclei of certain isotopes have angular momentum. The total angular momentum depends on the spin number I with value range from 0, 1/2, 1, 3/2,…. depending on the particular nucleus. If I=0, the nucleus does not have a spin and hence can't be observed by this method. Nuclei of I>0 have characteristic magnetic moments. When a magnetic nucleus is placed in an external uniform magnetic field, a discrete set of (2I+1) orientations will be adopted. For example, in nuclei with I=1/2 one of two possible orientations is assumed that correspond to energy level ± μH in applied magnetic field, where H is the strength of the external magnetic field and μ is the magnetic moment of the spinning nucleus. NMR spectroscopy utilises the magnetic spin energy of atomic nuclei of I= ½ such as ^{1}H, ^{13}C, ^{19}F, ^{31}P and ^{29}Si. A transition between these two energy levels is possible and may be affected by the absorption or emission of a discrete amount of energy such that E= hυ= 2 μH, where υ is the frequency of the electromagnetic radiation absorbed or emitted. The difference in energy between these two states is given by:

$$\Delta E = \frac{\gamma h H}{2\pi}$$

Where γ is the gyromagnetic ratio of nucleus under study.

The frequency of radiation that corresponds to this energy is called the resonance frequency.

Chemical shift

Each nucleus in a compound is surrounded by a cloud of electrons which are in constant motion, when a magnetic field of H is applied to a sample these electrons are caused to circulate to oppose the field. This effect will result in shielding the nucleus from the external field value and the effective magnetic field H_{eff} experienced by nuclei will not be the same.

$$H_{eff} = H (1-\sigma)$$

Where σ is the shielding constant.

This shielding constant will vary as the local environment changes, especially with the electron density around the nucleus under study. This will affect the energy and hence the frequency required to be applied to cause a transition and therefore the resonance frequency characterise the surrounding environment of the nucleus.

The chemical shift (δ) is the ratio of the change of field necessary to achieve resonance to the field strength of the standard. It is usually expressed in ppm.

$$\delta = \frac{H_{sample} - H_{eff}}{H_{ref}}$$

If the degree of shielding of the nucleus under study increases, H_{eff} and hence the resonance frequency decrease. Consequently, the peak will be shifted to lower ppm value. For example the proton NMR signal of HI is at lower δ than that of HF since the F is more electronegative so will withdraw more electron density from the H compared with I. Since the shielding of the nucleus is influenced by the type of atoms surrounding it, so the chemical shift of nucleus under study can be used to determine the type of chemical envirnment.

NMR spectra were collected using a Bruker AV300 equipped with an autosampler. The samples (~ 10 mg) were dissolved in deuterated benzene.

Solid State NMR

In the solid state, early NMR spectra gave broad, featureless bands which were of little use for structural work. Recently, practices have been developed for NMR study of solids. Magic Angle Spinning (MAS) NMR techniques are applied in which the sample is rotated at a high velocity at a critical angle of 54.74^{o} to the applied magnetic field and the broad bands collapse to reveal the fine structure. The spectra are composed of sharp peaks yeilding much structural information.

This technique has been applied to silicon –based nitride materials (aerogel, xerogel) in which ^{29}Si NMR spectra give peaks indications of the nature of the chemical environment of Si atoms through their chemical shift.

Solid-state NMR data were collected using Varian Unity Inova spectrometer operating at 59.56 MHz for ^{29}Si, Durham University and the spectral referencing is with respect to tetramethylsilane. Also a ^{29}Si NMR spectrum was collected in Southampton University using a Varian Infinity+ spectrometer at 9.4 T and with a 6.5 KHz spinning frequency and spectra referenced against silicone rubber.

2.9 Surface Area Measurement

A solid that contains pores, cavities, channels, or interstices which are deeper than they are wide is called a porous solid. The pores may vary greatly both in size and in shape within a given solid and between one solid and another. Nevertheless, pores have been classified into three different pore-size regimes according to their average width:[3]

- Micropores, pores which have diameter less than 2 nm.
- Mesopores, pores which have diameter between 2 and 50 nm.
- Macropores pores which have diameter larger than 50 nm.

The pore size is expressed either in terms of diameter (or radius), or with width of the slits. Gas adsorption measurements are widely used for determining the surface area and pore size distribution of a variety of different solid materials.[4] Surface area and porosity are important properties that can be used in catalyst design. Two measurable quantities can give a detailed description of a porous solid. **Specific Surface Area (S)** is a measure of the accessible surface area per unit mass of solid. It is the sum of its internal, S_{in}, and external, S_{ex}, surface areas ($S = S_{in} + S_{ex}$). **Pore Size Distribution (PSD)** is the distribution of the pore volume versus the pore size and depends on the shape of the pores present in the solid. This distribution can be homogeneous or heterogeneous according to the number of distinct pore maxima.

Adsorption Isotherms

The porous texture of solids can be determined using physical adsorption isotherms. When a gas comes into contact with a solid surface, which has been correctly outgassed, molecules of the gas will be adsorbed onto the surface in quantities that are a function of their partial pressure. The measure of the amount of gas adsorbed, ν, over a range of relative pressure, i.e. the pressure in the gas phase, P, divided by the saturation pressure, P_o, at a fixed temperature, results in a graph known as an adsorption isotherm and represented as:

$$\nu = f\,(P/\,P_o)_T$$

The adsorption is a consequence of force at the surface of the solid which attracts the molecules of the gas. This attraction force is physical and gives rise to physical (or "Van der Waals") adsorption.

Adsorption isotherms are grouped into five classes. These classifications were originally proposed by Brunauer, Deming, Deming and Teller (BDDT).[5] Nowadays they are commonly referred to as the Brunauer, Emmett and Teller (BET) classification.[6] These types are shown in Fig. 2.8. Type I isotherms characterize microporous adsorbents. Type II and III describe adsorption on macroporous adsorbents with strong and weak adsorbate- adsorbent interaction, respectively. Type IV and V represent adsorption isotherms with hysteresis. The former is common in mesoporous adsorbents while the latter is obtained with certain porous adsorbents.

The adsorption branch of the isotherm is obtained when the ν values are determined for increasing relative pressure (from $P/\,P_o \approx 0$ up to $P/\,P_o = 1$). The opposite is used to obtain the desorption branch. These two branches of the isotherm may not coincide with each other in which case a hysteresis loop is formed. This loop is characteristic of the pores present in the solid. The occurrence of a wider, more pronounced hysteresis loop indicates that the evaporation from the pore is a distinctly different process from the condensation within it.

BET measurements were performed at 77 K using a Micromeritics Gemini 2375 instrument. 20 mg of sample was placed in cleaned, dried tube, in the glove box. Then the sample and the balance tube were attached to the ports of the instrument. The sample tube is evacuated and then filled with the adsorbant gas (N_2). The quantities of adsorbed gas are measured at each desired point of relative pressure. This adsorption process continues until relative pressure reaches unity, then the desorption process is started following the pressure as vacuum is reapplied.

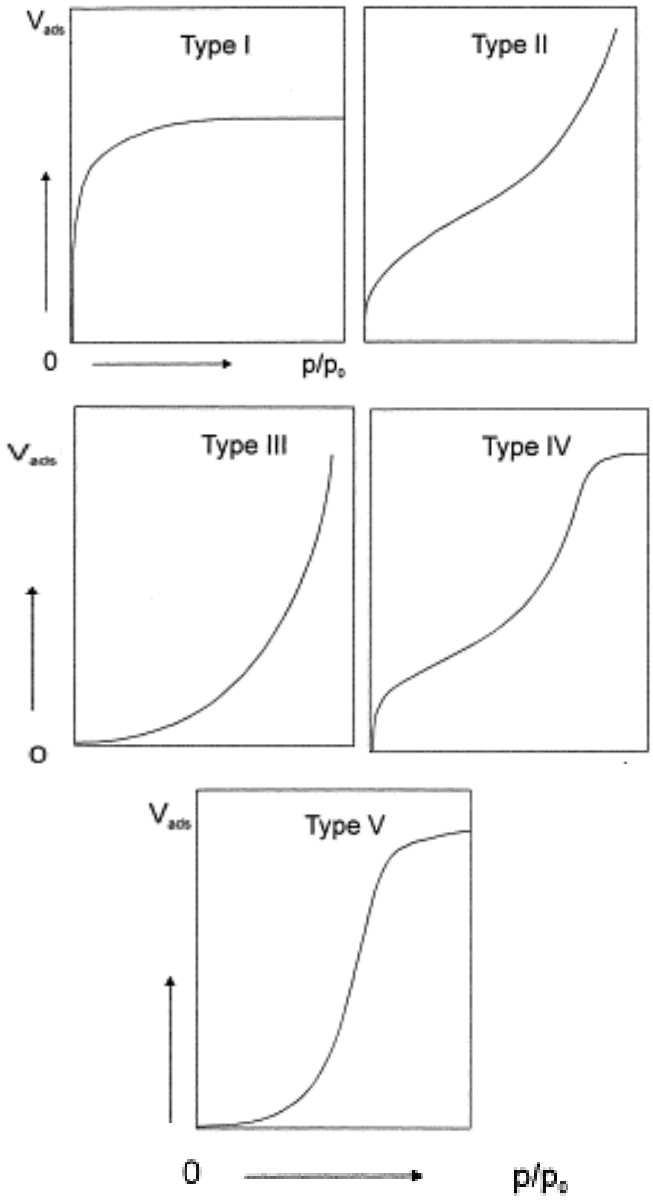

Fig. 2.8 Adsorption isotherm classifications. Reprinted with permission from S. Stork, H. Bretinger, W. F. Maier, *Appl. Catal. A,* 174, 1998, 137.

2.10 Photoluminescence Spectroscopy

Luminescence in solids is the phenomenon in which the electronic states of solids are excited by some energy from an external source and then that excitation energy is released as light. Photoluminescence is where the excitation source is light of high energy, often UV light. At excitation the electronic state of the molecule changes from the ground state to one of many vibrational levels in one of the excited electronic states. The excited electronic state is usually the first excited singlet state, S_1. Once the molecule is in this excited state, relaxation can occur via several processes. Fluorescence is one of these processes and results in the emission of light. Fluorescence intensity may be reduced or eliminated if the luminescing molecule is quenched. There are two main types of photoluminescence spectra:

• Excitation Spectrum.

In this spectrum the wavelength of the exciting light is varied and the intensity of the emitted light at a fixed emission wavelength is measured as a function of excitation wavelength. The excitation spectrum, like absorption, gives information on the position energy of the excited states but it differs in giving only the absorption bands that result in the emission light. For example it does not give any indication of nonradiative relaxation.

• Emission Spectrum.

The emission spectrum reflects the distribution of the probability of various transition from the lowest vibrational level of S_1 to the various vibrational level of S_o so its characteristics do not depend on the excitation wavelength source. This emission of photon with energy $h\nu_F$ varies depending on what S_o ground state level (e.g. 0, 1, 2, etc.) it returns to. Hence the light emitted by a substance is made up of a lot of different wavelengths. Each emission spectrum is characteristic of a given compound. For luminescence spectroscopy three elements are basics in the experiment; light source (excitation source), light- dispersing elements and light detection.

Fluorescence excitation and emission spectra were recorded using a Perkin Elmer LS 55 Luminescence spectrometer, Fig. 2.9. The excitation and emission wavelengths

used were 242 and 545 nm respectively. These wavelengths can be determined via the collection of two spectra, an excitation spectrum and an emission spectrum. Although the approximate excitation and emission wavelengths for many molecules are known, these wavelengths should generally be optimized for the specific conditions employed.

A sealed sample holder was filled with the sample and placed into the sample compartment, of the spectrometer with slit width adjusted at 10 and 2.5 for excitation and emission slit respectively. With the excitation wavelength fixed at 242 nm, the emission spectrum is obtained between 350 and 670 nm.

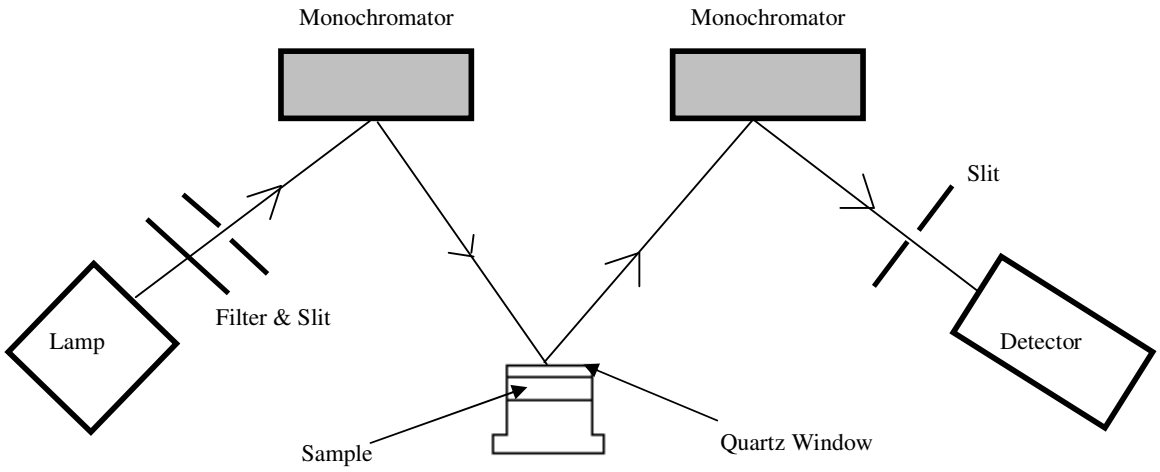

Fig. 2.9 A schematic Diagram of luminescence spectrometer.

2.11 References

[1] K. L. William, *Introduction to X-Ray Spectroscopy,* London: Allen & Unwin, 1987

[2] K. Nakamoto, *Infrared and Raman Spectra of Inorganic Compounds, Theory and Applicatios in Inorganic Chemistry,* Wiley-Interscience, 1997.

[3] M. M. Dubinin, *Quart. Rev. Chem. Soc.,* **9,** 1959, 101; *Chem. Rev.,* **60,** 1960, 235.

[4] K. S. W. Sing, D. H. Everett, R. A. W. Haul, L. Moscou, R. A. Pierotti, J. Rouquerol, T. Siemieniewska, *Pure & Appl. Chem.,* **57**, 1985, 603.

[5] S. Brunauer, L. S. Deming, W. S. Deming, E. Teller, *J. Amer. Chem. Soc.,* **62,** 1940, 1723.

[6] S. Brunauer, P. H. Emmett, E. Teller, *J. Amer. Chem. Soc.,* **60,** 1938, 309.

AMMONOLYSIS SOL-GEL ROUTE FOR SILICON NITRIDE THIN FILMS

3.1 Introduction

Silicon nitride films have good resistance to corrosion, high thermal stability, good hardness and wear resistance and good dielectric properties.[1] They can be utilised in cutting tools, as insulating layers in multilevel interconnects,[2] as dielectric antireflection coatings for silicon solar cells[3] and in the semiconductor industry as diffusion masks.[4]

Two general strategies are employed to prepare amorphous silicon nitride films.[5] One is the reactive sputtering of silicon in nitrogen using radio-frequency (rf) glow discharge to ionise gases that are used to deposit on a cold or heated substrate.[6] The other is chemical vapour deposition (CVD) in which typically a mixture of SiH_4 and NH_3 gases is pyrolytically decomposed on a substrate at high temperature.[7]

Low pressure chemical vapour deposition (LPCVD) and atmospheric pressure CVD (APCVD) techniques have been used for silicon nitride film formation at substrate temperatures in excess of 700 ^oC.[2] However, such high temperature results in substrate degradation and is not suitable for many devices. Electron cyclotron resonance plasma-enhanced CVD (ECR-PECVD) has been used to lower the deposition temperature of a SiH_4- NH_3 gas mixture and reduce the radiation damage.[8] Nevertheless, these films often contain a large amount of bonded hydrogen, which may sometimes degrade the device performance.[9] Reactive[10]and non-reactive[11] magnetron sputtering techniques have also been applied in which hydrogen- free silicon nitride thin films have been formed.

Sol-gel methods have been widely exploited for thin films, especially oxide films, in which large areas can be covered. Many metal oxide thin films are deposited using this method. Typically a sol is dip- or spin coated to produce thin films that are then heated to decompose to the oxide.

Silicon oxide thin films are used in optical,[12] microelectronics,[13] magnetic and thermal applications[14] including as anti-reflective[15] and thermal insulation coatings.[16] The sol-gel technique can be employed for silicon oxide film preparation using acid or base catalysis. Films with higher homogeneity and surface uniformity were obtained with

increasing amounts of water in acid catalysed (HCl) hydrolysis of tetraethylorthosilicate (TEOS) diluted in ethanol.[17] The prepared sols were dispersed on silicon wafers and spun at 2000 rpm for 15 s then pyrolysed at various temperatures from 100 to 1000 ^{o}C for 30 min. For high porosity silica films a base catalyst (NH_4OH) was added to TEOS solution followed by acetic acid addition to the gel solution to slow down the speed of condensation.[18] The SiO_2 gel was coated with polyvinyl alcohol (PVA) to restrict the growth of gel particles before spin coating onto Si substrates at 2500 rev/min for 10 min. It was then annealed at 550 ^{o}C. Uniform, crack-free porous SiO_2 films were formed.

TiO_2 has received a great deal of attention due to properties such as high chemical stability, low production cost, etc.[19] For use as the semiconductor in solar cell applications it has been prepared using a sol-gel method.[20] 0.1 mol $Ti(O\text{-}i\text{-}C_3H_7)_4$ and 100 ml ethanol were mixed with stirring at 0 ^{o}C. Then a mixture of ethanol (100 ml), water (0.15 mol) and hydrochloric acid (5 mmol) was added to the titanium solution under stirring at 0 ^{o}C. A titanium plate of 0.25 mm thickness was dipped into the titanium dioxide sol. The resulting TiO_2 films were heat treated at three different temperatures to select the anatase phase, rutile phase or a mixture of both. Yoko et al[21] used a similar method to prepare titanium dioxide in the anatase form.

Thin silica-titania films have been successfully obtained using a dip[22] or spin[23] sol-gel coating method. Silica[24] and titania[25] sols were prepared separately before mixing by dissolving silica and titania precursors in ethanol and hydrochloric acid. The mixed sols were aged for a few hours before deposition. Using dip coating, silica wafers were dipped into the mixed sols with a withdrawal speed of about 2 mms^{-1}. Thermal treatment at 500 ^{o}C for 1 hr resulted in films useful as an optical waveguide sensor with good optical and mechanical properties and a higher refractive index than SiO_2.[26] For spin coating, the film deposition was performed on (100) silicon wafer with spin speed of 3000 rpm at room temperature and then pyrolysed at 500 ^{o}C for 2 hr. The resulting TiO_2-SiO_2 composite thin film was constituted of TiO_2 nano-crystallites embedded in a silica network. This composite has a high catalytic activity for a wide variety of reactions such a complete photocatalytic oxidation of ethylene,[27] for decontamination of aquatic environments from organic and chloroorganic contaminants[28] etc. Furthermore, other metal oxide thin films such as ZnO have been made using sol-gel dip coating techniques.[29]

The extension of sol-gel techniques to nitride materials is still very limited. Recently, attention has been focussed on dip coating from sols as a simple method of preparing thin films of nitrides.[21]

Cheng *et al*[30] successfully prepared mesoporous silicon nitride membranes via a non-aqueous sol-gel process. A silicon diimide sol was prepared by acid-catalysed self-condensation of tris(dimethylamino)silylamine $[(Me_2N)_3SiNH_2]$ in THF at 50 ^oC to a cyclic trimer $[(Me_2N)_2SiNH]_3$ which was then treated with ammonia. A macroporous Al_2O_3 disk was dipped into the sol before gelation and fired at 1000 ^oC under NH_3 flow for 2 hr. The potential properties of this porous inorganic membrane such as oxidation resistance and high temperature mechanical properties were then examined and their use was demonstrated as a selective filter for gas sensors. Similarly, Kroke *et al*[31] synthesized silicon carbonitride membranes that can be used as a catalyst support in high temperature membrane reactors. Dimethyldichlorosilane $Me_2Si_2Cl_2$, bis(trimethylsilyl)carbodiimide $[(SiMe_3)_2NCN]$ and pyridine were mixed and heated at 150 ^oC for 24 hr. After cooling to room temperature, methyltrichlorosilane $MeSiCl_3$ was added to the reaction mixture. The resulting viscous sol was spin coated onto a macroporous Si_3N_4 substrate and pyrolysed at 1000 ^oC in Ar.

Using a related technique, nanocrystalline titanium nitride and carbonitride films have been formed.[32] Tetrakis(dimethylamino)titanium (TDMAT) was reacted with a controlled amount of primary amine. The resultant sol was coated onto a silica substrate via a dip coating method. The films were pyrolysed under ammonia or nitrogen leading to TiN and Ti(C, N) respectively. Jackson and Hector[33] also reported the effect of using extra amine and the use of TDMAT- ammonia sols. The former results in a solid precipitate that was converted to TiN powder after heating to 1000 ^oC under ammonia flow. It the latter case, 2-2` bipyridyl was added to the TDMAT precursor before addition of stoichiometric amounts of NH_3. Dip- coating of the silica slides with the sol, followed by annealing under ammonia forms TiN but the films were of very poor quality due to the lack of condensable species in the sol.

Since films are one of the easiest morphologies to process by sol-gel methods, in which the solvent has only to diffuse through a short path during the drying process, we focused here on preparation of silicon nitride thin films using ammonolysis sol-gel routes.

3.2 Experimental

3.2.1 General Remarks

All reagents were highly air and moisture sensitive therefore all procedures were performed under an anhydrous nitrogen atmosphere using standard Schlenk techniques and dry solvents or in a nitrogen filled glove box (O_2< 1 ppm, H_2O< 1 ppm).

The solvents, n-pentane and tetrahydrofuran (THF), were freshly distilled from sodium. The ammonia used in the preparation of sols was dried by condensation at -78^o C over sodium.

Reagents were purchased from Sigma-Aldrich, ammonia from Air Products and solvents from Fisher Scientific.

3.2.2 Investigation of $[Si(NMe_2)_4]$ as a Precursor

Initially the precursor chosen was tetrakis(dimethylamino)silane $[Si(NMe_2)_4]$ which is a clear liquid at room temperature. This precursor has been used in atmospheric pressure chemical vapour deposition (APCVD) with ammonia to make Si_3N_4 thin films, and was reported to be safer to handle than SiH_4 and SiH_2Cl_2 for this application.[34] A series of reactions with ammonia, with and without an acid catalyst, were investigated. A catalytic amount (one drop) of trifluoromethanesulfonic (triflic) acid was added to a solution of $[Si(NMe_2)_4]$ (1 mL, 4.33 mmol) in dry diethylamine (10 mL). This resulted in the formation of a small amount of white precipitate. An excess of dry ammonia was bubbled through the reaction mixture for over an hour. This reaction was also attempted with $[Si(NMe_2)_4]$ (0.5 mL, 2.16 mmol) in dry tetrahydrofuran (THF) (10 mL). Both reactions failed to produce any further precipitate or suspension. The solvent was removed by vacuum to yield a clear liquid. ^1H and ^{13}C NMR were collected on both starting material and product. For $[Si(NMe_2)_4]$, ^1H δ (ppm) was 2.55 (s) and ^{13}C δ (ppm): 37. The ^1H and ^{13}C for the product showed resonance at 2.5 (s) and 37 ppm respectively. Comparison with reported NMR spectra of $[Si(NMe_2)_4]$[35] reveals little difference. It was concluded that $[Si(NMe_2)_4]$ was not reactive enough with ammonia for coating sol formation under these conditions.

3.2.3 Synthesis of the [Si(NHMe)$_4$] (TMAS) Precursor

Tetramethylaminosilane [Si(NHMe)$_4$] (TMAS) contains smaller, more volatile methylamino groups than the dimethylamides in [Si(NMe$_2$)$_4$] and so should undergo ammonolysis at a faster rate. In fact its rate of ammonolysis has been shown to be comparable to those of reactive amides of metals such as [Ti(NMe$_2$)$_4$] and [Ta(NMe$_2$)$_5$].[36]

TMAS was synthesised using silicon tetrachloride $SiCl_4$ and methylamine, Fig.3.1. Methyl amine (99%, 100 ml, 2.253 mol, 14 equiv.) was passed through dry molecular sieves before being condensed onto a stirred solution of silicon tetrachloride (99%, 18 ml, 0.157 mol) in dry n-pentane (140 ml) at -78 ^{o}C (acetone/ dry ice bath). White solid formed immediately and the reaction mixture was allowed to warm to room temperature overnight. The reaction mixture was filtered though a sinter to remove the methylamine hydrochloride by- product. The solvent was removed from the filtrate under reduced pressure yielding an oily off-white solid.

$$SiCl_4 + 8\,H_2NCH_3 \xrightarrow{\text{n- pentane}} Si(NHCH_3)_4 + 4CH_3NH_2.HCl$$

Fig.3.1 Synthesis of tetramethylaminosilane (TMAS).

Purification of TMAS was achieved by sublimation,[37] as in Fig.3.2, of the crude material at 45 ^{o}C under vacuum in which a transparent, low-melting crystalline solid was formed. The solid was characterized with ^{1}H and ^{13}C NMR and microanalysis. The NMR data showed that sublimation successfully purified TMAS[38], Table 3.1.

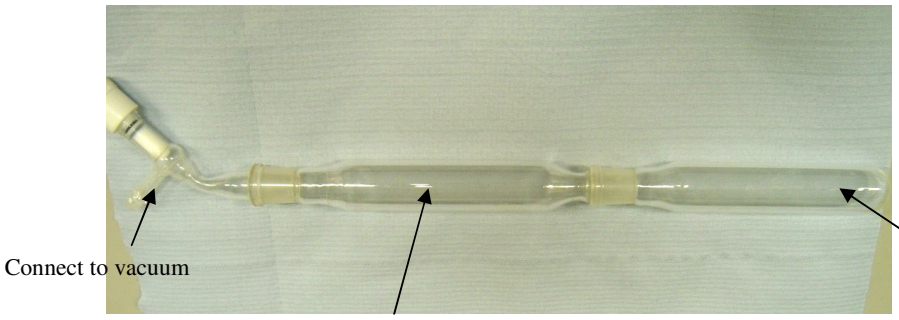

Fig. 3.2 Apparatus used for sublimation process.

Table 3.1 NMR of TMAS before and after sublimation.

NMR of crude product	^{1}H δ (ppm): 2.65 (m), 2.56 (m), 2.51(d), 0.27 (broad)
	^{13}C δ (ppm): many peaks between 29-27
NMR of sublimed solid	^{1}H δ (ppm): 2.51 (d, 3*H*, Si(NHC*H*$_3$)$_4$), 0.27 (broad, 1*H*, Si(N*H*CH$_3$)$_4$)
	^{13}C δ (ppm): 28

Microanalysis shows the expected carbon, hydrogen and nitrogen content, and a negligible amount of chlorine even in the crude, Table 3.2.

Table 3.2 Microanalysis of crude and sublimed products.

	Elemental Analysis (%)			
	C	H	N	Cl
Crude product	30.43	9.82	35.11	0.06
Sublimed product	31.82	11.04	36.67	not obtained
Theoretical	32.40	10.88	37.77	0

3.2.4 Reactions of TMAS with Dry Ammonia

Various quantities of sodium dried ammonia were condensed into [Si(NHMe)$_4$] solutions in dry THF, Fig. 3.3. Ammonia (0.04 mL, 0.5 equiv.) was reacted with a solution of TMAS (0.5g, 3.42 mmol) in dry THF (6 mL) at -78 ^{o}C.

$$[Si(NHMe)_4] + n\,NH_3 \xrightarrow{THF} [Si(NH)_x(NH_2)_y(NMe_2)_z]$$

Fig. 3.3 Non-catalysed reactions with purified TMAS.

This resulted in a clear solution after 18 hours of warming slowly to RT. A mixture of opaque (white) oil and clear crystals formed when the solvent was removed. This suggested that not all the TMAS had reacted. This procedure was repeated with 1 and 2

equiv. of NH_3. Little precipitate was formed but the sols were quite cloudy, indicating the growth of particles. The clearer the sol the better it is likely to be for dip coating, as smaller colloidal particles should pack better than larger ones to ultimately form a thin, continuous film on the surface after pyrolysis. Triflic acid (as catalyst) was tried to increase reactivity, Fig. 3.4.

$$[Si(NHMe)_4] + n\,NH_3 \xrightarrow[[H^+]]{THF} [Si(NH)_x(NH_2)_y(NMe_2)_z]$$

Fig. 3.4 Acid catalysed reaction with purified TMAS.

In section 1.1 and Fig 1.3 effect of acid catalyst on sol-gel silica formation was discussed. This mechanism seems unlikely in ammonolytic sol-gel and an alternative catalytic effect of triflic acid was proposed by Cheng *et* al.[39] The effect of catalyst would be displacement of NHMe groups as H_2NMe, resulting in precursor molecules containing triflate groups, Fig. 3.5. The electron withdrawing effect of a triflate group would render the precursor molecule more susceptible to nucleophilic attack. Triflate is then a good leaving group.

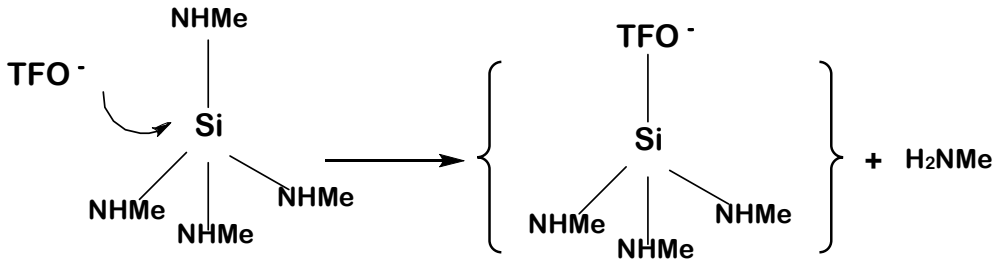

Fig. 3.5 Triflic acid effect on TMAS precursor.

Ammonia (0.068 mL, 0.63 equiv.) was condensed onto a solution of TMAS (0.7g, 4.72 mmol) in dry THF (6 mL) containing a drop of triflic acid at –78 °C. This was allowed to warm slowly to room temperature overnight. This reaction resulted in a precipitate and a clear sol. Separating the sol and evaporating the solvent revealed a solid that was not purely starting material. The NMR data showed presence of new small peaks formed combined with pure starting material peaks, ^1H (ppm): 3.5 (s), 2.66 (m), 2.51 and 1.4 (s), 0.41 and 0.27 (broad).

The acid catalysed reaction was then modified: Sodium dried ammonia (0.062 mL, 0.8 equiv.) was condensed onto a solution of TMAS (0.5 g, 3.37 mmol) in dry THF (6 mL) at

–78 °C. The mixture was allowed to warm to RT overnight (18 h) before treating the reaction mixture with one drop of triflic acid, Fig. 3.6. This resulted in a clear solution. This way, the reaction between TMAS and NH_3 (ammonolysis) occurs first, replacing some methylamino groups with amide groups. When the acid catalyst is added, the condensation reaction is enhanced. Very little precipitate was observed under these conditions. The reaction mixture was allowed to stand for at least 4 hours before use and most of the sol-gel processing work was performed with sols produced in this way.

$$[Si(NHMe)_4] + nNH_3 \xrightarrow{THF} [Si(NH)_x(NH_2)_y(NMe_2)_z] \xrightarrow{[H^+]} [Si(NH)_{>x}(NH_2)_{<y}(NMe_2)_{<z}]$$

Fig. 3.6 Steps of silicon diimide formation.

A sol obtained from the reaction with 0.8 equiv. of NH_3 was used for dip coating different tiles (section 3.2.5) which were then pyrolysed under dry ammonia (section 3.2.6).

The glassware used in this reaction is illustrated in Fig. 3.7. TMAS (0.5 g, 3.37 mmol) was dissolved in dry THF (6 ml) in a pressure tube then the required amount of ammonia was condensed into the graduated capillary tube of the glassware at -78 ^oC. The Young's tap was closed, the pressure withstanding tap opened and the capillary tube was allowed to warm outside the condensing bath in order for ammonia to be transferred. The mixture was allowed to warm to room temperature overnight, and then one drop of triflic acid was added. The clear sol was allowed to stand for 4 hours before use.

Larger amounts of ammonia (2–3 equiv.) resulted in monolithic gels. After at least 18 hours of standing the resultant sol was a very opaque emulsion. This was treated with one drop of triflic acid and allowed to stand overnight. A solid white gel formed occupying the whole volume of the original sol. These conditions were used for aerogel preparation and will be described in detail later (chapter 4).

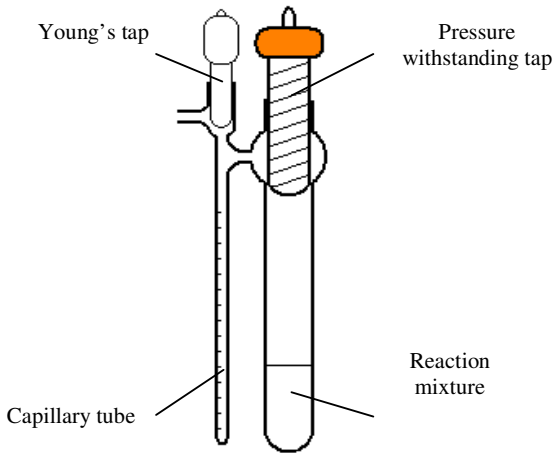

Fig.3.7 Ammonia transfer apparatus.

3.2.5 Preparing Sols for Dip Coating

On solvent removal in vacuo, the sol remained liquid until around 90% was removed. Then, suddenly, a solid formed, Fig. 3.8. An attempt to re-dissolve a small amount of this solid in excess THF showed that it was insoluble. This indicates that the gelation process is irreversible, which is important in terms of its use in coating because a substrate can be dipped into the sol, allowed to dry, and then dipped again to increase the thickness of the films if this is required.

For dip coating, sols were either used without pre-concentration or with around 40% of the solvent removed in vacuo. They will be referred to as *'as prepared* sol' and '*concentrated sol'* throughout this chapter. These different sols were dipped using various tiles and fired to several annealing temperatures

Fig 3.8 Silicon diimide xerogel.

3.2.6 Coating

Alumina, silica and silicon wafer substrates were cleaned before use by immersion in a 'Piranha Etch' mixture (3:1 H_2O_2: H_2SO_4) for 24 hours. This was performed to remove any organic material, grease, dirt and contaminants from the substrate surfaces that might cause poor adhesion of the coating-sol that would translate into cracking or flaking of the coating. Then the tiles were washed with copious amounts of deionised water and left to dry in an oven at of 300 ^oC for 24 hours.

As the sols were highly air sensitive, the dip coating of the tiles was performed inside the glove box. Using tweezers the tiles (typically 25 x 10 mm) were immersed into the coating sol for 5 seconds before removing from the solution. It was observed that when the tiles were removed slowly from the sol, the solvent evaporated almost instantly giving visibly shiny xerogel films. Removing the tiles from the sol more quickly caused the solvent to form drops on the surface that required at least one minute to evaporate. Some tiles were dipped more than once. These were allowed to dry horizontally for at least 3 minutes before dipping again. Once the coatings had been allowed to dry, the films were pyrolysed under anhydrous NH_3.

3.2.7 Pyrolysis of Xerogel Films and Powders

Coated tiles and bulk xerogels, Fig. 3.8, were loaded into a dry alumina boat then placed into a custom designed tube; see Fig. 3.9. The apparatus used was flushed first with sodium-dried ammonia for at least 30 minutes before beginning the heating program. They were heated initially to 200 ^{o}C at a rate of 2 ^{o}C per minute, held for duration of two hours then heated to the target temperature of 500, 700 or 1000 ^{o}C at the same rate and held again for 2 hours before allowing to cool back to room temperature.

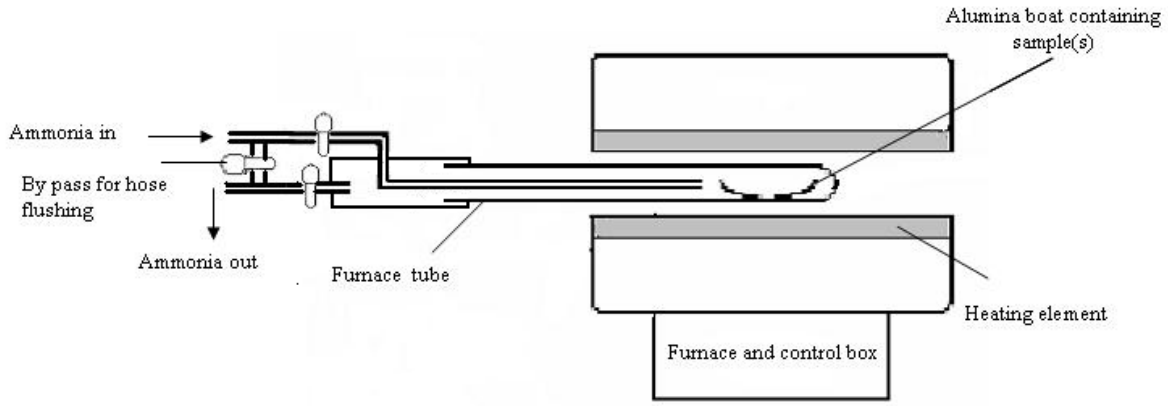

Fig. 3.9 Furnace tube apparatus used for pyrolysing samples under a flow of ammonia.

This heating program was similar to that used by Cheng *et al*,[40] during the pyrolysis of silicon boron imide gels, to reduce the amount of carbon present, the aim being to substitute the maximum number of alkylamide groups at low temperature before pyrolysis.

Due to the air-sensitivity of the precursors and the possible sensitivity of the annealed products, both were stored in the glove box and sample preparation for further analyses was carried out there.

For coated tiles, the surface morphologies were examined using scanning electron microscopy (SEM). The chemical compositions of the thin films were determined using X-ray photoelectron spectroscopy (XPS). The measurements were carried out at NCESS and at NNNC, University of Nottingham. At NCESS, a Scienta ESCA300 photoelectron

spectrometer, equipped with a high power rotating anode monochromatised Al K alpha (hv = 1486.6 eV) X-ray source combined with a high transmission hemispherical analyser and multichannel detector was used. At Nottingham, a Kratos Axis Ultra XPS spectrometer equipped with a mono-chromated Al K-alpha X-ray source, concentric hemispherical analyser and delay-line detector was used. The xerogel solids were analyzed using IR spectroscopy, microanalysis and X-ray diffraction.

3.3 Results and Discussion

3.3.1 TGA Studies of TMAS and its Ammonolysis Products

Thermogravimetric analysis is a thermal analysis technique that is used to determine a material's thermal stability and its fraction of volatile components by monitoring the weight change that occurs as a specimen is heated. TGA proved useful in comparisons made on the solids produced from the various ammonolysis reactions in which the weight loss was used as an indication of the amount of TMAS and small oligomers present and hence give a measure of the degree of condensation.

Figure 3.10 shows that increasing the amount of ammonia in each reaction resulted in solids that lose less mass when heated to 900 ^{o}C. The smaller mass losses with higher NH_3 quantities can be attributed to more Si-N-Si bonds being present i.e a more highly condensed polymer. Furthermore, the data also shows the large effect the catalytic triflic acid has on the products, especially when comparing the 1 NH_3 equiv. acid catalysed reactions with the 10 NH_3 equiv. non-catalysed reactions.

Comparison with related work using a TG-MS system[39] can give some insight into the processes likely to be occurring during heating. Generally, at the early stages of condensation small oligomer groups start to eliminate at temperature range from 200-400 ^{o}C. The mass loss of material depends on the amount of uncondensed groups that the material has. Hence the low mass loss during the heating cycle is evidence of the small amount of uncondensed groups that the material has. Hence the acid catalysed samples showed lower mass loss below 700 ^{o}C compared with the non-catalysed ones.

The appearance of the solids after the heating cycle also showed a trend. Samples with low final mass percentages contained more black particles (assumed to be carbon), whereas

those with higher final mass percentages were mainly white. This can be related to the amount of organic material remaining in the polymeric chains, a greater degree of ammonolysis and condensation is directly linked to lower product carbon content.

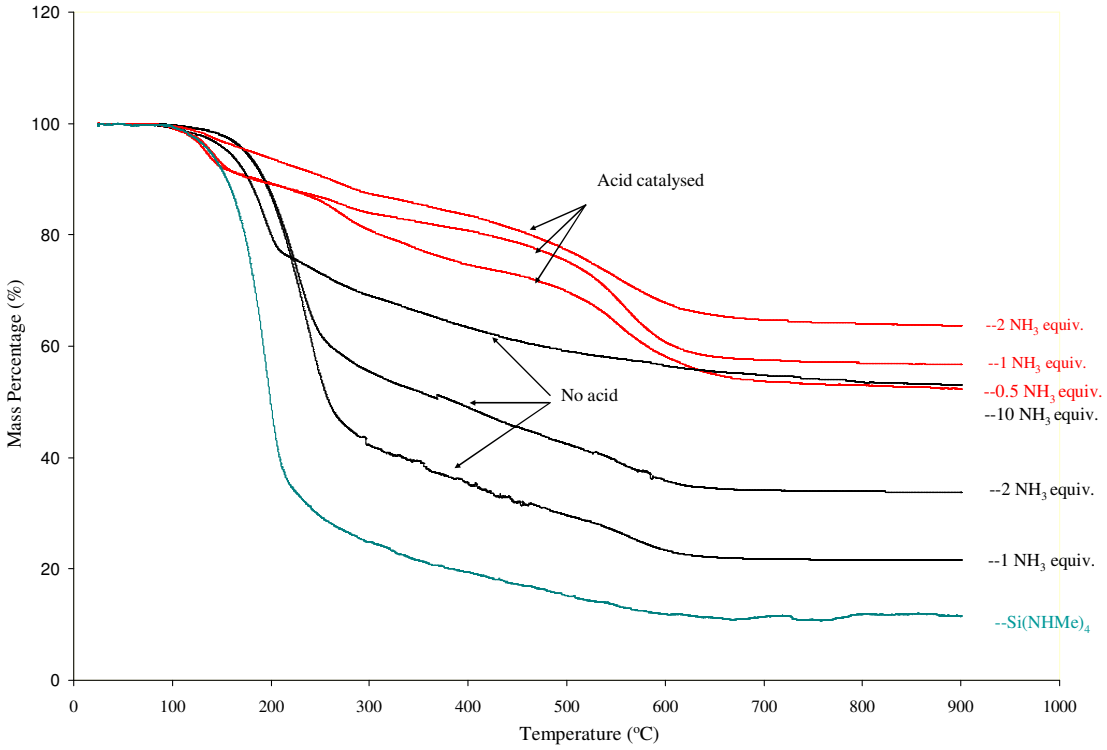

Fig. 3.10 Change in mass with temperature for $Si(NHMe)_4$ and xerogels under nitrogen flow.

Reduced mass loss is desirable in materials deposition terms and the displacement of more dimethylamino groups should result in lower product carbon content. However, use of an excess of NH_3 resulted in a lot of precipitate, and more than 2 equivalents of NH_3 in acid-catalysed reactions resulted in gelation. An acid catalysed reaction with around 0.8 equiv. NH_3 produced clear sols with almost no precipitate and it was these conditions that were used for all the coatings described herein.

3.3.2 IR Studies of Xerogels Before and After Firing

The film composition was checked from xerogels obtained under the same conditions as the films. The acid catalysed sols were made with 0.8 equivalents of ammonia and the solvent was evaporated in vacuo, 3 mins. after the gel was formed. The gel was then fired at different temperatures under a flow of dry ammonia. The IR spectra of a xerogel before firing and the products fired at different temperatures (500, 700 and 1000 ^{o}C) are illustrated in Fig. 3.11.

The IR spectrum of the xerogel shows (cm^{-1}): 3391 (N-H stretch), 2810-2929 (C-H stretch), 1597 NH_2 bending, 1469 NH bending, 1373, 1196 and 1100 (C-N stretch).[15] Further, a strong Si-N peak centred on 921 cm^{-1} was observed (similar to the Si-N stretch reported by Cheng *et al.* for sol-gel derived silicon nitride powders [30]).

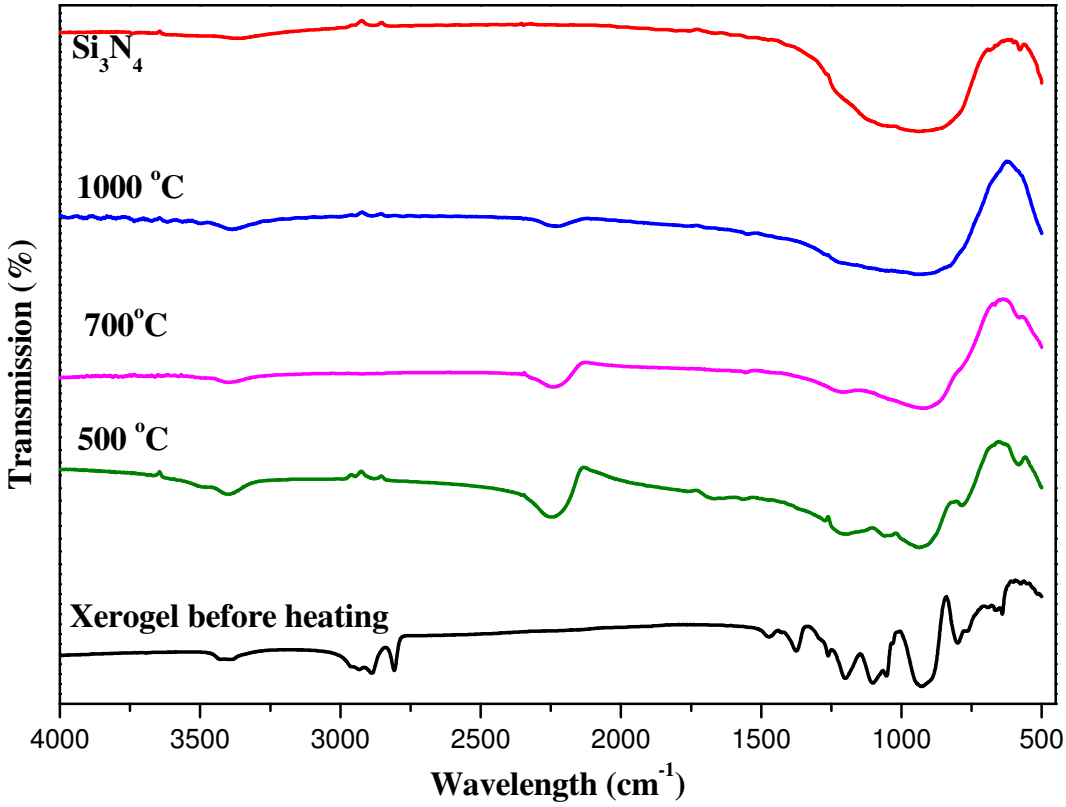

Fig. 3.11 IR spectra of 0.8 equiv. xerogel before and after annealing at 500, 700 and 1000 ^{0}C compared with commercial Si_3N_4.

The IR spectra of the residues pyrolyzed at 500 and 700 ^{o}C are similar. They show a large decrease in, and complete disappearance of, the ν(C-H) band between 2810- 2929 cm^{-1} at 500 and 700 ^{o}C respectively. A new ν(C≡N) band at 2236 cm^{-1} was formed. The intensity of this band decreased at 700 ^{o}C. The loss of the ν(C-H) suggests that most of the dimethylamino groups in the gel have been removed under these conditions. However, the appearance of a new nitrile band indicates that some of the dimethylamino groups have been pyrolysed into nitrile groups rather than being replaced by amide (NH_2) groups through reaction with ammonia. Furthermore, a weak peak appeared at around 1660 cm^{-1}, attributed to H-N-H bending, which indicates the presence of amide NH_2 groups in the solid formed at 500 ^{o}C. At 700 ^{o}C, this peak is no longer present. Hence increasing the pyrolysis temperature from 500 to 700 ^{o}C removes the amide/imide groups and minimises the intensity of the nitrile and the C≡N stretch bands.

For the material fired at 1000 ^{o}C, a considerable decrease in the ν(C≡N) band occurred and a broad band at 959 cm^{-1}, ascribed to ν(Si-N), was observed. The literature suggests that the Si-N-Si asymmetric stretch is typically centred at around 930 cm^{-1}.[41] Comparison with the IR spectrum of commercial Si_3N_4 (Aldrich, nanopowder +98 %) showed that it closely resembled that of the residue pyrolysed to 1000 ^{o}C except that the ν(C≡N) band was absent in the commercial sample.

Microanalysis also confirms the sample heated to 1000 ^{o}C to be similar to the commercial Si_3N_4 powder, Table 3.3. Si_3N_4 is resistant to oxidation at high temperature and combustion analysis can fail to give the full nitrogen content. Comparison to a standard sample suggests a composition close to Si_3N_4.

Table 3.3 Microanalysis of different fired products and commercial silicon nitride.

	Elemental Analysis after pyrolysis (%)		
	C	H	N
Pyrolysed product at 1000 ^{o}C	< 0.1	1.57	34.57
Commercial Si_3N_4	< 0.1	< 0.1	34.215

(Theoretical value for Si_3N_4: N 39.92%)

3.3.3 Film Morphologies

3.3.3.1 SEM of Films Produced by Dipping Concentrated Sols

The surface morphologies of thin films were investigated using SEM. Alumina tiles were used for dipping and slowly removed from the sol. The dipped tiles were fired at 500 and 1000 ^{o}C. A white surface with small black and faint brown spots was observed for 500 and 1000 ^{o}C respectively, which may indicate carbon contamination. Changing the rate of heating did not overcome this contamination even at higher temperature. SEM images showed that the use of concentrated sols did produce fairly continuous films, Fig. 3.12. Note that the alumina crystallites were visible through the films.

3.3.3.2 SEM of Films Produced by Dipping into the as- Prepared Sol

The as prepared 0.8 equiv. sols were used with two different dipping rates (section 3.2.5). The films were dipped as above and fired at 1000 ^{o}C. The tiles have a clear, white coloured surface. For thicker films, more dipping steps were required.

The SEM images of the two types of films, Fig. 3.13, showed a great deal of variation in the surface topography and smooth coating that was cracked during the coating process. Generally, areas with thicker coatings contained more severe cracking, whereas thinner coatings showed little or no cracking. These coatings were found to be similar in texture before and after firing, suggesting that the cracking is occurring during the pyrolysis process, probably as the solvent evaporates.

In both cases the crystalline alumina substrate is also visible, between the cracks (top) or through the thin film (bottom).

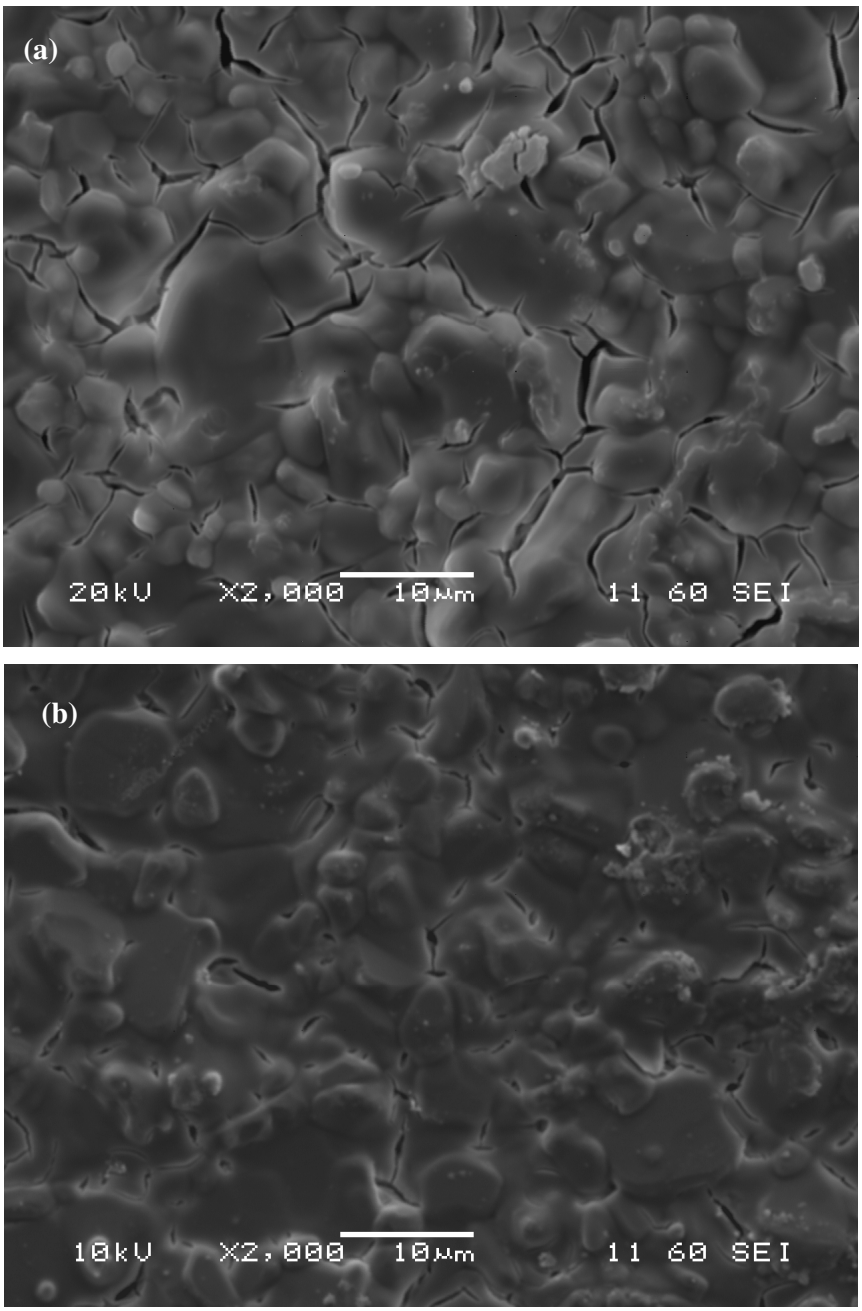

Fig. 3.12 SEM of silicon nitride films using a concentrated sol, fired at 500 ^{o}C (a) and 1000 ^{o}C(b).

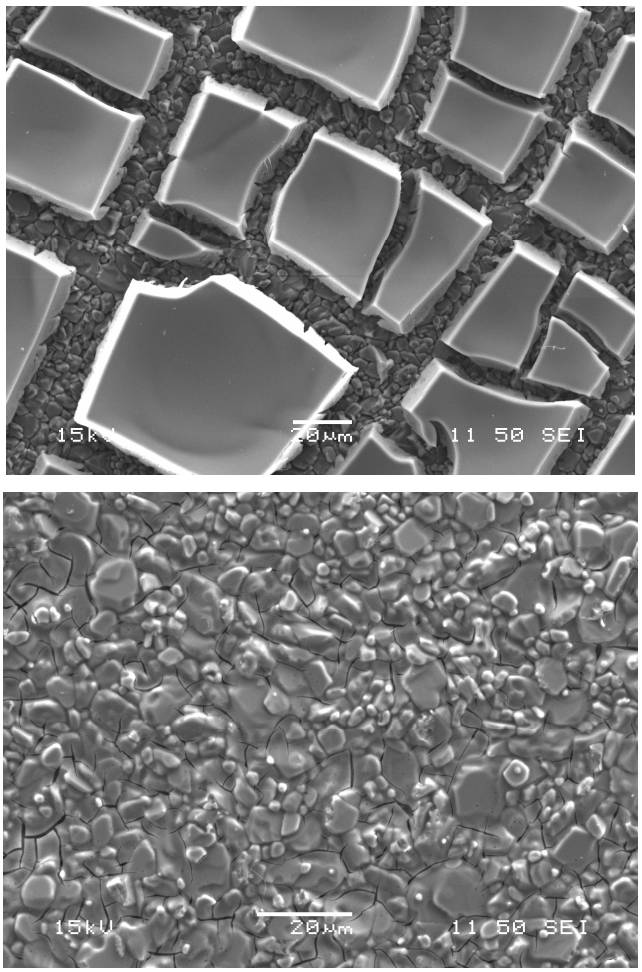

Fig. 3.13 SEM of a thick film produced by withdrawing a tile from the sol quickly (top) and a thin film from slow tile withdrawal with less severe cracking (bottom).

EDX microanalysis was performed on all of the above surfaces. For the thicker areas a strong Si signal was observed alongside a weak O signal. For the thinner areas a strong Al signal was observed alongside weak Si and O signals, Fig. 3.14. The instrument was insensitive to nitrogen due to a boron nitride detector window to the SiLi detector. Hence any presence of nitrogen within the sample was rendered invisible and thus the composition could not be resolved by this technique. Generally, elements with low atomic number (less than 8) cannot be detected. However, all the films showed weak carbon signals caused by the conductive carbon coating.

According to the above results, the as prepared sol with slow dip coating rates produced the most promising films so the work continued with these conditions.

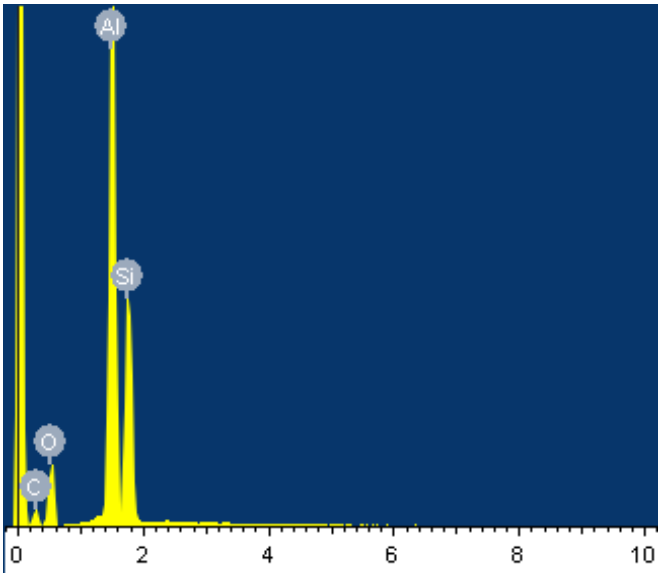

Fig. 3.14 EDX microanalysis of a thin silicon nitride film.

3.3.3.3 Variation of Substrate and Firing Temperature

3.3.3.3.a Coating of Alumina and Silica Tiles

Different substrates and annealing temperatures have been used for comparison: alumina, silica, silicon and gold-coated silicon tiles were used. Four dipping layers were formed and fired at 500, 700 and 1000 ^{o}C separately. The conditions are summarized in Table 3.4. SEM images of coated alumina and silica tiles fired at different temperatures are shown at Figs. 3.15 and 3.16 respectively. For alumina tiles, smooth thin film formation is evidenced in which the alumina structure was seen through the coating, though a little cracking was observed at higher annealing temperatures.

Films on alumina fired at 500 and 700 ^{o}C were light brown, while those fired at 1000 ^{o}C have a clear white surface. The SEM of films on silica tiles showed less cracked surfaces but surfaces were contaminated with unidentified particles of 'dust', Fig. 3.16. Coating onto silica produced better films than alumina, presumably because the tile itself is smoother or the thermal expansion is better matched.

Table 3.4 Different substrates and temperatures applied for silicon nitride thin film synthesis.

Kind of tiles	Annealing temperature	Appearance
Alumina	500 °C	Light brown surface Fig. 3.14 (a) and (b) respectively
	700 °C	
	1000 °C	Clear white surface Fig. 3.14 (c)
Silica	500 °C	Less cracking Fig. 3.15 (a) than with alumina
	1000 °C	Smooth film with some surface particles Fig. 3.17 (b)
Uncoated silicon wafer	1000 °C	Homogeneous surface, Fig. 3.16 (a)
Gold coated silicon wafer	1000 °C	Smooth surface with some particle underneath and little cracking Fig. 3.16 (b)

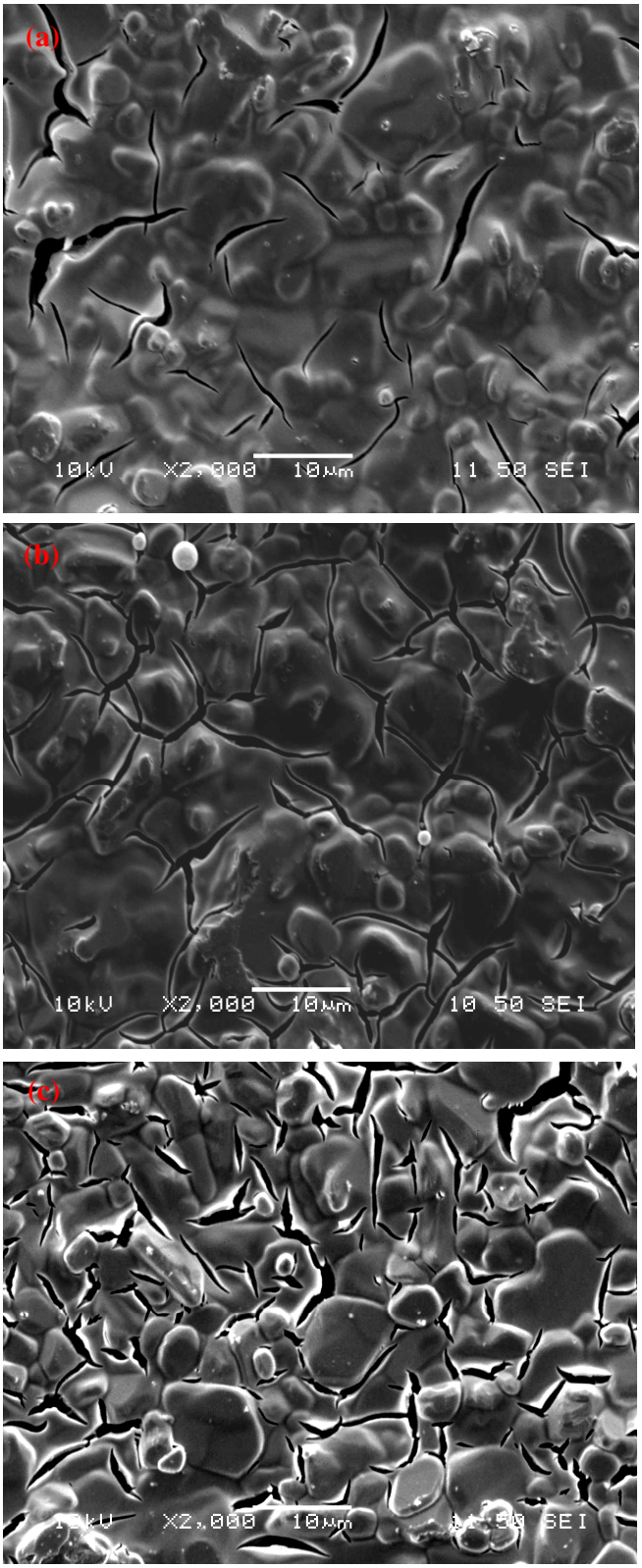

Fig. 3.15 SEM images of Si_3N_4 films on Al_2O_3 tiles fired at 500 (a), 700 (b) and 1000 ^oC (c).

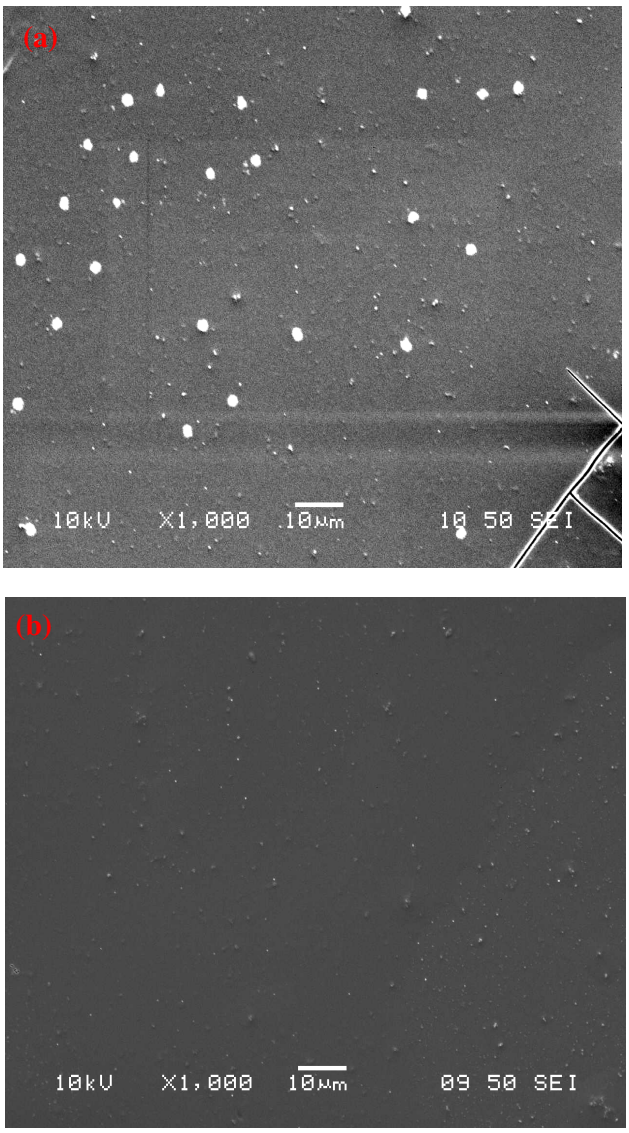

Fig. 3.16 SEM images of Si_3N_4 films on SiO_2 tiles fired at 500 (a) and 1000 ^oC (b).

3.3.3.3.b Coating of Silicon Wafers and Gold Coated Silicon

Silicon wafers and gold-coated silicon were coated in the same way as alumina and silica. Fig. 3.17 illustrates the topographies of films on those two substrates. The SEM images reveal that less cracked thin film surfaces were produced than with the oxide substrates. The uncoated silicon wafer tiles fired at 1000 ^{o}C, Fig. 3.17 (a) are promising as films are smooth and relatively crack free. Coating the silicon wafer with gold did not achieve the required goal of a completely clear, homogeneous thin film. It appears that some of the gold peeled away from the substrate at some point in the process, and cracks and bumps are observed in the SEM (Fig. 3.17 (b)).

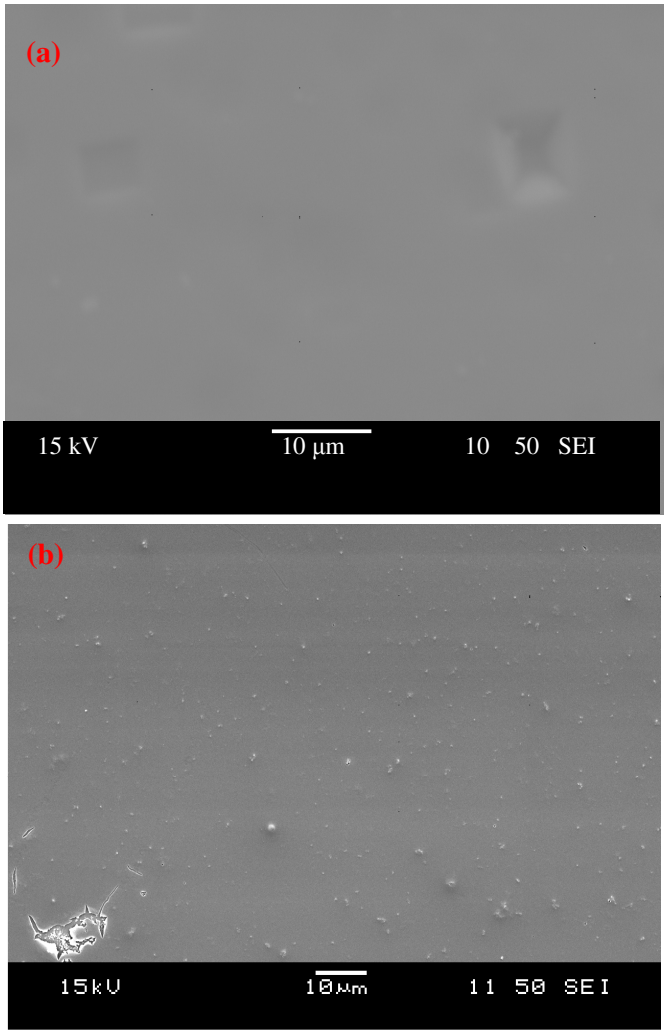

Fig. 3.17 SEM of uncoated Si wafer fired at 1000 ^{o}C (a) and gold coated Si tile fired at 1000 ^{o}C (b).

The silicon nitride films described above were dipped four times, using a slow dipping rate (section 3.2.5). To examine formation of thicker films, eight, ten and twelve dipping cycles were applied and the SEM results of these tiles are shown in Fig. 3.18. It has been observed that the more dipping cycles applied, the more severe the cracking of the films. However, for tiles dipped ten or twelve times, the regions between cracks appear as smooth films, Fig. 3.18 (b and c). This suggests that the film strength at this stage of processing is insufficient to survive thermal expansion of the substrate. It may be that the thinner films stretch to some extent. The film thickness ranged from 18 μm for eight dippings to 18.5 μm for ten dippings and 22 μm for twelve dippings.

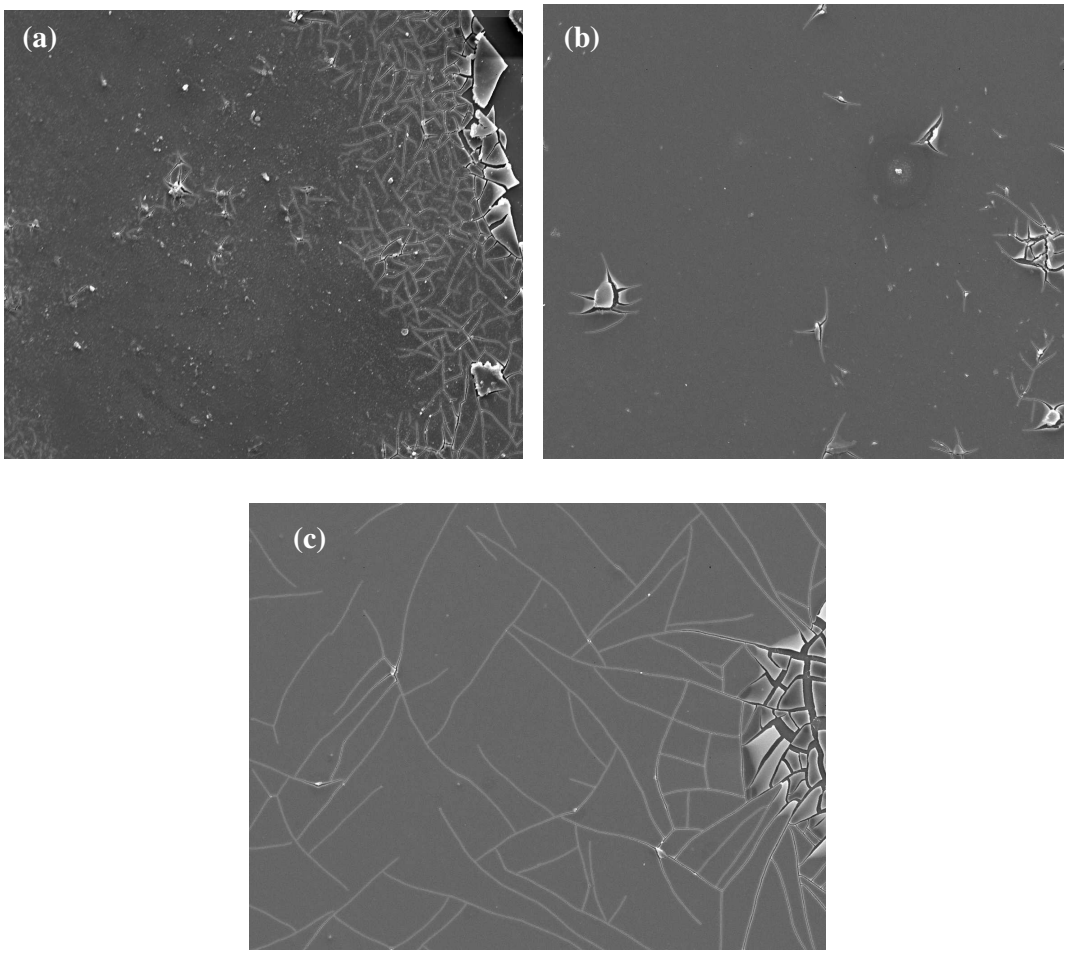

Fig. 3.18 SEM of tiles dipped eight (a), ten (b) and twelve (c) times.

3.3.4 X-ray Photoelectron Spectroscopy (XPS)

The chemical compositions of the films were examined by XPS using monochromatic Al K alpha radiation. XPS is a quantitative technique in the sense that the number of electrons recorded for a given transition is proportional to the number of atoms at the surface. Photoelectron spectra of C 1s, N 1s, O 1s and Si 2p were recorded at a take-off angle of 45^{o}. Etching of the samples was performed with a Kratos Minibeam III. Standard ion bombarding conditions: 4 keV sputter energy and 10 mA emission current producing an effective 0.5 μA current at the sample. Argon gas was used for tile etching to remove the surface and to examine the composition deeper in the films. The XPS of the numerous thin films fired at different temperatures have been examined. The tiles have been etched for 30 sec. before measurements. The calculated atomic concentrations of Si, C, N, and O at different condition of tiles and annealing temperatures are shown in Table 3.5.

3.3.4.1 Films on Alumina Tiles

The XPS spectra of a film fired at 500 ^{o}C showed high oxygen and carbon contents. The former high percentage may be due to the rapid oxidation of the silicon nitride films on exposure to air.[42] The source of carbon contamination must be the methyl groups in the silicon-containing sol since the complete substitution of these groups was no achieved. This result was confirmed from the presence of a nitrile peak in the IR spectrum. Tiles were etched for an extra 30 sec. to remove a surface oxygen layer. Although the carbon content was reduced, the silicon and nitrogen contents were also reduced. This suggested that the film thickness was not enough to allow removal of the top layer by etching. At the same time, this process did not reduce the oxygen content but a further excess of oxygen was detected and a new peak relating to aluminium was observed due to the Al_2O_3 substrate.

Increasing the firing temperature to 700 ^{o}C, resulted in the silicon and nitrogen peaks becoming a little more intense. A small increase in the nitrogen content and a decrease in carbon atom % were obtained. Raising the firing temperature increased the exposure time to ammonia (crosslinking agent) which results in much crosslinking and elimination of methyl groups as methylamine. These results were in agreement with the IR spectra and microanalysis data. However a high oxygen percentage was still observed.

Comparing the XPS spectra of the films on alumina tiles fired to 1000 ^{o}C with the other two temperatures, there were significant changes of element contents. The nitrogen and carbon contents were increased and decreased respectively. Furthermore, the silicon content increased since the oligomer molecules that contained silicon atoms have undergone condensation reaction rather than eliminating out of the film. The oxygen content was still high. There was no evidence of an aluminium peak. This was an indication of thicker or denser silicon nitride film formation. Generally, all films on alumina contained a high oxygen concentration despite careful handling.

Table 3.5 Atomic concentration (%) of elements (Si, C, N and O) in the silicon nitride films deposited onto several tiles and fired at different temperatures.

Tiles used	Annealing temperatures	Silicon	Carbon	Nitrogen	Oxygen
Alumina	500 ^{o}C	38.11	14.7	2.9	53.29
	700 ^{o}C	37.82	9.9	3.4	43.8
	1000 ^{o}C	40.61	6	10.5	39
Silica	500 ^{o}C	46.36	5.91	1.642	46.1
	700 ^{o}C	32.8	18.72	4.182	44.31
	1000 ^{o}C	40.11	13.23	8.96	37.7
Silicon wafer	700 ^{o}C	42.856	9.66	3.867	43.6
	1000 ^{o}C	52.95	3.843	30.13	13.08
Gold-coated silicon wafer	700 ^{o}C	47.47	5.7	5.32	39.3
	1000 ^{o}C	50.73	6.34	19.3	23.63

3.3.4.2 Films on Silica Tiles

A silicon nitride film on a silica tile fired at 500 ^{o}C was found to have a low nitrogen content compared to that obtained at the same temperature using an alumina tile while the silicon and oxygen percentages were high. Since the substrate is SiO_2 it is not possible to say how much of this signal comes from there. The tiles fired at 700 and 1000 ^{o}C were similar to the alumina tiles at the same temperature. However, the oxygen content at both temperatures was lower than that with alumina.

The 1000 ^{0}C firing temperature again yields the highest nitrogen content and increased the oxidation resistance.

3.3.4.3 Films on Silicon and Gold-Coated Silicon

These films were fired at 1000 ^{o}C and were handled in a vacuum suitcase. A higher nitrogen atomic percentage has been achieved with considerable reduction in carbon contamination. Furthermore, the oxygen content is decreased enormously compared with other tiles fired at the same or lower temperatures.

The XPS spectrum and the element peak positions of this silicon nitride film is shown in Fig. 3.19 and Fig 3.20 respectively. The binding energies of Si 2p and N 1s peaks were 101.1 and 397.0 eV, respectively. These signals are close to literature values, 101.8 and 397.5, for stoichiometric Si_3N_4.[36] The binding energy of Si 2p in a silicon oxynitride was 103.5 eV and the N 1s peak centred at 400.1 eV was ascribed to nitrogen present in oxynitride like network.[43] These values indicate the incorporation of oxygen in the film. These peaks were absent in the silicon nitride films so the presence of oxygen was considered to be due to surface oxidation. This was in agreement with the IR of the xerogels in which no Si-O peak could be detected.

In reactions of silica powders with ammonia to form silicon nitride it has been observed that only small amount of silicon nitride was formed in reactions below 1400 ^{o}C.[44] Consequently, the firing temperature used herein was not high enough for significant conversion of oxide, suggesting that the effect of the higher temperature was to increase the stability of the film surface to oxidation rather than replacing oxide with nitrogen. For films on gold-coated silicon fired at 700 and 1000 ^{o}C, similar results were obtained.

More oxygen was detected due to the cracking of the gold coating; the oxygen was seen through the cracks as confirmed by SEM.

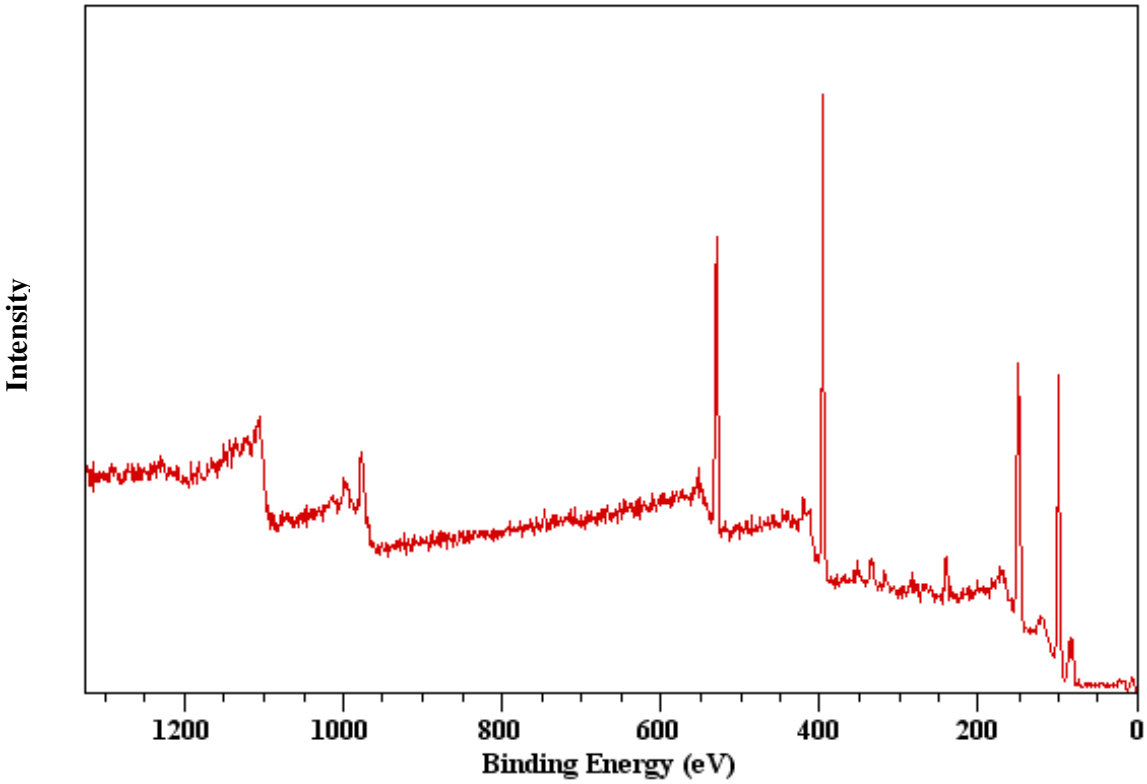

Fig. 3.19 XPS spectra of silicon nitride film on silicon wafer fired at 1000 °C

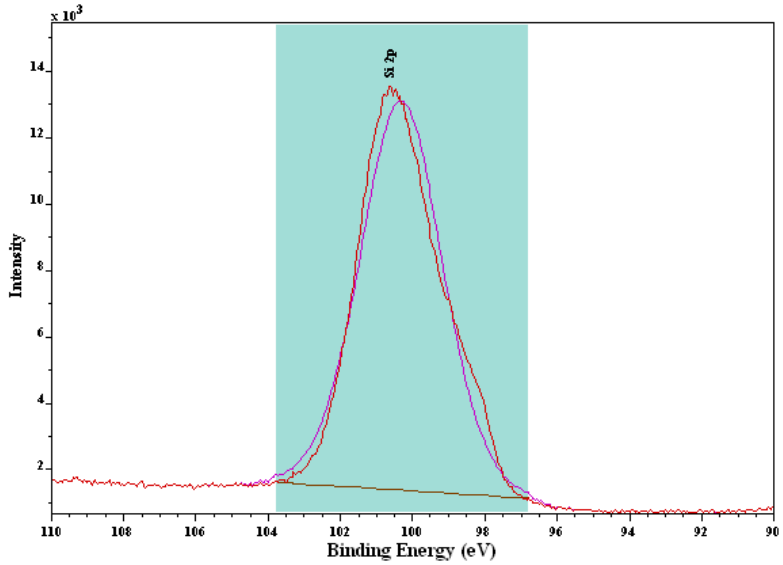

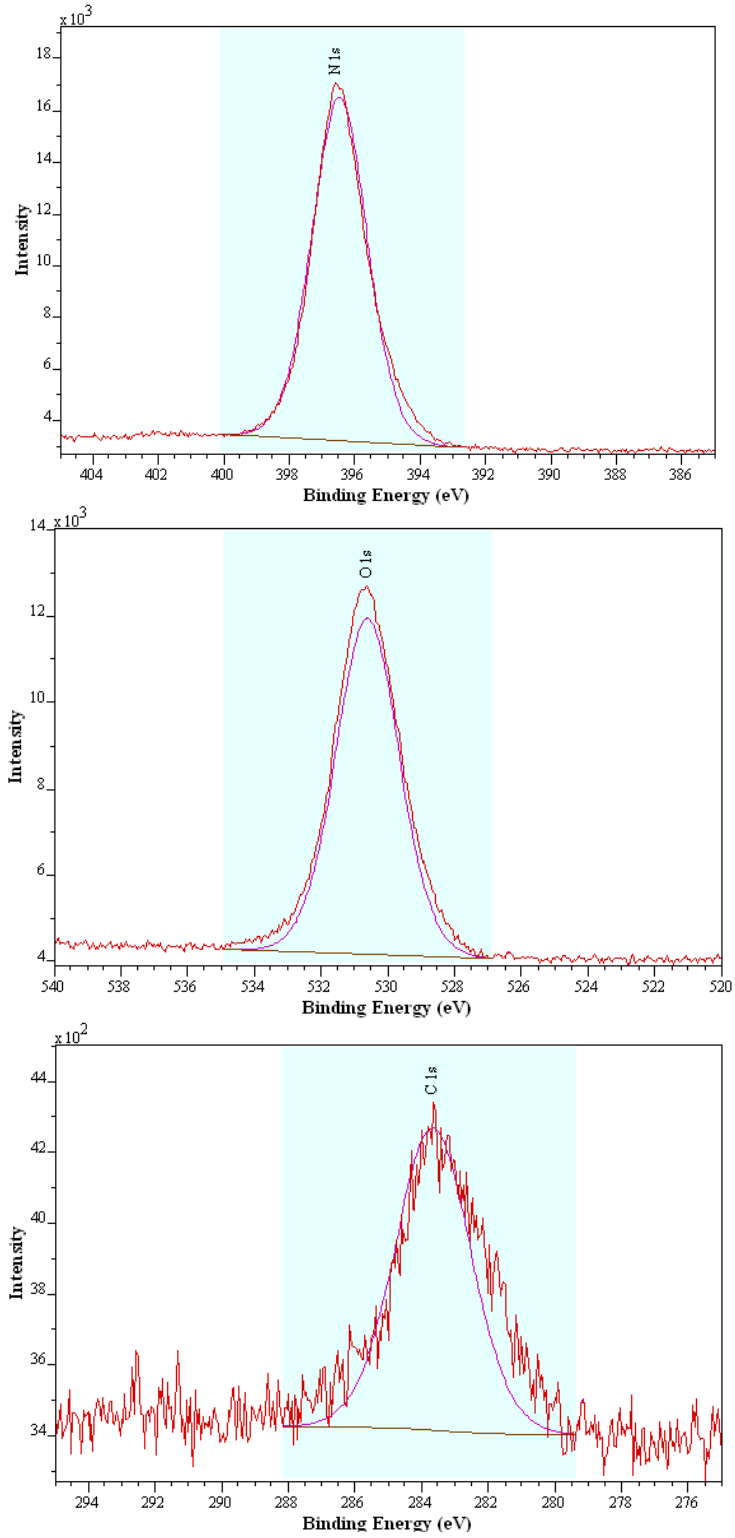

Fig. 3.20 The Si 2p, N 1s, C 1s and O 1s peak positions silicon nitride film on silicon wafer fired at 1000 ^{o}C.

3.4 Conclusions

Silicon nitride films were prepared from tetra(methylamino)silane, which was found to have an acceptable ammonolysis rate for this purpose. Triflic acid has been used to catalyse condensation, and showed a large effect on obtaining a clear and effective sol. Acid catalysed sols exhibited less loss of volatile material when samples were heated in nitrogen. Various amounts of ammonia were used to produce sols and it was found that 0.8 molar equivalents of NH_3 produced clear sols that could be used for coating.

Various substrates were used for dipping. Fast withdrawal of the substrate from the sol produced films with severe cracking once fired. Slow withdrawal of the substrate resulted in a thin layer with less cracking. Consequently for thicker layers more dipping cycles were applied. The dipped substrates were fired at 500, 700 or 1000 ^{o}C with flow of dry ammonia. Although a heating programme was applied in order to reduce the amount of carbon present, this aim was only achieved at higher temperature. Another way to get thicker films was to concentrate the sol by pumping off some solvent before using for dipping. However, this method resulted in heavy cracking of the thicker films and carbon contamination was detected even with higher firing temperatures. The least cracked films obtained were deposited on silicon wafers.

XPS showed that films deposited on Si wafers and fired at 1000 ^{o}C contained a large amount of nitrogen and little oxygen. Those deposited on oxide substrates had very high oxygen contents. All films also contained significant amounts of carbon. Higher temperature firing at 1000 ^{o}C reduced oxygen contents as analysed by XPS but did not result in oxygen-free films.

3.5. References

[1] M. Lattemann, E. Nold, S. Ulrich, H. Leiste, H. Holleck, *Surf. Coat. Technol.,* **174-175,** 2003, 365.

[2] S. K. Patra, G. Mohan Rao, *Mater. Sci. and Engin. B,* **90***,* 2002, 90.

[3] R. Hezel, K. Jaeger, *J. Electrochem. Soc.,* **136,** 1989, 518.

[4] G. C. Han, P. Luo, K. B. Li, Z. Y. Liu, Y. H. Wu, *Appl. Phys.,* **A 74,** 2002, 243.

[5] E. A. Taft, *J. Electrochem. Soc.: Solid State Science,* **118,** 1971, 1341.

[6] H. F. Sterling, R. C. G. Swann, *Solid State Electron.,* **8,** 1965, 653.

[7] V.Y. Doo, D. R. Nichols, G. A. Silvey, *J. Electrochem. Soc.,* **113,** 1966, 1279.

[8] T. Hirao, K. Setsune, M. Kitagawa, Y. Manabe, K. Wasa, S. Kohiki, *Jpn. J. Appl. Phys.,* **26,** 1987, L544.

[9] G. N. Parsons, J. H. Souk, J. Batey, *J. Appl. Phys.,* **70,** 1991, 1553.

[10] F. Stedie, I. Baumvol, W. Schreiner, F. Freire Jr., *J. Vacuum Sci. Technol.,* **A 10,** 1992, 462.

[11] I. Sugimoto, K. Yanagisawa, H. Kuwano, S. Nakano, A. Tago, *J. Vacuum Sci. Technol.,* **A 12,** 1994, 2859.

[12] G. M. Wu, J. Wang, J. Shen, *J. Phys. D Appl.,* 2002, 1301.

[13] I. M. Thomas, *Appl. Optics,* **31,** 1992, 6145.

[14] S. M. Attia, J. Wang, G. M. Wu, J. Shen, J. H. Ma, *J. Mater. Sci. Technol.,* **18,** 2002, 211.

[15] C. J. Brinker, A. J. Hurd, P. R. Schunk, G. C. Frye, C. S. Ashley, *J. Non-Cryst. Solids,* **147/148,** 1992, 424.

[16] Y. Zhang, D. Wu, Y. H. Sun, S. Y. Peng, *J. Sol-Gel Sci. Technol.,* **33,** 2005, 19.

[17] M. A. Fardad, E. M. Yeatman, E. J. C. Dawnay, Mino Green, F. Horowitz, *J. Non-Cryst. Solids,* **183,** 1995, 260.

[18] Y. Liu, W. Ren, L. Zhang, X. Yao, *Thin Solid Films,* **353,** 1999, 124.

[19] H. A. Macleod, in; Thin Optical Filters, second Ed., MacMillan, New york, 1986, p. 370.

[20] Y. Hamasaki, S. Ohkubo, K. Murakami, H. Sei, G. Nogami, *J. Electrochem. Soc.,* **141**, 1994, 660.

[21] T. Yoko, A. Yuasa, K. Kamiya, S. Sakka, *J. Electrochem. Soc.,* **138,** 1991, 2279.

[22] A. Lukowiak, R. Dylewicz, S. Patela, W. Strek, K. Maruszewski, *Optic. Mater.,* **27,** 2005, 1501.

[23] M. Houmard, D. Riassetto, F. Roussel, A. Bourgeois, G. Berthome, J. C. Joud, M. Langlet, *Surf. Sci.,* **602,** 2008, 3364.

[24] M. Houmard, D. Riassetto, F. Roussel, A. Bourgeois, G. Berthome, J. C. Joud, M. Langlet, *Appl. Surf. Sci.,* **254,** 2007, 1405.

[25] M. Langlet, A. Kim, M. Audier, C. Guillard, J. M. Hermann, *J. Mater. Sci.,* **38,** 2003, 3945.

[26] X. M. Du, R. M. Almeida, *J. Mater. Res.,* **11,** 1996, 353.

[27] X. Fu, L. A. Clark, Q. Yang, M. A. Anderson, *Environ. Sci. Technol.,* **30,** 1996, 647.

[28] G. Dagan, S. Sampath, O. Lev, *Chem. Mater.,* **7,** 1995, 446.

[29] K. R. Murali, *J. Phys. Chem. Solids,* **68,** 2007, 2293.

[30] F. Cheng, S. M. Kelly, S. Clark, J. S. Bradley, M. Baumbzch and A. Schütze, *J. Membr. Sci.,* **280**, 2006, 530.

[31] C. Balan, K. W. Völger, E. Kroke, R. Riedel, *Macromolecules*, **33**, 2000, 3404.

[32] A. W. Jackson, A. L. Hector, *J. Mater. Chem.,* **17,** 2007, 1016.

[33] A. W. Jackson, A. L. Hector, *Mater. Res. Soc. Symp.Proc.,* **848,** 2005, FF2.2.1.

[34] R.G. Gordon, D.M. Hoffman, U. Riaz, *Chem. Mater.*,**2**, 1990, 480.

[35] B. J. Aylett, L. K. Peterson, *J. Chem. Soc.,* 1964, 3429.

[36] J. Löffelholz, J. Engering, M. Jansen*, Z. Anorg. Allg. Chem*., **626**, 2000, 963.

[37] H. Andersch, M. Jansen, *Acta Cryst.,* **C46**, 1990, 1985.

[38] J. E. Drake, N. P. C. Westwood, *J. Chem. Soc.(A),***22,** 1971, 3617.

[39] F. Cheng, S. Clark, S. M. Kelly, J. S. Bradley, *J. Amer. Ceram. Soc.,* **87**, 2004, 1413.

[40] F. Cheng, S. J. Archibald, S. Clark, B. Toury, S. M. Kelly, J. S. Bradley, *Chem. Mater.,* **15,** 2003, 4651.

[41] A. L. Smith, *Spectrochim. Acta,* **16,** 1960, 87.

[42] S. I. Raider, R. Flitsch, J. A. Aboaf, W. A. Pliskin, *J. Electrochem. Soc.,* **123,** 1976, 560.

[43] P. Singh, S.M. Shivaprasad, M. Lal, M. Husain, *Solar Energy Materials & Solar Cells,* **93,** 2009, 19.

[44] A. Pawelec, B. Strojek, G. Weisbrod, S. Podsiadlo, *Ceram. Intern.,* **28,** 2002, 495.

POROUS SILICON NITRIDE MONOLITHS

4.1 Introduction

Aerogels are materials in which most of the pore structure of the gel is maintained after replacing the pore liquid by air. These 3-dimensional network materials have extraordinary properties derived from their very low density, large specific surface area, extremely high porosity monolith structures and high thermal stability.[1] These unique properties make aerogels interesting for the manufacture of catalysts, sensors and thermal or sound insulation materials. Typically sol-gel processes are applied for aerogel synthesis: first, a sponge-like gel network is formed, through a series of hydrolysis and condensation reactions. Second, a drying technique that can maintain the filigrane solid network is used. Supercritical drying is the most common method. The solvent is heated under pressure until it is in the supercritical state and then depressurised above its critical temperature directly to the gas phase so there are no liquid/gas interfaces in the pores during drying. Thus destructive surface tension effects are avoided. SiO_2 aerogels are the most studied ones. Their unique physical and chemical properties make them useful for various applications such as thermal insulators, optical materials, radiation detectors, sensors and catalyst supports. Aerogels made from other oxides,[2] carbon[3] and recently II-VI semiconductor materials[4] have been investigated.

There are few examples of nitride aerogels. Hexagonal BN aerogel monoliths have been prepared by CO_2 critical point drying of gels produced from $[(BCl)(NH)]_3$ and $[(Me_3Si)_2NH]$.[5] Ammonolysis of vanadium oxide aerogels or foams have also been shown to result in catalytically active vanadium oxynitrides that retain some of their porous structure.[6] However, high temperature ammonolysis of oxides requires forcing conditions and is not viable as a general route to nitride aerogels as either the aerogel framework will disintegrate, or the pores will close during the reaction.

The aim of this chapter is to synthesise silicon nitride aerogels using a non-oxide sol-gel route. Some of this work has been published [7] and will be discussed in detail through this chapter. One of the major sources of interest in forming aerogels of nitride materials is the possibility of using them in catalysis, since nitrides exhibit useful activities for hydroprocessing and a range of other reactions.[8]

4.2 Experimental

All experimental procedures were carried out in a controlled inert atmosphere of nitrogen gas; using either a Schlenk-line for the synthesis, or a glove-box for the handling of reagents, products and storage. Diethyl amine, the solvent used as a supercritical fluid for aerogel drying, was dried by distillation from barium oxide. The amide used (tetramethylaminosilane [$Si(NHMe)_4$] (TMAS)) was prepared and purified as described in chapter 3.

4.2.1 Preparation of Monolith Gel

Monolith gels were produced by reacting [$Si(NHMe)_4$] with two equivalents of dry NH_3. Two different high-pressure glassware sizes have been used, (18.2 mm, left, 14.8 mm, right, internal diameter) as shown in Fig. 4.1.

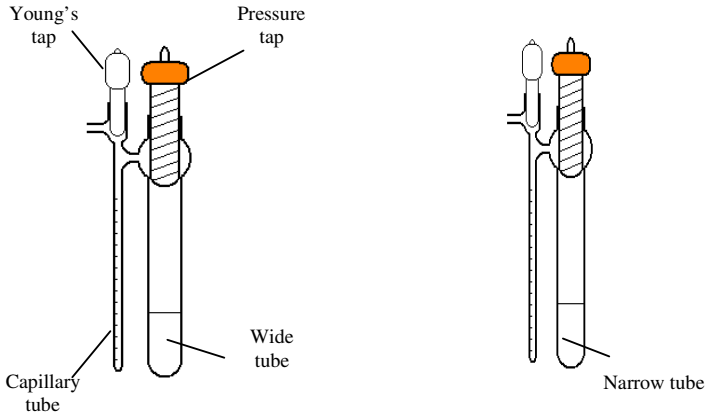

Fig. 4.1 Different glassware sized used for aerogel preparation.

2 eq.(0.16 mL) condensed ammonia was transferred to a cold (-78 ^oC) solution of TMAS (0.5 g, $3.3x10^{-3}$ mol) in 6 ml THF. The mixture was allowed to warm to room temperature overnight. Two significant observations were made. The narrow glassware size showed a white suspended solid while the wider tube contained a clear transparent sol. This suggested that the narrow tube resulted in uneven ammonolysis of the precursor due to inhomogeneous mixing. After a drop of triflic acid was added to catalyse condensation, a glass tube was inserted into the sol so that a plug of gel could be removed. The clear solution rapidly showed signs of turbidity and could maintain its

shape when the vessel was tilted after 40 min. At this point the gel was white, Fig. 4.2. No further changes in appearance were observed even over a period of 4 weeks. The effects of these two different glass sizes on the composition structure of gel 1 (using wide glassware) and gel 2 (using the narrow tube) were investigated using microanalysis, infra-red spectroscopy and thermogravimmetric analysis.

Fig. 4.2 The turbid solution after adding acid (left) and the formed gel after 40 min (right).

For drying purposes, two different methods have been applied to the formed gels. Drying at ambient pressure results in xerogels while supercritical fluid drying produces aerogels. The effect of these methods on the final product shape was compared.

4.2.2 Supercritical Extraction of THF

Supercritical CO_2 is the commonest supercritical fluid used in aerogel preparation, but due to concerns about reactivity with these gels diethylamine Et_2NH has been employed here. First, diethylamine was saturated with dry ammonia for 30 min. The sample to be dried was loaded into a steel reactor tube in the glove box. The back pressure regulator was set to the required pressure, the pump rate required (2 ml/min) was set on the HPLC pump and the system was flushed with supercritical ammonia/ diethylamine solution at 300 °C and 80 bar pressure for one hour, followed by controlled depressurization of the system to 5 bar over a period of 60 mins. The system was then flushed with nitrogen to

remove the solvent vapour before cooling under nitrogen flow to room temperature. The apparatus used for supercritical fluid drying is shown in Fig. 4.3. The formed aerogels were stored in the glove box for further characterization. These experiments were performed with Jason. S. Hyde (Physics Department, Southampton University).

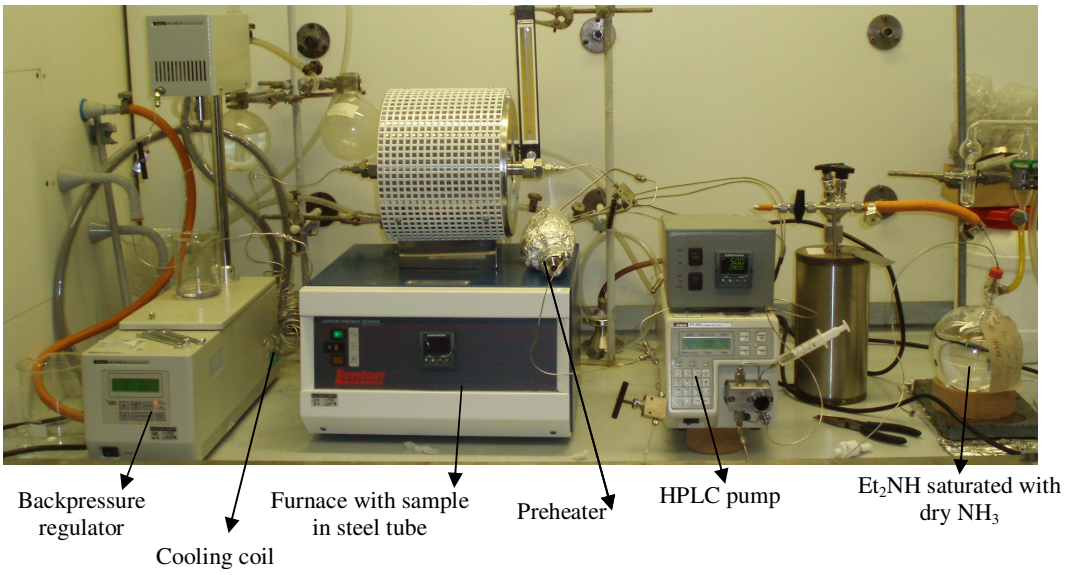

Fig. 4.3 Supercritical fluid drying system.

4.2.3 Bomb Drying

The same supercritical fluid drying principle has been applied using a Parr 7470 autoclave with a silica-tube lining. This was rigorously dried before use by heating at 100 ^{o}C under vacuum in an oil bath for 24 hours. The bomb was then backfilled with nitrogen via the Schlenk-line, sealed and transferred to the glove box.

The silica liner was removed from the bomb, the glass tube containing a plug of gel prepared using wide glassware tube (gel 1) was placed inside and then was covered with 20 ml of diethylamine saturated with ammonia, Fig. 4.4. This was then placed back inside the main body of the bomb and the apparatus was reconstructed.

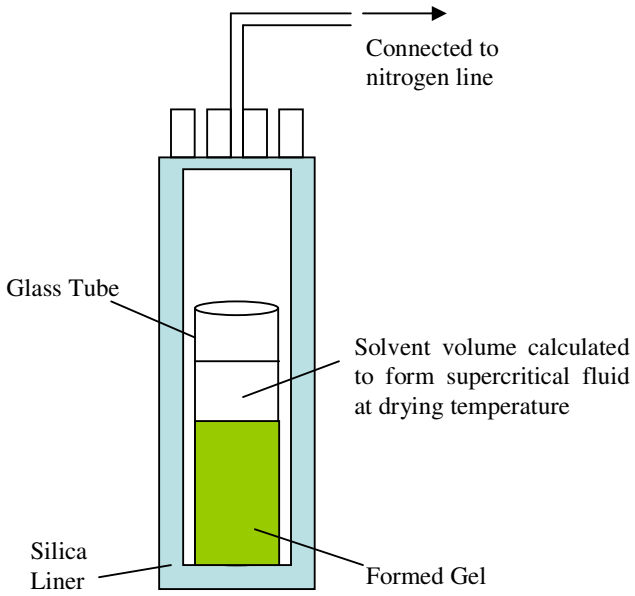

Fig. 4.4 Bomb apparatus used for supercritical drying of gel.

The head unit of the bomb was screwed hand-tight onto the main body and all valves were shut. The apparatus was then removed from the glovebox and, using a torque-wrench, the bolts on the head-unit were tightened.

The bomb was placed into a heater and adjusted above the critical temperature of diethylamine (300 ^{o}C). Once the temperature was reached, the bomb was left for one hour to equilibrate. The fluid was removed by gradual opening of the bomb inlet/outlet valve that was connected to the nitrogen Schlenk-line via a trap filled with dry ice and acetone allowing the excess pressure to be released and the diethylamine to evaporate.

4.2.4 Ambient Pressure

To obtain a xerogel, the same steps were followed to form the wet gel, which was dried by pumping off the solvent and the resultant solid was pyrolysed under a flow of ammonia in a furnace tube. The ammonia used here was passed through a column of molecular sieves to minimise its moisture content. The samples were placed under the flow of ammonia for 15 minutes before beginning the heating program. The samples were

heated to 300 °C at a rate of 5 °C per minute and then were held at this temperature for 2 hours before allowing to cool down to room temperature. The resultant solids were mainly brown in colour. This suggested the presence of carbon.

The resulting xerogel and aerogels were characterized using infrared spectroscopy (IR), microanalysis, scanning electron microscopy (SEM), transmission electron microscopy (TEM), ^{29}Si solid state MAS-NMR, Themogravimetric analysis (TGA), powder X-ray diffraction (XRD) and nitrogen adsorption/desorption analysis.

Solid-state NMR data were collected using Varian Unity Inova spectrometer operating at 59.56 MHz for ^{29}Si, Durham University and the spectral referencing is with respect to tetramethylsilane.

For surface area measurements, nitrogen adsorption isotherms were obtained at 77 K using a Micromeritics Gemini 2375 instrument and surface area measurements were determined from BET analysis. For aerogel 1, the sample was sent to MCA Services, Meldreth, Cambs for BET analysis using the same instrument type.

4.3 Results and Discussion

4.3.1 Compositional Studies of Synthesised Gels

Microanalysis, IR spectra and TGA data were recorded for both gel 1, prepared using the wide glassware and gel 2, obtained using the narrow tube, after pumping off solvent under vacuum. Microanalysis of gel 1 and 2 is shown in Table 4.1.

Table 4.1 Elemental analysis of different gels before firing.

Synthesized	Elemental Analysis before pyrolysis (%)		
	C	H	N
Gel 1	11.56	4.69	23.23
Gel 2	11.76	4.4	19.49

The gels showed very similar elemental analysis for carbon and hydrogen with 4% more nitrogen in gel 1. The only plausible explanation for the increased N content in gel 1 is the larger surface area with the wide glassware that may enhance the ammonolysis reaction.

IR spectra of gels 1 and 2 showed $\nu_{C\text{-}H}$ (~2900 cm^{-1}) and a broad $\nu_{N\text{-}H}$ (~3400 cm^{-1}) feature plus two further bands at ~900 and ~1200 cm^{-1} corresponding to $\nu_{Si\text{-}N}$. Generally, the spectra are similar to those observed for $[Si(NH)_x(NH_2)_y(NMe_2)_z]$ gels and the differences can be explained by the presence of NHMe groups rather than NMe_2.[9]

TGA under nitrogen showed a stepped mass loss of ~30% and ~40% by 400 °C for gel 1 and 2, respectively, followed by a gradual loss of a further 10% by 900 °C. These features correspond to rapid initial condensation with loss of any small, volatile oligomers, $MeNH_2$ and NH_3, followed by slower condensation as the polymeric xerogel becomes a rigid ceramic.[10] The lower mass loss of gel 1 shows that more condensation occures in this gel than in gel 2, again this can be related to the better availability of ammonia in the solutions/sols.

The xerogel and the different two aerogels obtained from the aforementioned reaction method were analysed using IR, TGA, microanalysis, PXD and ^{29}Si MAS-NMR. The product topographies were characterised using SEM and TEM.

The effect of different drying methods on the volume change of the final product is illustrated in Fig. 4.5. Slow drying of gels under nitrogen at ambient pressure resulted in massive shrinkage of the monolith body to around 10% of its original dimensions. However, flushing with supercritical diethylamine at 300 ^{o}C and 8 MPa pressure followed by controlled depressurisation yielded aerogel monoliths with very little dimensional change (approx. 2 mm shrinkage in the length of a 30 mm sample). For the bomb-dried aerogel the shrinkage of sample length was a little more than that of the flow-dried aerogel (approx. 4.5 mm dimensional change in the same length sample).

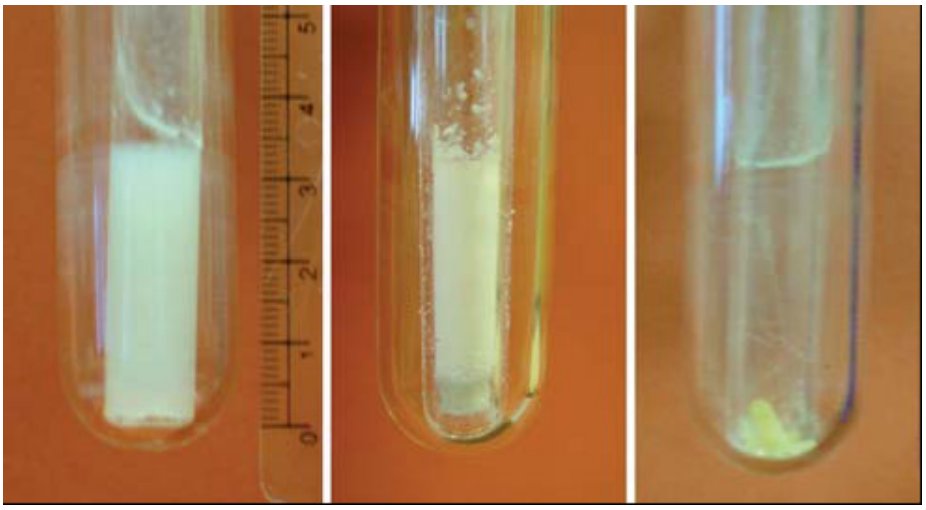

Fig. 4.5 Photographs of a wet gel (left), a SCF dried aerogel (centre) and a xerogel dried at ambient temperature under dry nitrogen (right).

4.3.2 Compositional Studies of Aerogels and Xerogel

4.3.2.1 Infrared Spectroscopy and Microanalysis

IR spectra of the xerogel and aerogels are shown in Fig. 4.6. All gels had been prepared using the same wide glassware tube except aerogel 2 that used narrow glassware tube. The IR spectra of aerogels 1 and 2 were similar but with different peaks intensities. Two characteristic peaks centered at 925 and 1200 cm^{-1}, assigned to ν_{Si-N}, were observed in both aerogels. Aerogel 1 has a peak at 3365 cm^{-1} which is attributed to ν_{N-H} with a weak shoulder at 3470 cm^{-1} corresponding to ν_{NH2}, ν_{C-H} at 2960-2800 cm^{-1} and δ_{NH2} at 1545 cm^{-1}. For aerogel 2, the broad band of the ν_{N-H} and the low intensity of the δ_{NH2} may due to presence of NH groups with different environments such as Si-NH-Si and $SiNH_2$. This is similar to powdered gels pyrolysed under nitrogen at the same temperature except that no $\nu_{C\equiv N}$ stretch due to pyrolysis of amide groups (~2250 cm^{-1}) was observed.[11] For the bomb-prepared aerogel, a small peak at 2265 cm^{-1} attributed to $\nu_{C\equiv N}$ was observed and a higher intensity at 1374 cm^{-1} that could be due to C-N stretch were also present presumably due to pyrolysis of amide groups. These different environments of carbon were confirmed with microanalysis.

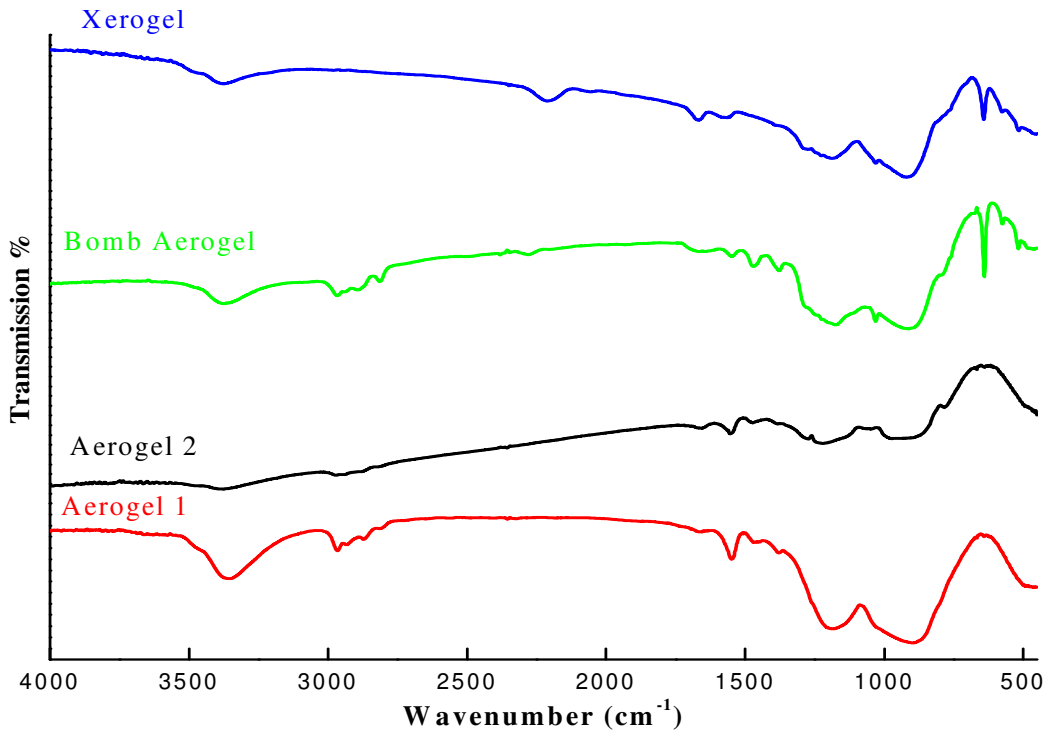

Fig. 4.6 IR spectra of silicon imidonitride aerogels and xerogel.

The IR spectrum of the xerogel pyrolysed at 300 °C under NH_3 closely resembled those of the aerogels except that the $\nu_{C\text{-}H}$ bands were absent and a $\nu_{C\equiv N}$ peak was observed at 2230 cm^{-1} suggesting that organic substituent groups had decomposed under these conditions.

Microanalysis (C, H, N) of the pyrolysed products is shown in Table 4.2.

Table 4.2 Microanalysis of different gels after pyrolysis.

Product to be pyrolysed	Elemental Analysis after pyrolysis (%)		
	C	H	N
Xerogel pyrolysed at 300°C	3.58	2.46	19.32
Aerogel 1	8.47	4.59	35.3
Aerogel 2	6.13	3.54	26.43
Aerogel bomb	17.455	5.73	27.85

The microanalysis showed that the N percentage of the xerogel was low compared to the aerogels and aerogel 1 had higher nitrogen content than the others. Although the bomb dried aerogel was prepared using the same glassware size as used for aerogel 1,

the microanalysis results showed that the former had nearly the same nitrogen content as that of aerogel 2 but with more significant carbon and hydrogen contents. Theoretically, Si_3N_4 contains 40% N but these gels contain NH, NH_2 and NHMe groups, so the expected nitrogen content should be higher. It can be difficult to obtain good nitrogen analysis because Si_3N_4 has good oxidation resistance. This was tested with a commercial Si_3N_4 sample (Aldrich, <50 nm particle size), which showed nitrogen content of 35%.

4.3.2.2 Thermogravimetric Analysis

The thermogravimetric analysis under N_2 of various gels pyrolysed at different conditions is shown in Fig. 4.7. Aerogels 1 & 2, and the bomb dried aerogel have the same trend but with different mass losses compared with the xerogel. For aerogel 1, the TGA under nitrogen showed a mass loss of around 16% between 400 and 600 °C giving some indication of the proportion of the mass due to condensable groups. The mass loss of aerogel 2 was around 30% between 400 and 700 °C, suggesting a larger number of unreacted methylamide groups, followed by a further gradual loss of ~12% up to 900 °C. The TGA trend of the bomb dried aerogel was similar to that of aerogel 2 but the mass loss starts earlier at 155 °C. By 700 °C the mass is around 67 % of its original value which was attributed to loss of the volatile byproducts $MeNH_2$ and NH_3 of condensation, the presence of which explains the high C and H contents. Generally mass loss over 500 °C is due to further condensation of amide/imide groups and the elimination of NH_3.

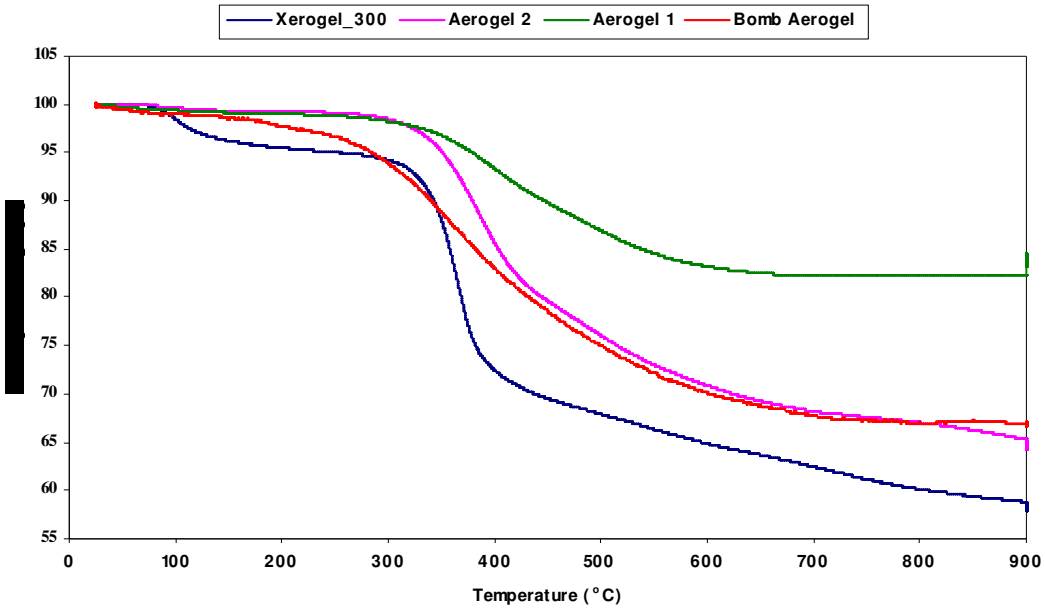

Fig. 4.7 Thermogravemitric analyses of aerogel 1, aerogel 2, bomb aerogel and xerogel.

The trend lines of the aerogels were similar to those of silicon diimide gels[11] in which dimethyl amine and ammonia were the principle gases evolved below 700 °C because of the elimination of the $–NMe_2$ and $–NH_x$ groups present in the gel due to further condensation reaction during heating.

For the xerogel, TGA under nitrogen showed a different trend. The mass loss takes place in two district steps rather than one. The first starts at 120 °C with mass loss around ~5% which was probably due to loss of adsorbed ammonia, since the sample was cooled under ammonia flow. The second mass loss of 29% occurred between 350 and 700 °C followed by a further gradual loss of ~12% up to 900 °C. This was a similar profile to the gel itself but with smaller mass losses. Powder X-ray diffraction showed that aerogels and the xerogel were amorphous.

Overall according to the TGA results, all the products showed the presence of residual methylamino groups that suggest that the transamination reactions were not yet 100% complete at the time rigid gel formation.

4.3.2.3 ^{29}Si MAS-NMR Spectroscopy

^{29}Si MAS-NMR is a powerful method to structurally characterise silicon compounds.[12] The ^{29}Si MAS-NMR of the aerogels and xerogel are illustrated in Fig. 4.8. Aerogel 2 and 1 showed a broad resonance centred near -40 ppm for aerogel 2 (Fig. 4.8, a) and at -41 ppm for aerogel 1 (Fig. 4.8 b). Crystalline Si_3N_4 has signals at -47 to -49 ppm [13] but a broad resonance at -41 ppm has previously been observed in gel derived silicon imidonitride samples and ascribed to SiN_4 tetrahedra containing a significant number of amide/imide groups which produced Si_3N_4 when pyrolysed at higher temperature.[11]

The xerogel showed a similar resonance to that of the aerogel at -43 ppm, with weaker peaks at around -50, -69 and -90 ppm. These resemble signals seen in oximide gels and attributed to SiN_3O, SiN_2O_2 and $SiNO_3$ groups.[14] From the relative intensity of these different four peaks the N: O ratio can be estimated. Simply, the percent of nitrogen and oxygen atoms at each peak is calculated separately by multiplying the number of each atom by the area of that peak. For example, peak of SiN_3O group has three N and 1 O atom, the amount of N and O at this peak is 3 and 1 times the peak area (0.2) respectively. The whole amount of nitrogen and oxygen in these environments is obtained by sum their individual values separately (3.5 and 0.46). Then the estimated N: O ratio is obtained by divided this sum value of N and O individually by that of N and O together (3.5/3.96: 0.46/3.96 = 0.88: 0.12). The ammonia used for the pyrolysis was dried over a column of molecular sieves and this data shows how moisture sensitive the gels are during heating. The lack of these resonances in the NMR spectra of the aerogels demonstrates that these contain very low levels of oxygen.

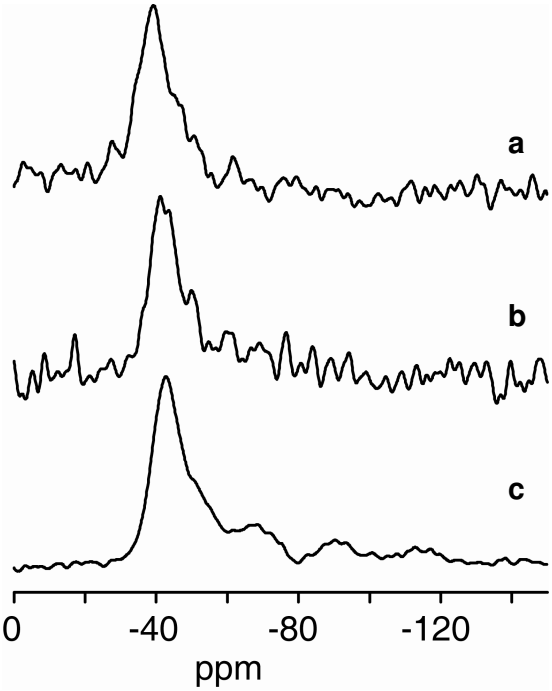

Fig. 4.8 ^{29}Si MAS-NMR spectra of three silicon imidonitride samples prepared under different conditions: An aerogel 2(a), aerogel 1(b) and a xerogel heated at 300 °C under NH_3 (c).

4.3.3 Surface Measurements

The adsorption isotherm is the first important source of information about surface area and porosity that can be obtained from a physisorption experiment. The full isotherm of aerogel 1 is illustrated in Fig. 4.9. The physisorption experiment showed that the aerogel displays a type II nitrogen adsorption isotherm typical of macroporous material with a narrow pore-size distribution and a BET (Brunauer, Emmett and Teller) surface area of 833 m^2/g. This has been confirmed with the pore size distribution measurements that pores in the macroporous size range predominate and most are around 80 nm, Fig. 4.10(a). For the bomb dried aerogel the type II N_2 adsorption-desorption isotherm revealed a macroporous material and the BET surface area was calculated as 760 m^2/g. The pore-size distribution was centred on 103 nm, Fig. 4.10(b). This increase of the pore size diameter can be linked to the surface area reduction.

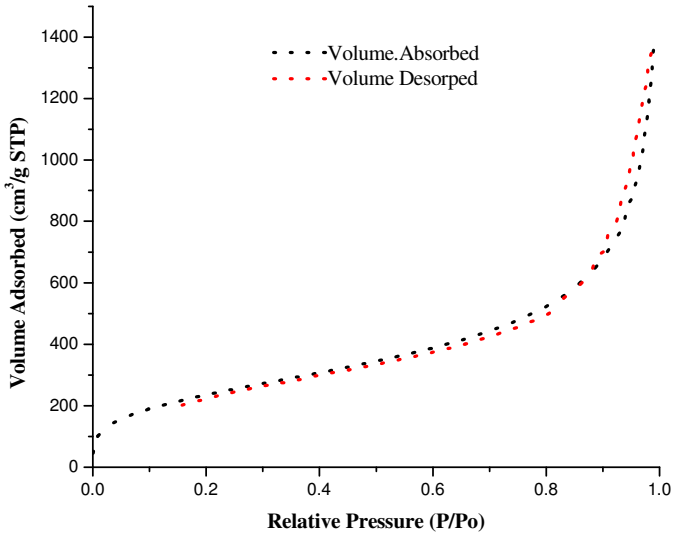

Fig. 4.9 Nitrogen physisorption isotherm of aerogel 1.

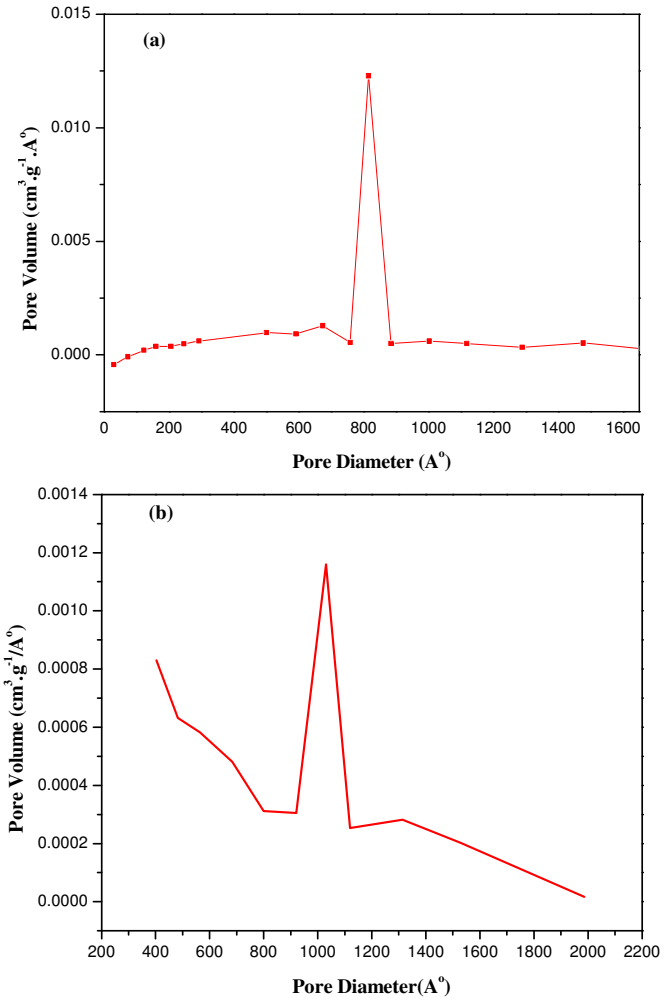

Fig. 4.10 Pore size distribution of aerogel 1(a) and bomb prepared aerogel (b).

4.3.4 Morphology of the Xerogel and Aerogel

The SEM images of the products are shown in Fig. 4.11. At low magnification there is no obvious porous structure in the xerogel or aerogels. The SEM of aerogel 1 in Fig. 4.11(c) showed sheer faces where the fragment studied had been fractured from the monolith body. At higher magnification the porous surface morphology was clearly observed for the aerogels. For the xerogel product at the same magnification (Fig. 4.11b), a porous structure was observed but with fewer pores and larger grains.

TEM of aerogel 1 showed a network of small pores separated by thin walls, Fig. 4.12 (a, b) with large (~80 nm) pores running through this random structure. The large pores were in good agreement with the macropore diameter of 80 nm as estimated from nitrogen adsorption. EDX showed strong silicon and nitrogen signals plus some oxygen (since samples were handled in air prior to analysis). For the bomb dried aerogel, TEM images, Fig. 4.12(c, d), showed a similar structure but with the presence of thicker walls and larger particles. No such network structure was found in xerogels heated under NH_3 at 300 °C. These results show a very close relationship between the nitrogen adsorption, SEM and TEM data.

Silica aerogels have been made by a sol-gel technique and dried using supercritical ethanol.[15] The temperature used was not stated but the critical temperature of ethanol is 245 °C. SEM photographs showed some pores in the silica aerogel with pore size 20-80 nm. The specific surface area was measured as 470 m^2/g. The supercritical drying technique was applied after several days of alcogel (the gel with alcohol instead of water as the dispersion medium) aging. The structures obtained in silica closely resemble those observed here.

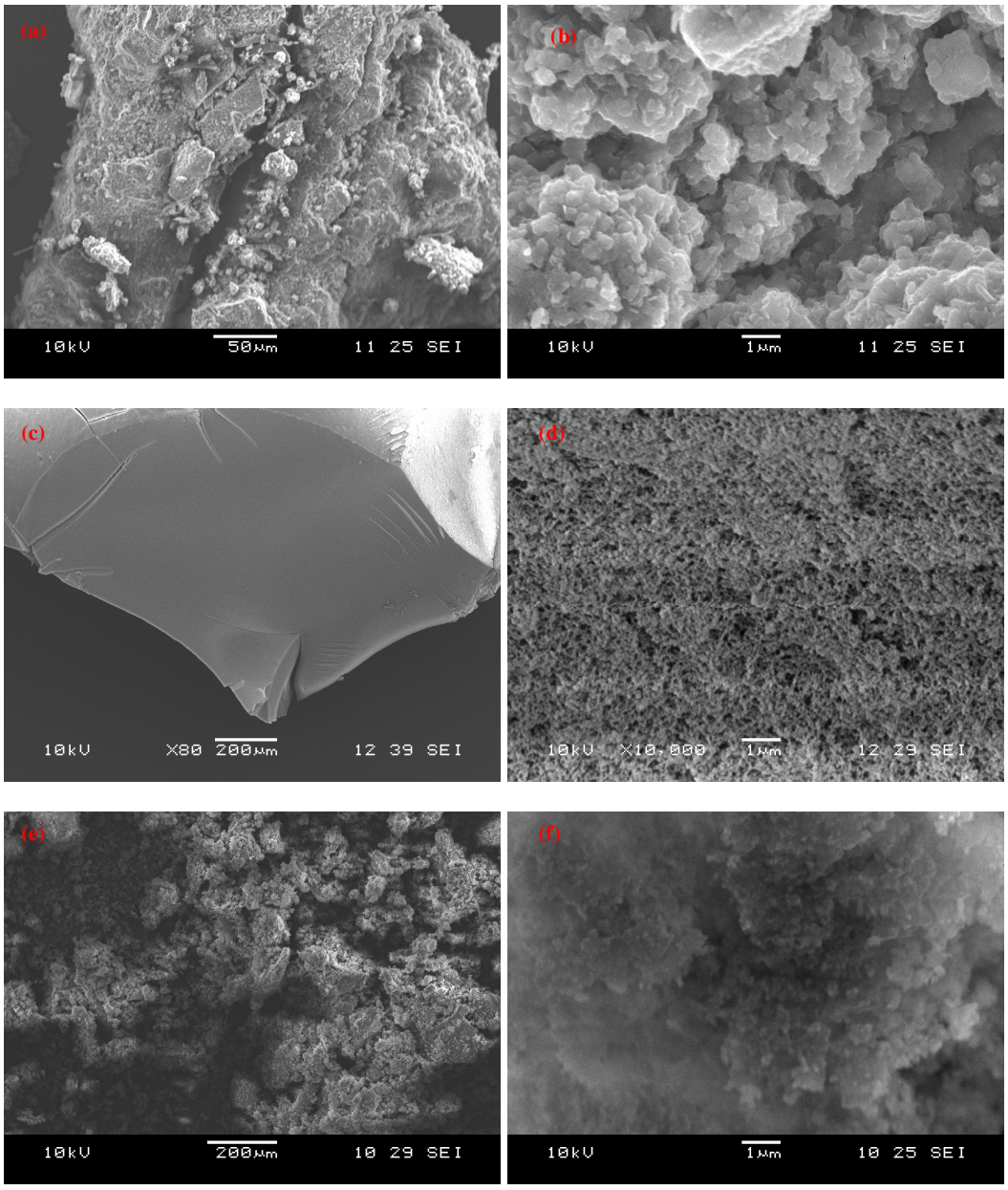

Fig 4.11 SEM of xerogel (a,b), aerogel (c,d) and bomb aerogel (e,f) at low and high magnification.

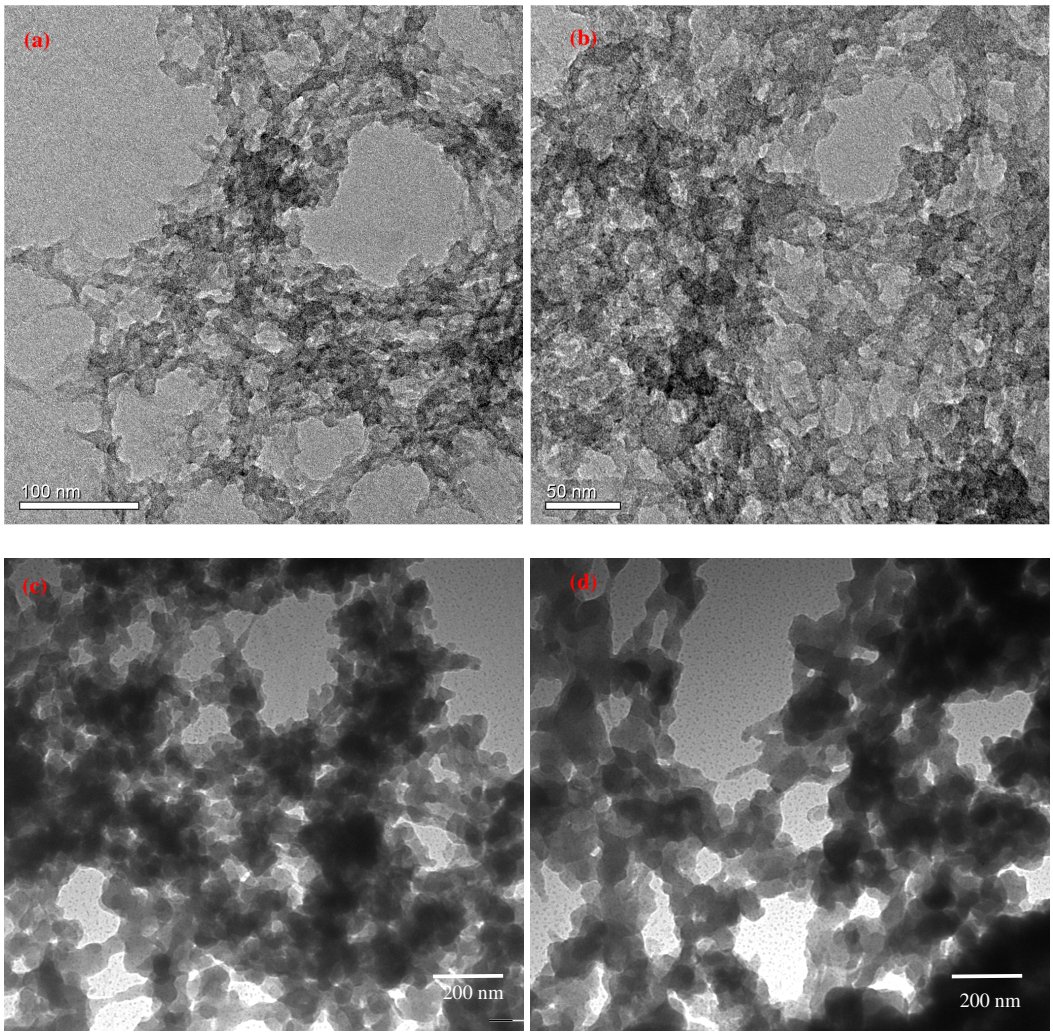

Fig. 4.12 TEM of aerogel 1 (a,b) and bomb aerogel (c,d).

4.4 Conclusions

Silicon nitride aerogels have been prepared using a sol-gel method followed by supercritical drying. Two equivalents of dry ammonia were reacted with a TMAS solution in THF. After overnight reaction the sol was acidified and left for 40 mins to form a translucent gel. The width of the glassware showed an effect on the sol appearance and on the final gel formation. Drying techniques such as supercritical fluid drying, autoclave drying and heating the gel directly under flow of ammonia have been applied separately. The effects of these methods on the final composition, surface area, pore size distribution and morphologies were studied using infrared spectroscopy, elemental microanalysis, thermogravimetric analysis, nitrogen adsorption measurements, scanning electron microscopy and transmission electron microscopy.

High nitrogen percentage gels were formed using supercritical fluid drying. This aerogel showed a high surface area and the full nitrogen isotherm revealed the aerogel to be type II macroporous with a pore size range from around 65 to 130 nm. The surface morphology demonstrates an open porous structure that was confirmed with TEM in which a network structure with pores connected together through thin walls has been achieved.

An attempt to prepare the same aerogel using bomb apparatus was successful in terms of high surface area products and similar pore network; however more shrinkage and high carbon and hydrogen content were detected in the product. Ambient pressure drying under flow of ammonia destroyed the porosity.

4.5 References

[1] N. Hüsing, U. Schubert, *Angew. Chem. Int. Ed.,* **37,** 1998, 22.

[2] A. M. Orlovic, D. T. Janackovic and D. U. Skala, Aerogels in Catalysis, in *New Developments in Catalysis Research*, ed. L. P. Bevy, Nova Science Publishers, Hauppauge NY, 2005. Ch. 2

[3] C. Moreno-Castilla and F. J. Maldonado-Hódar, *Carbon*, **43**, 2005, 455.

[4] S. L. Brock, I. U. Arachchige, K. K. Kalebaila, *Comments Inorg. Chem.,* **27,** 2006, 103; Y. P. Geo, C. N. Sisk, L. J. Hope-Weeks, *Chem. Mater.,* **19,** 2007, 6007.

[5] R. T. Paine and C. K. Narula, *Chem. Rev.,* **90**, 1990, 73.

[6] O. Merdrignac-Conanec, K. El Badraoui and P. L'Haridon, *J. Solid State Chem.*, **178**, 2005, 218; P. Krawiec, P. L. de Cola, R. Gläser, J. Weitkamp, C. Wiedenthaler and S. Kaskel, *Adv. Mater.*, **18**,2006, 505.

[7] S. Hassan, A. L. Hector, J. R. Hyde, A. Kalaji, and D. C. Smith, *Chem. Commun.,* 2008, 5304.

[8] J. S. J. Hargreaves and D. Mckay, *Catalysis, Specialist Periodical Report*, RSC, London, 2006, **19**, 84; E. Furimsky, *Appl. Catal. A*, **240**, 2003, 1.

[9] F. Cheng, S. M. Kelly, S. Clark, J. S. Bradley, M. Baumbach, A. Schütze, *J. Membr. Sci.,* **280,** 2006, 530.

[10] O. Vollmer, F. Lefebvre, J. S. Bradly, *J. Molec. Catal. A: Chemical,* **146,** 1999, 87.

[11] F. Cheng, S. Clark, S. M. Kelly, J. S. Bradley, *J. Amer. Ceram. Soc.,* **87**, 2004, 1413.

[12] G. Engelhardt, H. Koller< NMR Basic Principles and Progress, vol. **31**, Springer, Berlin, 1994, p.1.

[13] K. R. Carduner, C. S. Blackwell, W. B. Hammond, F. Reidlinger, G. R. Hatfield, *J. Am. Chem. Soc*., **112**, 1990, 4676.

[14] F. Cheng, S. M. Kelly, F. Lefebvre, S. Clark, R. Supplit, J. S. Bradley, *J. Mater. Chem*., **15**, 2005, 772.

[15] Z. Deng, J. Wang, J. Wei, J. Shen, B. Zhou, L. Chen, *J. Sol-Gel Scien. Techn.,* **19**, 2000, 677.

SILICON NITRIDE ORDERED MACROPOROUS MATERIALS

5.1 Introduction

Ordered macroporous materials may be formed either as two-dimensional films or three-dimensional bulk structures. The commonest ordered macroporous structures are inverse opals. They have received considerable attention due to their periodic structures that can interact with light, uniform pore sizes that are large enough to allow liquids to diffuse readily, and high specific surface areas. These materials have been utilised in photonic band gap materials,[1] battery electrodes,[2] gas sensors,[3] optoelectronic devices,[4] catalysis,[5,6] membranes[7,8] and biomaterials.[9]

Arrays of close-packed spheres (typically silica or polystyrene) are used as the templates.[10] For these material syntheses the void space between the spheres is infiltrated with precursors to the target material. Upon removal of the template spheres (by thermal processing, solvent extraction, or chemical etching), ordered macroporous structures are obtained.

Until now, attention has been focussed mainly on ceramic structures of binary oxides such as SiO_2, TiO_2, Al_2O_3, ZrO_2,[11,12] and ternary transition/main-group metal oxides,[13] as well as metals[14] and organic polymers,[8,15] semiconductors,[16] and carbon.[2] However, there are only a few examples of templated porous nitride materials. Inverse opals of WN [17] and Ta_3N_5 [18] have been produced by atomic layer deposition (ALD) through a silica template. This method was found suitable for making Ta_3N_5 with a photonic band gap at optical wavelengths. While ALD yields extremely high quality materials, it is expensive, time-consuming and not suitable for yielding bulk structures. High-quality photonic crystals of GaN have been prepared by opal-SiO_2 templating with Ga_2O_3 followed by annealing in an atmosphere of nitrogen hydrides.[19] Ordered macroporous SiCN has been formed by templating silica spheres with a preceramic precursor, polysilazane.[6] The material obtained is promising as a catalyst support for high-temperature fuel reforming because of its surface geometry and good stability up to 1200 ^{o}C. High-surface-area mesoporous boron nitride was synthesized by nanocasting mesoporous carbon with a molecular boron nitride precursor.[20]

There is a clear need to develop routes to other nitride materials, as their properties vary significantly from those of oxides and new macroporous metallic, semiconductor or insulator nitride compositions will be of significant interest. Very recently Fischer *et al*.,[21] demonstrated some progress in this by infiltrating a template of 60 nm silica spheres with molten cyanamide and pyrolyzed to make a macroporous graphitic C_3N_4 powder. After dissolution of the SiO_2 spheres, $TiCl_4$ and ethanol were infiltrated and samples were fired under N_2 at 800 ^oC to yield TiN/amorphous carbon nanocomposite powders, in which TEM showed that an ordered macroporous structure was maintained. These authors suggested application of the porous metal nitride as a catalyst or catalyst support. However, applications as electrodes could be envisaged for high surface area films of such an inert yet highly conductive material.[22,23]

Sol-gel synthesis has the potential to yield nitride materials in various useful morphologies.[24] Infiltration of a precursor or templating of a sol-gel process are the routes used to produce many of the macroporous oxides described above,[13,25] but there are few examples of templating processes to yield nitrides. Microporous silicon nitride has been prepared using sol-gel templating on long chain amines and showed a higher selectivity over nontemplated silicon nitride in the catalysis of alkylation and isomerisation reactions.[26] A number of porous silicon nitride structures have also been prepared using sol-gel chemistry without a template, including high surface-area aerogels,[27] membranes,[28,29] and mesoporous powders.[30]

In this chapter, ordered macroporous templated nitride materials have been synthesised. Since the precursor-derived silicon nitride typically varies in composition from Si_3N_4, herein we use the "SiN_x" notation to describe silicon nitride containing low levels of other functional groups. Inverse opal films of insulating silicon nitride (SiN_x) were synthesised by infiltrating templates of close-packed 500 nm polystyrene spheres with precursor solutions then firing to different temperatures with programmed heating rate. Some of these results have been published with related work within our research group on TiN inverse opal.[31] The method described herein is simple yet effective for yielding new nitride materials with the inverse opal morphology. Because infiltration is carried out from nonaqueous solutions, it could also have more general applicability to nonoxide materials.

5.2 Experimental

5.2.1 General Remarks

All the solvents used were freshly distilled. Tetrahydrofuran (THF), diethyl ether and hexane were dried using sodium / benzophenone. Barium oxide was used for diethyl amine distillation. All preparations of sols and solutions were carried out under dry N_2 conditions using a Schlenk line or glove box.

5.2.2 Preparation of Silicon Imide Sol and Silicon Amide Solution

For silicon imide sol preparation, 0.8 equiv. of dry ammonia was condensed into 0.5 g of sublimed tetra(methylamino) silane (TMAS) starting material dissolved in 6 mL of different dried solvents such as: THF, diethyl ether, diethyl amine and hexane separately, followed by a drop of triflic acid catalyst (using the method described in chapter 3). However, these sols failed in obtaining ordered macroporous films. THF dissolved the polystyrene sphere arrays while diethyl ether and diethyl amine caused disruption of the array structure, as confirmed with SEM. Attempts at sol formation in non polar solvents led to precipitation. Hence filling of templates using silicon amide solutions directly was attempted. Typically 0.5 g of TMAS was dissolved in 6 mL of solvents. Furthermore, several amounts of solvent and the solution were used to fill templates in the glove box.

5.2.3 Generation of Polystyrene Arrays

Silica tiles for coating were cleaned with Piranha etch (1 H_2SO_4: 3 H_2O_2) then rinsed thoroughly with distilled water and dried. Thin film arrays of polystyrene (PS) spheres were generated as follows: An array of divinylbenzene-cross-linked, amidine-capped polystyrene microspheres (4% w/v, 500± 17 nm, Invitrogen) was sonicated for 15 minutes then diluted to 1% using distilled water. This solution (0.15 cm^3 per array) was syringed into PTFE wells (diameter 7 mm) sealed onto the surface of the silica tiles by clamping between stainless steel plates, Fig. 5.1 (top). These were allowed to evaporate slowly in a refrigerator (~ 4 ^oC) over 7-10 days yielding iridescent green arrays, Fig. 5.1 (bottom).

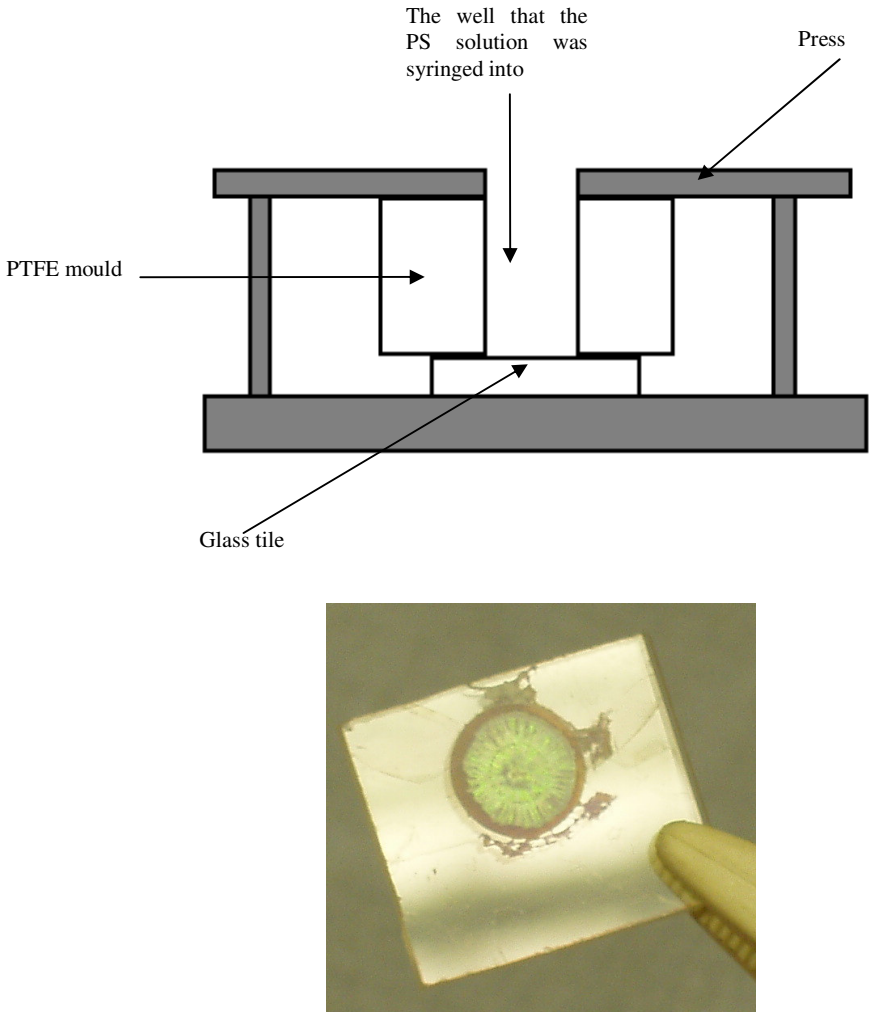

Fig. 5.1 The press used to generate the arrays (top). A photograph showing the iridescence of the PS arrays and the radial pattern formed (bottom).

5.2.4 Array Filling

Three different methods (dropping, dipping and capillary infiltration) were tried for filling the polystyrene arrays. A solution of TMAS was prepared in the glove box. For dropping, the precursor solution was dropped onto the horizontal polystyrene array via a Pasteur pipette, left to dry for 3 minutes and further dropping was applied if required, Fig. 5.2 (top). Dipping and infiltration techniques were carried out by placing TMAS solution into a sample vial. For the former, the polystyrene tile was dipped vertically in

the TMAS solution using tweezers for 1 minute then pulled out for drying, Fig. 5.2 (middle). In the latter case a sample vial containing 1 array was filled with TMAS solution until the level of the solution was just touching the edge of the array and left to stand for approximately 1 hour with the lid on, Fig. 5.2 (bottom). The tiles were then removed from the solution and allowed to dry.

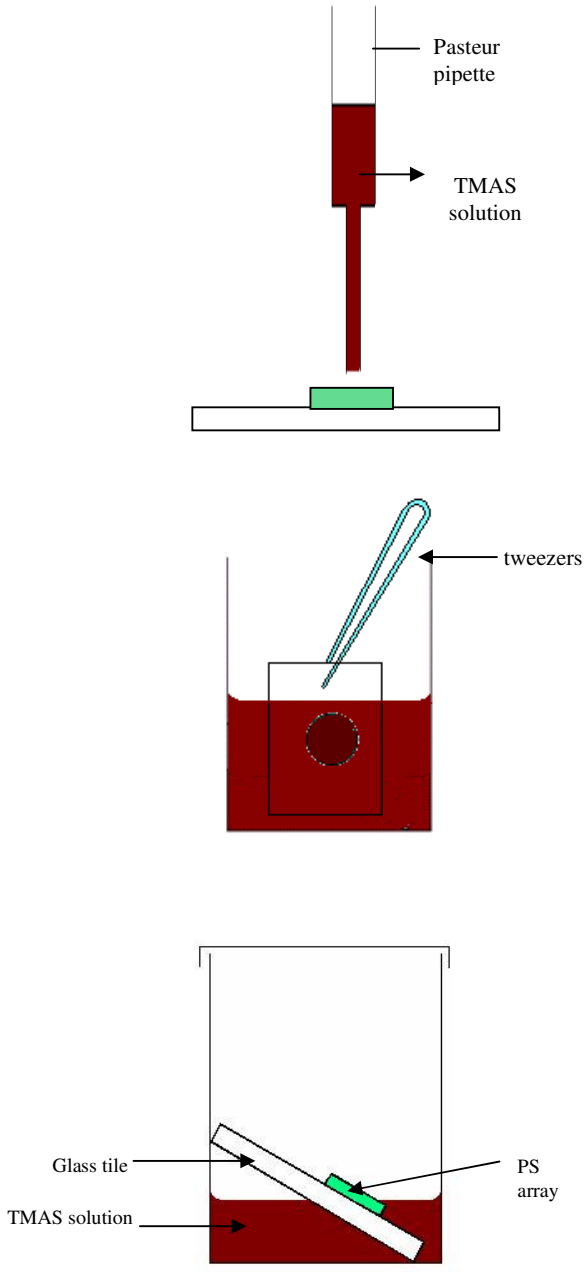

Fig. 5.2 A schematic diagram of dropping (top), dipping (middle) and capillary infiltration (bottom) techniques.

5.2.5 Ammonolysis of Templated Film and TMAS Material

The pyrolysis of the arrays was performed using a Lenton LTF 12/50/300 (max. temperature 1200 °C) tube furnace equipped with a Eurotherm 2416 controller. The different templated films were placed in an alumina boat and into a reactive gas furnace tube as shown in Fig. 3.8, in the glove box. Pipework was thoroughly flushed, then the arrays fired under a flow of dry ammonia to 50 ^{o}C at 0.5 °C/min and maintained for 1h, then ramp to 500 or 600 ^{o}C with rate 1 °C/min and maintained for 1 h or 4 hrs respectively, before the furnace was allowed to cool down.

The effect of different conditions on the final surface morphology of the templated silicon nitride films has been checked using JEOL JSM5910 scanning electron microscope (SEM). For further characterisation of chemical composition and crystallinity, samples of bulk [$Si(NHMe)_4$] were also pyrolysed under ammonia in the same manner to yield white SiN_x powder. Fourier Transform-Infrared spectroscopy (FT-IR), microanalysis and X-ray diffraction (XRD) techniques have been applied. Differential scanning calorimetry (DSC) of a sample of the polystyrene template was performed on a Mettler Toledo DSC 821e using a 1.77 mg sample in a 40 μL aluminium crucible.

5.3 Results and Discussion

5.3.1 Template Characterisation

The effects of different preparation conditions (type and amount of solvent used, template filling method and firing temperature) on the morphologies of the product were checked using SEM.

First, the array of PS spheres was examined by SEM to reveal polycrystalline lattices with close-packed domains and amorphous regions, Fig. 5.3. The diameters of the spheres are confirmed by SEM to be unchanged at 500 nm. DSC showed that the PS polymer has a glass transition temperature at ~110 ^{o}C, but does not melt below 300 ^{o}C. This is important because the infiltrated material will cross-link as the temperature is raised under ammonia flow and needs to become rigid before the template structure is

disrupted. It is also important for the polystyrene to be removed by heating in ammonia. Pyrolysis of a polystyrene sample at 500 ^{o}C in ammonia left no residue confirming the process occurs clearly.

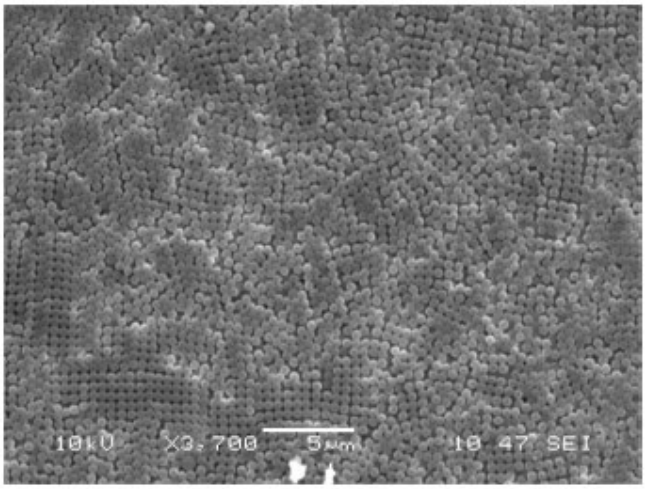

Fig. 5.3 SEM micrograph of an array of DVB cross-linked PS microspheres displaying regions of close-packing.

5.3.2 Solvent Used for Template Filling

The polystyrene arrays were filled with the precursor sol and solutions prepared using 6 mL of THF, diethyl ether, diethylamine or hexane, and then fired at 500 ^{o}C. The effect of each solvent on the morphology of the products was investigated using SEM.

5.3.2. A Tetrahydrofuran

Dry THF was used in the preparation of sols and of solutions of TMAS. Firstly polystyrene arrays were dipped into the sol and fired. SEM images, Fig. 5.4, showed that this result in destruction of the PS array due to dissolution, though some pores are still observed in the film and some regions still appear partially ordered. Using the silicon amide solution, SEM showed similar results to those obtained with the sol. A small amount of THF, 1 mL, with the precursor was then used with the aim of introducing the precursor with minimal solvent exposure. Different amounts of this solution were dropped onto polystyrene tiles. The SEM of a fired tile is illustrated in Fig. 5.5. It reveals that in spite of small amounts of THF being used, the material

formed a thick film over the beads. There was however, some evidence of templated structure underneath, that could be observed through the cracks.

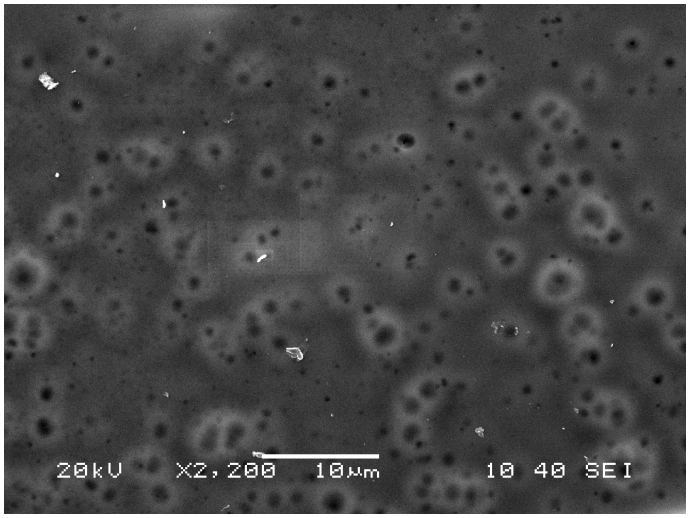

Fig. 5.4 SEM of a film produced by dipping a polystyrene array in a THF-based sol and firing at 500 ^{o}C in ammonia.

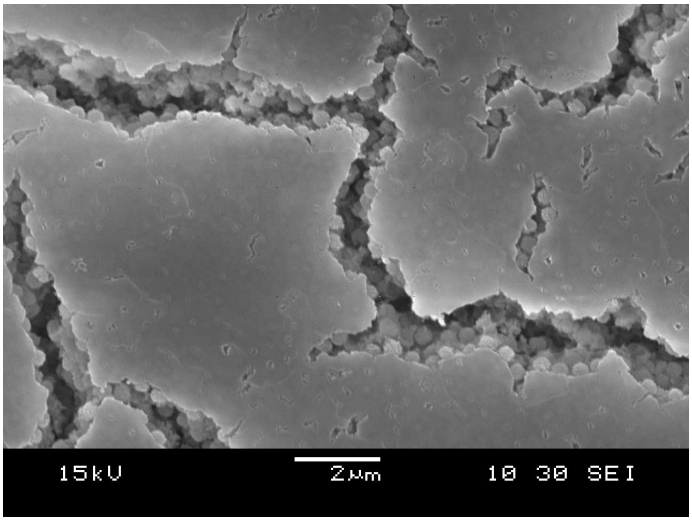

Fig. 5.5 SEM of a film produced by dropping a concentrated TMAS solution onto a polystyrene array and firing at 500 ^{o}C in ammonia.

5.3.2. B No-Solvent

Since THF had a negative effect on the polystyrene arrays, molten starting material (without solvent) was dropped onto a polystyrene array and fired to the same

temperature. SEM, Fig. 5.6, showed that using one or two drops resulted in thick layer formation with some pores but no evidence of regular structure.

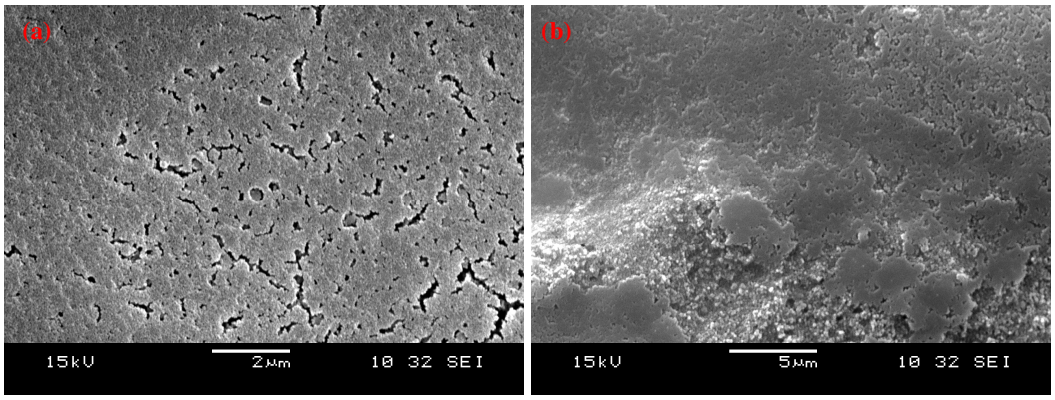

Fig. 5.6 SEM of a film produced by dropping one (a) or two (b) drops of TMAS onto a polystyrene tile then firing at 500 °C in ammonia.

5.3.2. C Diethylamine or Diethyl ether

An attempt to produce an SiN_x precursor sol in diethyl ether failed. It resulted in immediate precipitation. This was also observed for diethylamine. In addition, capillary infiltration of TMAS dissolved in 6 mL diethylamine into a polystyrene array was tried. SEM, Fig. 5.7, showed a thick layer over the surface with material underneath that may be porous but does not appear to have any ordered porosity. This result was quite similar to that obtained with no solvent.

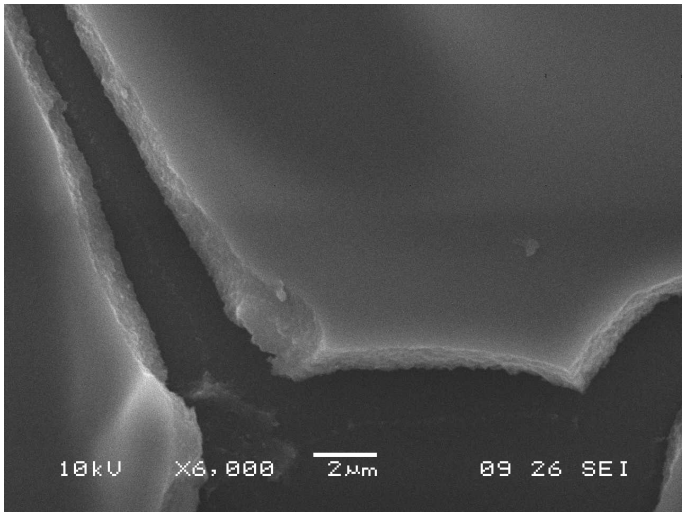

Fig. 5.7 SEM of a film produced by capillary infiltration of a TMAS/ diethylamine solution into a polystyrene array followed by firing in ammonia at 500 °C.

5.3.2. D Hexane

Initially, attempts were made to produce an SiN_x precursor sol in hexane. These were unsuccessful resulting in immediate precipitation since the solubility of the oligomers containing polar Si-NH_2 and Si-NH-Si groups in non-polar solvent is low. TMAS was dissolved in 6 mL dry hexane, the solution was capillary infiltrated into a polystyrene array for 1 hr then this was fired at 500 ^{o}C under flowing ammonia. SEM showed that the regular pore structure survived. Hence, the following discussion is based on using hexane to introduce TMAS and the effect of different conditions on the final morphology of films.

5.3.3 Template Filling Methods

Dipping, dropping and capillary infiltration have been applied to fill the gaps in the opal arrays with precursor solution. Then the arrays were fired under ammonia flow at 500 ^{o}C with a programmed heating rate of 0.5 ^{o}/min until 50 ^{o}C, a dwell of 1 hr then ramped heating with a rate of 1 ^{o}/min to 500 ^{o}C, where the temperature was held for 1 hr before step cooling down to room temperature.

5.3.3. A Capillary Infiltration

Infiltration for different time periods and amounts of hexane was performed. The SEM images of samples produced under these different conditions are illustrated in Fig. 5.8. For TMAS dissolved in 1 mL hexane, infiltration for 3 or even 60 mins resulted in poorly formed films. On infiltration for a short time, it appeared that TMAS was not efficiently carried into the polystyrene array due to the higher viscosity of the solution, Fig 5.8(a). Increasing the infiltration to 60 mins., more amide was carried into the template and the structure seen in Fig. 5.8(b) appears to be a partial templated film but with only the layer in direct contact with the substrate filled in.

Hence more hexane (6mL) was used and the TMAS solution was infiltrated into a polystyrene array for 60 mins. SEM of the fired film, Fig. 5.8(c), showed a remarkable improvement. Using a suitable concentration of TMAS (6 mL hexane) for infiltration does lead to well ordered macroporous films.

5.3.3. B Dropping

Different dropping cycles of 1 and 6 mL hexane were tested. When 1 drop of TMAS dissolved in 1 mL hexane was used, SEM, Fig. 5.9, reveals an ordered array of features underneath a thin film. It is not clear whether these features are pores or regions in which the polymer or a pyrolysis product is trapped. By increasing the number of drops to drop 3, Fig. 5.9(b), a thicker layer was deposited over the template. This thick layer was cracked and irregular templated areas were observed between these cracks. Further drops (5 drops), Fig.5.9(c), yielded a still thicker layer over the surface.

With 6 mL hexane, using one drop of the solution gave a nice templated array, Fig. 5.10. Increasing the amount of solvent decreases the TMAS solution viscosity and enhances the penetration of the solution to fill the gaps between polystyrene spheres. Nevertheless, using more drops produced the same effects as with 1 mL hexane, a solid film was observed over the top of the templated material.

5.3.3. C Dipping

Polystyrene arrays were dipped into TMAS/6 mL hexane solutions and allowed to dry horizontally in the glove box. SEM images of the fired products are shown in Fig. 5.11. A significant improvement in the templated films, with well ordered macroporous structure was obtained using a single dipping. The film thickness was around 5.5 μm, Fig. 5.11(a). The porosity extended throughout the structure and was observed through the first layer, Fig. 5.11(b), into subsequent layers. Double dipping the polystyrene arrays increased the layer thickness deposited onto its surface and hence more cracking through firing was observed, Fig. 5.11(c). Furthermore, the uncracked area was covered with a flat surface layer in places, Fig. 5.11(d). These covered areas were more significant if the array was subjected to further dipping cycles.

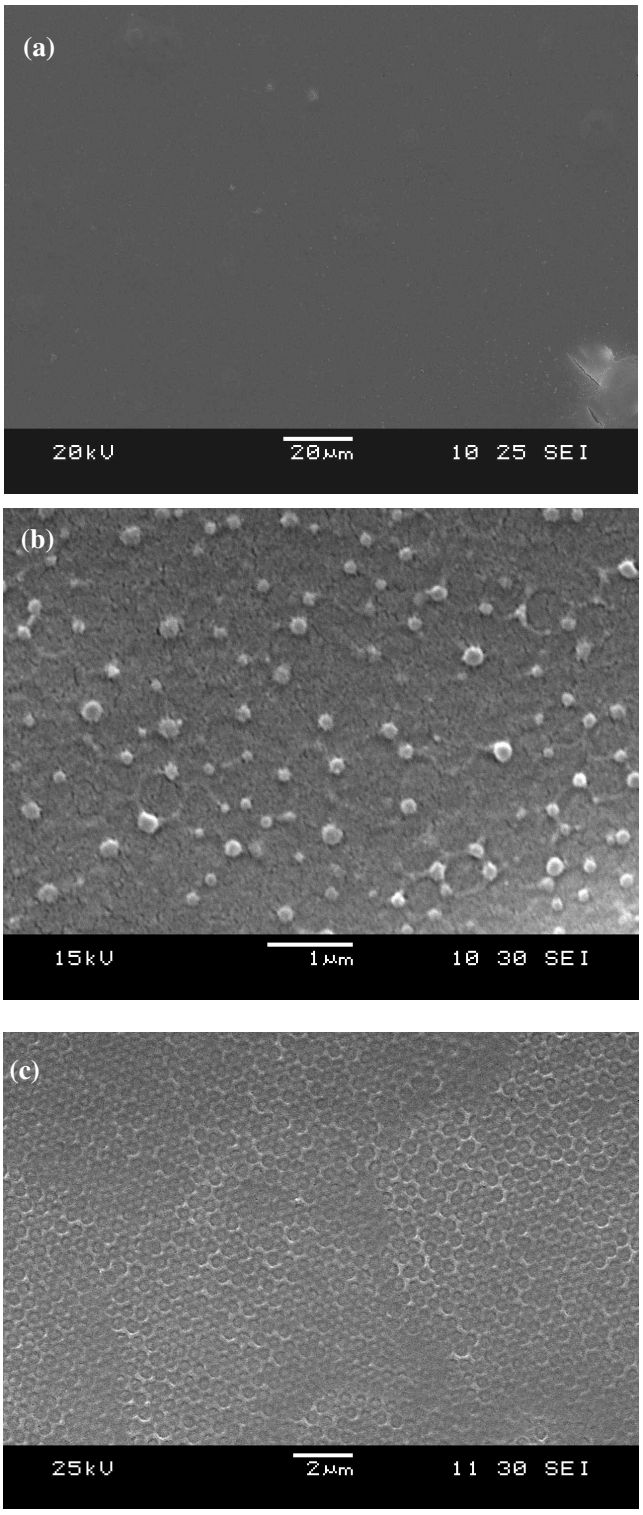

Fig. 5.8 SEM of films produced by capillary infiltration of TMAS solution (1 mL hexane) into a polystyrene array for 3 (a) and 60 (b) mins and that produced by capillary infiltration of TMAS solution (6 mL hexane) into a polystyrene array for 60 mins (c). All were fired in ammonia at 500 ^{o}C.

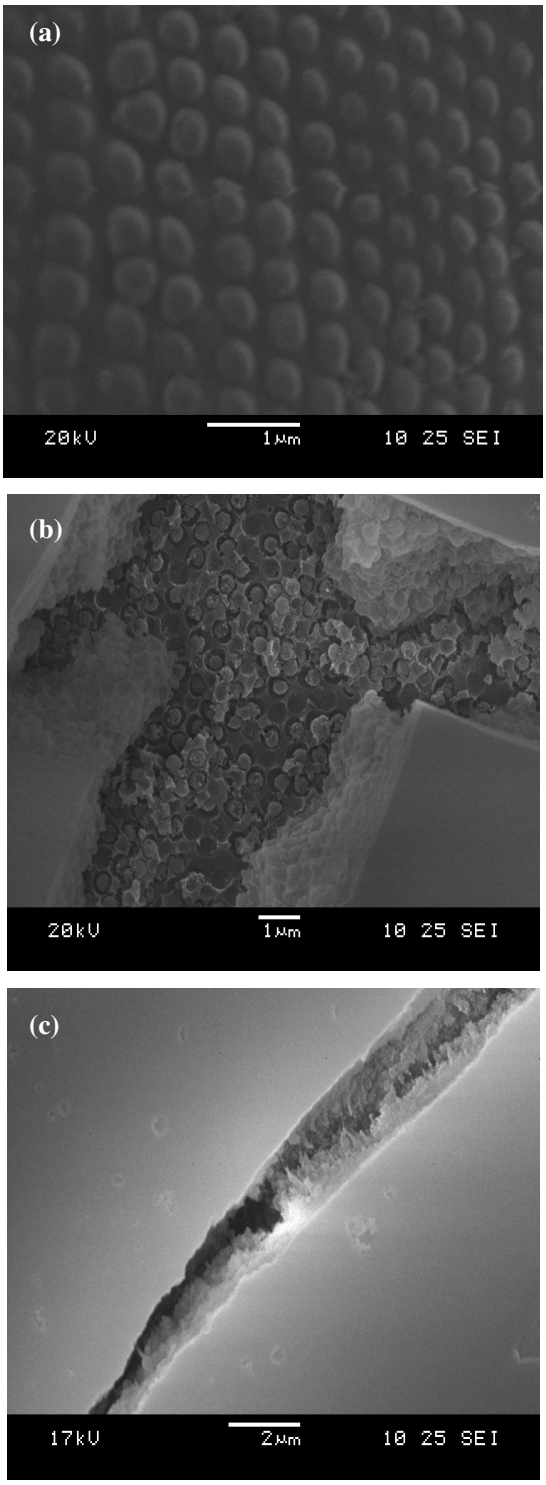

Fig. 5.9 SEM of films produced by dropping 1(a), 3(b) and 5 (c) drops of a TMAS/1 mL hexane solution into a polystyrene array followed by firing in ammonia at 500 ^{o}C.

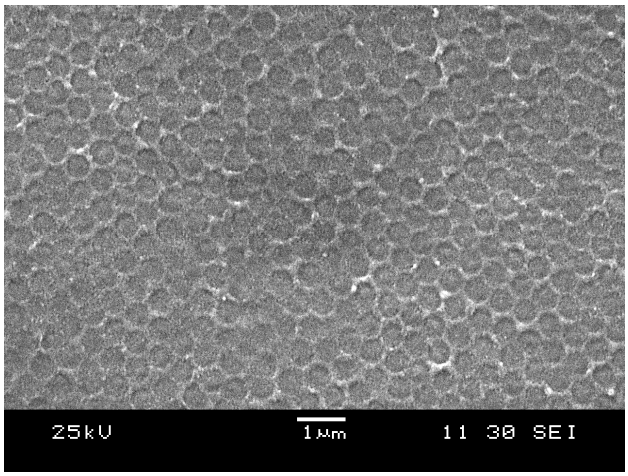

Fig. 5.10 SEM of a film produced by dropping 1 drop of a TMAS/6 mL hexane solution into a polystyrene array followed by firing in ammonia at 500 ^{o}C.

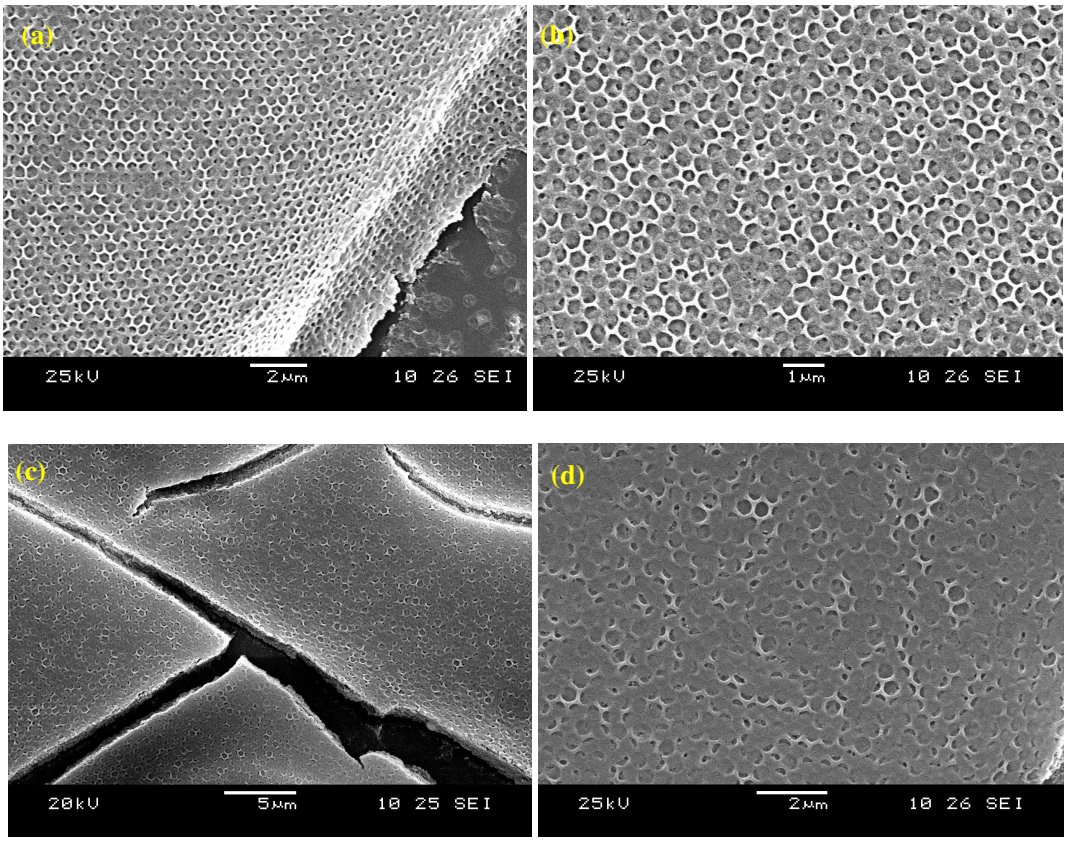

Fig. 5.11 SEM of films produced by single dipping of polystyrene tile into TMAS/6 mL hexane solution (a,b) and the effect of double dipping on the morphology of templated film (c,d) followed by firing at 500 ^{o}C in ammonia.

5.3.4 Firing Conditions

All the coated tiles discussed so far were fired under flowing ammonia at 500 ^{o}C using a programmed heating cycle, (section 5.3.3). Films fired at this temperature contain significant amounts of Si-NH groups (as seen in section 5.3.5). Higher temperature firing was tested (600 ^{o}C) using the same heating rates and the effect of this different firing condition on the chemical structure and film morphology was determined. Films were also fired at 500 ^{o}C using a single ramp rate (10 ^{o}/min) rather than using a programme designed to maximise opportunities for cross linking. These comparisons used films produced with a single dipping into a TMAS solution made with 6 mL hexane. The SEM images are illustrated in Fig. 5.12 (a) and (b) respectively.

Firing the dipped polystyrene tile at 500 ^{o}C using a programmed heating cycle gave ordered porous films with porosity extending through the film, Fig. 5.12(a). This heating programme was designed to give enough time for the TMAS solution to be cross-linked before the polystyrene array was removed at higher temperature. Clearly this was successful.

Faster heating resulted in a porous film, but the structure (Fig. 5.12(b)) is irregular, presumably because the ammonia did not produce sufficient cross links before the template was removed.

Films fired to 600 ^{o}C with a heating programme, Fig. 5.12(c), had an ordered macroporous structure, as in the inset to Fig. 5.12(c). However, the increased temperature produced more cracking and surface distortion of the film compared with that fired at 500 ^{o}C.

According to the above results, dip- coating the polystyrene array into a TMAS solution in 6 mL of hexane, then firing to 500 ^{o}C with a heating programme gave the best ordered macroporous structures of silicon nitride.

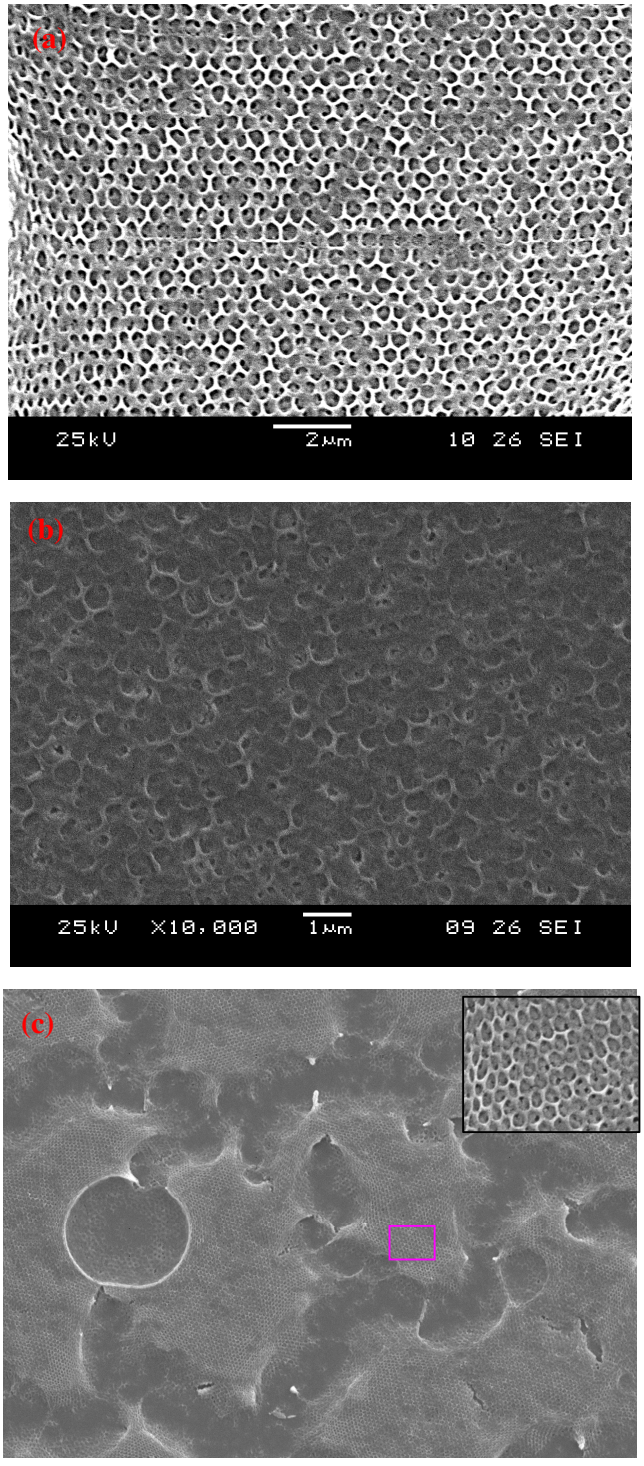

Fig. 5.12 SEM images of films produced by dipping polystyrene arrays into TMAS/6 mL hexane solutions and firing in ammonia at (a) 500 ^{o}C with a heating programme, (b) 500 ^{o}C with a fast ramp or (c) 600 ^{o}C with similar heating programme.

5.3.5 Infra-red Spectroscopy (IR) and Microanalysis of Bulk SiN_x Material

The ordered macroporous films were of very low density so obtaining detailed analysis directly is difficult. To obtain further analytical information, bulk xerogels were produced by heating [$Si(NHMe)_4$] under the same conditions as the films. However, it was found that most of the precursor sublimed under these conditions, so the precursor was mixed with a dried sample of the PS template then heated under the same conditions to 500 or 600 ^oC. The microanalysis of the former yielded a sample containing 41.4% N, 2.2% C and 2.6% H. This suggests a N-rich silicon nitride (Si_3N_4 would contain 39.9% N) with some residual carbon and hydrogen. Presumably some interaction with the surface capping amidine groups on the PS spheres results in retention of the precursor during heating. A sample fired at 600 ^oC contained 34.145 % N, <0.1 % C and 1.4 % H which suggests that increasing the heating temperature enhances removal of any remaining amide groups and the residual carbon and hydrogen have been reduced.

The IR spectra of the bulk SiN_x xerogels fired at both temperatures are shown in Fig. 5.13. They reveal the presence of similar peaks in samples fired at both temperatures such as ν_{N-H} (3378 cm^{-1}) and two typical ν_{Si-N} peaks present at 1218 and 917 cm^{-1}. However, a weak ν_{C-H} stretching (2808 and 2900 cm^{-1}) and small NH_2 band present at 1550 cm^{-1} were observed at the 500 ^oC. At 600 ^oC the former peak disappeared and the latter decreased as confirmed with microanalysis. Furthermore, there is a small peak at 1043 cm^{-1} which may relate to ν_{Si-O} (~ 1030 cm^{-1}). This spectra was similar to that obtained by pyrolysing the silicon diimide gel under ammonia flow at 600 ^oC except the presence of $\nu(C\equiv N)$ band at 2236 cm^{-1} due to the decomposition of residual dimethylamino group under those conditions.[30] Powder X-ray diffraction on both bulk xerogels showed no Bragg scattering, i.e. the SiN_x samples are amorphous.

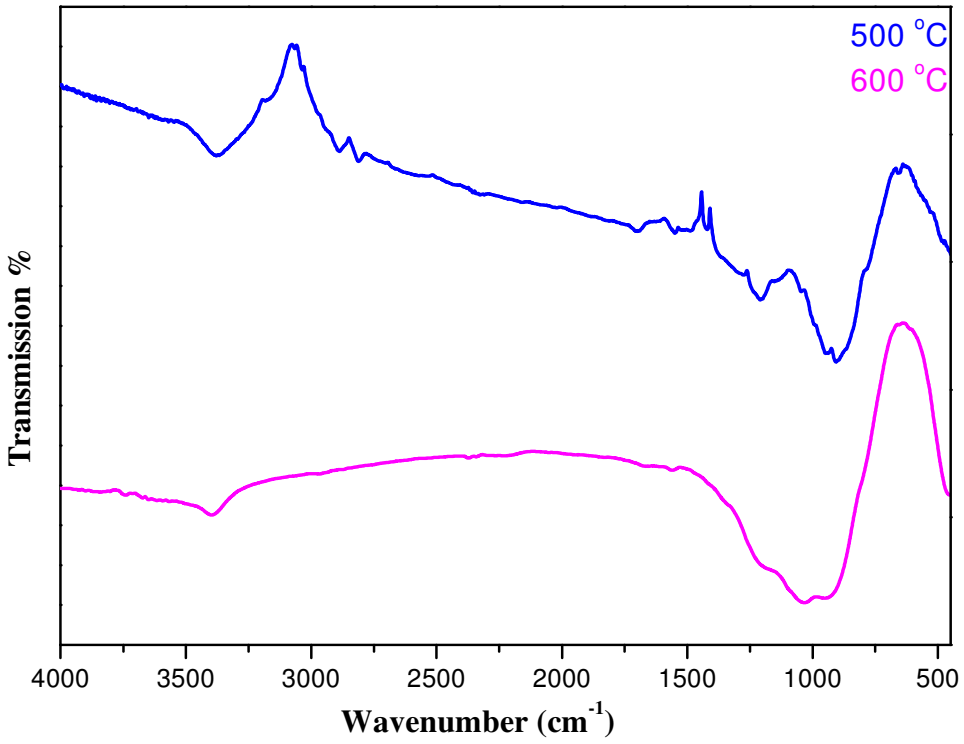

Fig. 5.13 IR spectra of bulk SiN_x xerogels.

5.4 Conclusions

Ordered macroporous SiN_x thin films were prepared by simple templating methods with crosslinked polystyrene sphere arrays. Different solvents, coating methods and firing temperatures have been applied. The effects of these conditions on the morphologies of the final templated films were characterised using scanning electron microscopy. Of the various solvents used to produce solutions for filling the polystyrene arrays, hexane caused the least interference with the array structure and yielded the best results. Dip-coating the array into a precursor solution and annealing at 500 ^{o}C with a structured heating rate in ammonia removed the polystyrene template and resulted in a well ordered macroporous structure with the porosity extending throughout the structure. Increasing pyrolysis temperature to 600 ^{o}C did not improve the porous structure but caused a remarkable distortion and further cracking of the templated structure.

5.5 References

[1] D. J. Norris, Y. A. Vlasov, *Adv. Mater.*, **13**, 2001, 371. A. Stein, F. Li, N. R. Denny, *Chem. Mater.,* **20,** 2008, 649.

[2] K. T. Lee, J. C. Lytle, N. S. Ergang, S. M. Oh, A. Stein, *Adv. Funct. Mater.,* **15,** 2005, 547.

[3] R. J. W. Scott, S. M. Yang, G. Chabanis, N. Coombs, D. E. Williams, G. A. Ozin, *Adv. Mater.,* **13,** 2001,1468. M. Acciarri, R. Barberini, C. Canevali, M. Mattoni, C. M. Mari, F. Morazzoni, L. Nodari, S. Polizzi, R. Ruffo, U. Russo, M. Sala, R. Scotti, *Chem.Mater.,***17,** 2005, 6167.

[4] A. Mihi, H. Mı´ guez, *J. Phys. Chem. B*, **109,** 2005, 15968. M. Imada, S. Noda, A. Chutinan, T. Tokuda, *Appl. Phys. Lett.*,**75,** 1999, 316.

[5] M. A. Carreon, V. V. Guliants, *Chem. Mater.*, **14,** 2002, 2670. M. A. Al-Daous, A. Stein, *Chem. Mater.,* **15,** 2003, 2638.

[6] I.-K. Sung, M. M. Christian, D.-P. Kim, P. J. A. Kenis, *Adv. Funct. Mater.,* **15,** 2005, 1336.

[7] S. H. Park, Y. Xia, *Adv. Mater.,* **10,** 1998,1045.

[8] B. Gates, Y. Yin, Y. Xia, *Chem. Mater.,* **11,** 1999, 2827.

[9] H. Yan, K. Zhang, C. F. Blanford, L. F. Francis, A. Stein, *Chem.Mater.,* **13,** 2001, 1374. B. J. Melde, A. Stein, *Chem. Mater.,* **14,** 2002, 3326. K. Zhang, H. Yan, D. C. Bell, A. Stein, L. F. Francis, *J. Biomed. Mater. Res.,* **66A,** 2003, 860.

[10] Y. Xia, B. Gates, Y. Yin, Y. Lu, *Adv. Mater.,* **12,** 2000, 693.

[11] M. Abdullah, F. Iskandar, S. Shibamoto, T. Ogi, K. Okuyama, *Acta Mater.,* **52,** 2004, 5151. M. A. Carreon, V. V. Guliants*, Eur. J. Inorg. Chem.,* **27,** 2005.

[12] M. C. Carbajo, A. Gómez, M. J. Torralvo, E. Enciso, *J. Mater.Chem.,* **12,** 2002, 2740.

[13] S. Madhavi, S. Ferraris, T. White, *J. Solid State Chem.,* **179,** 2006, 866.

[14] R. Han. W. Pan S. Shi, H. Wu, S. Liu, *Mater. Let.,* **61,** 2007, 5014.

[15] M. A. Ghanem, P. N. Bartlett, P. de Groot, A. Zhukov, *Electrochem. Commun.,* **6,** 2004, 447.

[16] F. Meseguer, A. Blanco, H. Mı´ guez, F. Garcı´ a-Santamarı´ a, M. Ibisate, C. L_opez, *Colloids Surf.,* **202,** A 2002, 281. Y. A.Vlasov, X.-Z. Bo, J. C. Sturm, D. Norris, *J. Nature* , **414,** 2001, 289.

[17] A. Rugge, J. S. Becker, R. G. Gordon, S. H. Tolbert, *Nano Lett.,* **3,** 2003,1293.

[18] A. Rugge, J.-S. Park, R. G. Gordon, S. H. Tolbert, *J. Phys. Chem. B,* **109,** 2005, 3764.

[19] G. Gajiev, V. G. Golubev, D. A. Kurdyukov, A. B. Pevtsov, A. V. Selkin, V. V. Travnikov, *Phys. Status Solidi B,* **231,** 2002, R7.

[20] P. Dibandjo, F. Chassagneux, L. Bois, C. Sigala, P. Miele, *Micro. Meso. Mater.,***92,** 2006, 286.

[21] A. Fischer, Y.-S. Jun, A. Thomas, M. Antonietti, *Chem. Mater.,* **20,** 2008, 7383.

[22] C. N. Kirchner, K. H. Halmeier, R. Szargan, T. Raschke, C. Radehaus, G. Wittstock*, Electroanalysis* , **19,** 2009,1023.

[23] D. Choi, P. N. Kumta, *J. Electrochem. Soc.,* **153,** 2006, A2298.

[24] A. L. Hector, *Chem. Soc. Rev.,* **36,** 2007, 1745. B. Mazumder, A. L. Hector, *J. Mater. Chem.*, **19,** 2009, 4673.

[25] J. C. Lytle, A. Stein, Recent progress in syntheses and applications of inverse opals and related macroporous materials prepared by colloidal crystal templating. In *Annual Reviews of Nano Research.* G. Cao, C. J. Brinker, Eds.; World Scientific Publishing Co.: River Edge, NJ, **1,** 2006; 1-79 and references therein.

[26] D. Farruseng, K. Schlichte, B. Spliethoff, A. Wingen, S. Kaskel, J. S. Bradley, F. Schüth, *Angew. Chem.,* Int. Ed. **40,** 2001, 4204.

[27] S. Hassan, A. L. Hector, J. R. Hyde, A. Kalaji, D.C. Smith, *Chem. Commun.,* 2008, 5304.

[28] F. Cheng, S. M. Kelly, S. Clark, J. S. Bradley, M. Baumbach, A. Schütze, *J. Membr. Sci.,* **280,** 2006, 530.

[29] K. W. Völger, R. Hauser, E. Kroke, R. Riedel, Y. H. Ikuhara, Y. Iwamoto, *J. Ceram. Soc. Jpn.*, **114,** 2006, 567.

[30] F. Cheng, S. Clark, S. M. Kelly, J. S. Bradley, *J. Am. Ceram. Soc.,* **87,** 2004, 1413.

[31] B. M. Gray, S. Hassan. A. L. Hector, A. Kalaji, B. Mazumder, *Chem. Mater.,* **21,** 2009, 4210.

TERBIUM DOPED SILICON NITRIDE

6.1 Introduction

Much of the interest in rare earth doped silicon nitride and oxynitride materials is related to potential applications as highly stable, efficient phosphors. The stability of these materials is linked to their strongly bonded structures based on networks of covalent SiN_4 units. Attention has focussed on their use as conversion phosphors for solid state lighting based on blue, NUV or UV LEDs,[1,2,3] which have exceptional lifetime and reliability and promise large efficiency savings in terms of power consumption.

Recently there has also been interest in producing rare earth doped silicon nitride films as emitters. Rare earth doped SiO_2 is an effective source of light emission,[4] but the large bandgap of SiO_2 leads to inefficient carrier injection and electroluminescence based on these materials depends on excitation by impact of high energy electrons.[5] High working temperatures, device degredation and incompatibility with some technologies are the result. Tb^{3+} implantation into PECVD-grown silicon nitride was shown to result in significantly higher quantum efficiency of photoluminescence from the terbium ions.[5] Similarly Er^{3+}-doped silicon nitride films produced by a co-sputtering method show strong photoluminescence.[6]

There have also been studies of rare earth doping into other nitrides. BN based phosphors have been proposed for use in extreme environments such as high temperatures and high radiation levels.[7] Tm, Tb, Sm, Eu or Yb doped AlN films have been produced using reactive radiofrequency sputtering and show strong photoluminescence and cathodoluminescence.[8] Eu^{2+} doped AlN shows stronger blue cathodoluminescence than the Ce^{3+}:Y_2SiO_5 blue phosphor normally used in field emission displays.[9] There are various other reports of high emission efficiencies from rare earth centres in III-nitride matrices, largely for field emission applications.[10,11,12,13]

Sol-gel methods have advantages in materials synthesis. They are often a lower cost option than vapour deposition techniques and they can readily be used to coat very large areas. In addition, several morphologies such as films with ordered pore structures or

monolithic materials can be produced. Oxide or fluoride based phosphors can readily be produced by doping lanthanide ions into sols.[14]

For silicon nitride-based phosphors a sol-gel route could offer better control and homogeneity in the rare earth concentration than when ion implantation methods are used since the concentration in the sol is directly related to that in the powder or film. The accurate doping of more than one rare earth or of rare earth/transition metal combinations (e.g. to produce phosphorescent materials or to mix emission colours) and an expansion of the range of forms in which these materials can be produced beyond powders and films, are further possible outcomes. It also offers an opportunity to produce morphologies other than films, including periodic structures of potential interest as photonic materials.[15]

The use of such routes to incorporate other ions into silicon nitride and hence modify its properties is also a general interest. Jansen[16] that showed B, Ti or Ta could be doped into SiN_x by adding the respective dimethylamide to the reaction between $[Si(NHMe)_4]$ and ammonia. These silicon nitride materials are referred to as SiN_x rather than Si_3N_4 because they are amorphous materials with composition that deviates from Si_3N_4, similar to the vapour deposited SiN_x films extensively used as capping layers and dielectrics in electronics. Amorphous ceramic metal/boron silicon nitrides were formed after annealing in NH_3 at 1000 °C while calcining at 1500 °C in N_2 atmosphere partially crystallised nanoparticles of the metal nitrides (TiN/TaN) which were distributed in the amorphous silicon metal nitride matrix. Others have incorporated Al[17] or Ti[18] into silicon nitride using single source precursors designed so that the active groups are amide ligands attached to silicon.

It has been shown that rare earth *tris*(*bis*-trimethylsilyl)amides react with ammonia to produce polymers which decompose on heating to yield the rare earth nitrides.[19] In this chapter doping of Tb^{3+} ions into silicon nitride starting from mixtures of $[Tb(N(SiMe_3)_2)_3]$ and $[SiCl(NEt_2)_3]$ in solution has been investigating and the composition, morphology and photoluminescence behaviour of the products have been examined.

6.2 Experimental

6.2.1 General Remarks

For all the following reactions, reactants were measured out in a nitrogen filled-glove box and all the reactions were carried out under nitrogen using Schlenk line equipment due to the high air and moisture selectivity of the reactants and products.

Solvents were obtained from Fisher Scientific and freshly distilled; THF and pentane used a combination of sodium metal as drying agent, benzophenone as the indicator and 2-methoxyethyl ether to aid benzophenone dissolution. Barium oxide was used as the drying agent for diethylamine distillations.

$SiCl_4$ and $[Na(N(SiMe_3)_2]$ were obtained from Aldrich and $TbCl_3$ from Strem. Anhydrous ammonia was obtained from Air Products and further dried by passing through a column of molecular sieves.

6.2.2 Investigation of $[Si(NMe_2)_4]$ as a Precursor

A number of different precursors could potentially be used in sol-gel processes to yield silicon nitride. The obvious approach is to react a silicon amide with ammonia yielding a polymeric network containing Si-NH-Si bridging groups, Fig. 6.1. This approach has been used by Bradley[20] using $[Si(NH_2)(NMe_2)_3]$ and by Jansen[16] and ourselves (chapter 3 and 4) with $[Si(NHMe)_4]$.

$$M(NR_2)_4 + (x+y)NH_3 \rightarrow M(NH)_x(NH_2)_y(NR_2)_z + (4-z)HNR_2$$

Fig. 6.1 Ammonolysis of a silicon amide precursor.

Initially, $[Si(NMe_2)_4]$ (0.25 mL, 99.99 %, Aldrich) dissolved in 20 mL THF was used. Exposure to ammonia resulted in no precipitate formation. An attempt to add a drop of trifluoromethanesulfonic acid gives an oily product even after an extended exposure to dry ammonia.

Oily solids were formed after solvent removal when a solution of $[Si(NHMe)_4]$ exposed to ammonia. While it leads to solid xerogels when a trifluoromethanesulfonic acid catalyst is used[21] and may be suitable for production of phosphors similar to those described herein as films or other forms, it was not used here due to concern that by mixing terbium precursor $[Tb(N(SiMe_3)_2)_3]$ with $[Si(NHMe)_4]$ in THF solution the Tb ions would not be immobilised in the oily products and so Tb rich regions could form. It was concluded that these precursors were too unreactive to be useful in an initial study of coprecipitated phosphors, and a precursor that would precipitate on contact with NH_3 was sought.

6.2.3 Synthesis of $[SiCl(NEt_2)_3]$

Trikisdiethylaminechlorosilane $[SiCl(NEt_2)_3]$ is simple to prepare and purify, and precipitation was found to occur rapidly on exposing it to ammonia in THF solution. The expected reaction scheme for ammonolysis of the silicon reagent is shown in Fig. 6.2.

$$[SiCl(NEt_2)_3] + (4\text{-}z)NH_3 \rightarrow [Si(NH)_x(NH_2)_y(NEt_2)_z] + HNEt_2.HCl + (2\text{-}z)HNEt_2$$

Fig. 6.2 Ammonolyis of $[Si(NEt_2)_3]$.

$[SiCl(NEt_2)_3]$ was synthesised using silicon tetrachloride and diethyl amine, Fig. 6.3. $HNEt_2$ (100 mL) was added to a solution of $SiCl_4$ (10 mL) in THF (40 mL) at 0 °C. The mixture was stirred for 12 h, the $HNEt_2{\cdot}HCl$ by-product precipitate was removed by filtration and the solvent removed *in vacuo* to obtain the crude product.

$$SiCl_4 + 6\ HNEt_2 \xrightarrow{THF} [SiCl(NEt_2)_3] + 3HNEt_2{\cdot}HCl\downarrow$$

Fig. 6.3 Silicon amide preparation using silicon tetrachloride.

Purification of the crude product was achieved by vacuum distillation, as in Fig. 6.4, at ~75 °C in which a transparent liquid was formed. The liquid was characterised with ^1H and ^{13}C NMR. ^1H δ(ppm) was 2.89 (q) C*H*$_2$ [2H], 0.95 (t) C*H*$_3$ [3H] and $^{13}C\{^1H\}$ δ(ppm) was 39.8, 14.8.

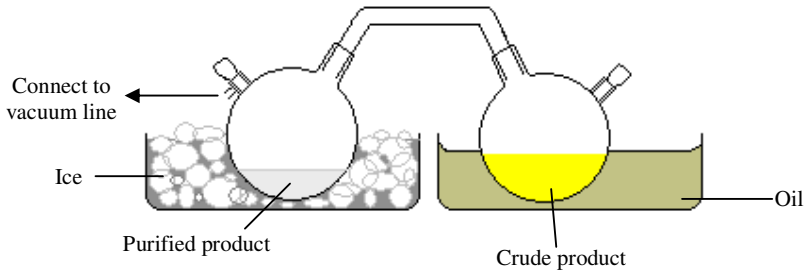

Fig. 6.4. Apparatus used for [$SiCl(NEt_2)_3$] distillation.

6.2.4 Synthesis of the Terbium Amide Precursor [$Tb(N(SiMe_3)_2)_3$]

Tris(bis-trimethylsilyl)amides [$Tb(N(SiMe_3)_2)_3$] was obtained by a literature method using anhydrous terbium chloride $TbCl_3$ and bis(trimethylsilyl)amido sodium [$NaN(SiMe_3)_2$].[22] 24 mL of [$NaN(SiMe_3)_2$] solution (1.0 M in THF) was added to a solution of $TbCl_3$ (2.05 g, $7.7x10^{-3}$ mol) in THF (10 mL) at 0 °C and kept stirring at room temperature for 48 hr. The solvent was removed *in vacuo*, the remaining solid was dissolved in dry n-pentane (20 mL), and sodium salts were removed by filtration giving a clear [$Tb(N(SiMe_3)_2)_3$] solution. Under vacuum the solvent was pumped off and the remaining solution was chilled to allow crystallisation. NMR measurement has been collected on the final product. It showed a single peak at 0.125 ppm (^{1}H NMR) which is shifted to lower chemical shift, due to the paramagnetic shift effect of the terbium precursor. The same effect has been observed in other lanthanide trimethylsilylamides.[23]

6.2.5 Formation and Firing of Tb:SiN_x Xerogels

A solution of [$Tb(N(SiMe_3)_2)_3$] (various amounts in 10 mL THF) was mixed with a solution of [$SiCl(NEt_2)_3$] (0.5 mL / 0.53 g in 10 mL THF). Dry ammonia was flowed over the stirred mixture for 1 hr. The resultant precipitate was collected by filtration and dried *in vacuo*, then heated to 800 °C at 10 °/min under flowing dry ammonia and held at this temperature for 2 hr. before cooling down. This procedure was carried out with 0.03, 0.035, 0.04, 0.045, 0.05, 0.055, 0.06 or 0.065 g of [$Tb(N(SiMe_3)_2)_3$].

The xerogel has been characterised using thermogravimetric analysis (TGA) and infrared spectroscopy (IR). The final ceramic phosphor products were examined by TGA, IR spectroscopy, microanalysis, PXD and TEM. The photoluminescence spectra were collected on neat or NaCl-diluted phosphor samples with a Perkin Elmer LS55 spectrometer. Then ^{29}Si MAS-NMR spectrum of this solid was recorded with a Varian Infinity+ spectrometer at 9.4 T and with a 6.5 KHz spinning frequency. Spectra were referenced against silicone rubber (-22.4 ppm) and collected through direct observation (178 scans, 900 s relaxation) or after 5 ms cross-polarisation (128 scans, 5 s relaxation).

6.3 Results and Discussion

6.3.1 Characterization of SiN_x Produced from $[SiCl(NEt_2)_3]/NH_3$ Xerogel Pyrolysis

$[SiCl(NEt_2)_3]$ was reacted with ammonia in solution and pyrolysis of the resultant xerogel to 800 °C under a flow of dry ammonia led to a white ceramic solid. The IR spectrum of the ceramic silicon nitride after pyrolysis at 800 ^{o}C is shown in Fig. 6.5. It shows υ_{N-H} at 3348 cm^{-1}, $\upsilon_{C\equiv N}$ at 2157 cm^{-1}, δ_{NH2} at 1543 cm^{-1} and a broad, intense υ_{Si-N} peak at 951 cm^{-1}. No evidence of residual organic groups (υ_{C-H}) was found. This closely resembles spectra of silicon nitride samples produced by heating $Si(NH_2)(NMe_2)_3/NH_3$-derived gels under similar conditions, where the presence of the $\upsilon_{C\equiv N}$ peak was attributed to pyrolysed organic substituent groups.[24] Powder X-ray diffraction showed the fired ceramic materials to be amorphous.

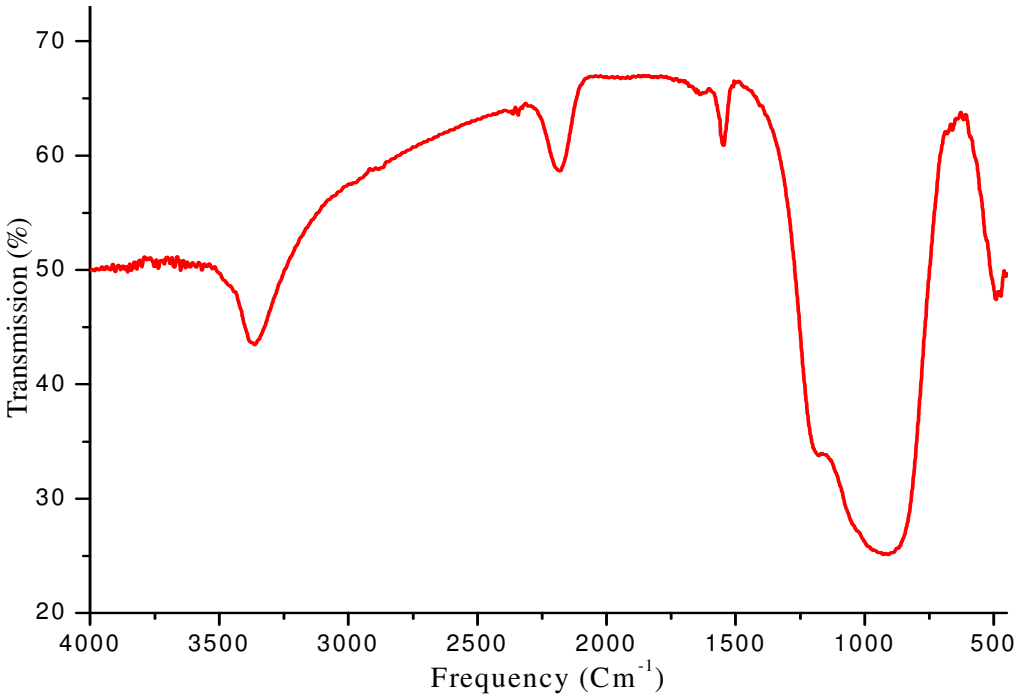

Fig. 6.5 IR spectrum of silicon nitride produced by heating $SiCl(NEt_2)_3/NH_3$-derived gels under ammonia.

Solid state ^{29}Si MAS-NMR, Fig. 6.6, showed a single strong peak with a maximum between -43.7 and -45.5 ppm. This is particularly significant as MAS-NMR is sensitive to oxide incorporation into silicon nitride – every oxygen atom results in three SiN_3O tetrahedra. In chapter 4 the production of silicon nitride xerogels from another route led to the detection of low level oxide contamination in these through the observation of SiN_4, SiN_3O, SiN_2O_2 and $SiNO_3$ groups.[20] The chemical shift observed for the ceramic produced herein is consistent with SiN_4 and no other environments are seen.

Combustion microanalysis resulted in a nitrogen content of 35.1-35.7%, 2% hydrogen and no detectable carbon. Si_3N_4 contains 40% N but its high oxidation resistance often results in low analysis values, 35% N was also analysed in a commercial Si_3N_4 sample (Aldrich, <50 nm particle size). A significant signal enhancement was observed using cross polarisation, though the appearance of the spectrum did not change. This shows that many silicon centres are still close to protons as expected in these gel-derived materials.

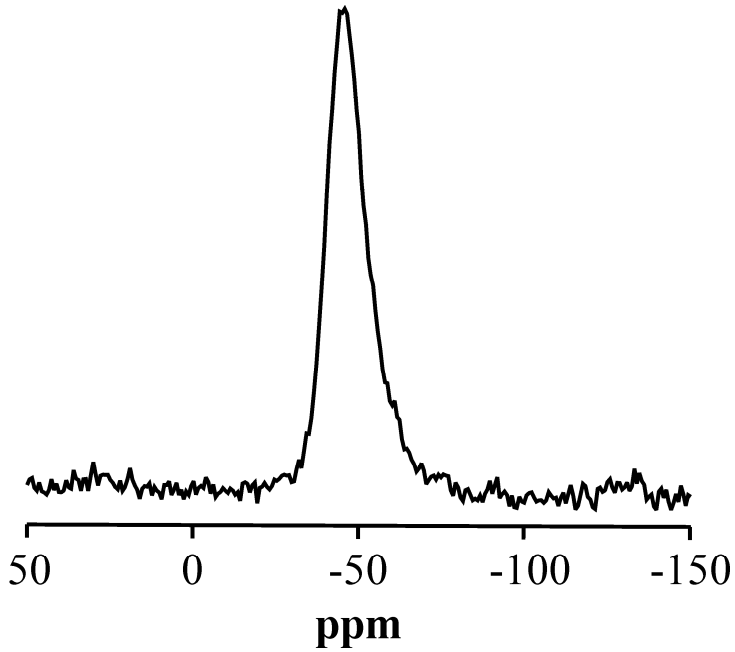

Fig. 6.6 ^{29}Si MAS-NMR spectrum of silicon nitride produced by pyrolysis of a $SiCl(NEt_2)_3/NH_3$ xerogel at 800 ^oC.

6.3.2 Characterization of Tb:SiN_x Xerogels and Ceramics

The mass loss of the gel under N_2 has been investigated using thermogravimetric analysis, Fig. 6.7. A sharp 60% mass loss around 200 °C corresponding to loss of the amine hydrochloride by-product and ammonia/amine, due to some further condensation of the xerogel, was observed. Further slow mass loss of another 14% due to additional condensations which were complete by 800 °C has been followed.

The chemical structure of as obtained Tb:SiN_x xerogel has been characterised using IR. The IR spectrum of a gel, Fig. 6.8(a), contained a broad band centred at 3136 cm^{-1} (υ_{N-H}) and peaks at 2850-2720 cm^{-1} (υ_{C-H}), 1448 (δ_{NH2}), 1405 cm^{-1} (υ_{C-N}), 1200 and 916 cm^{-1} (υ_{Si-N}). Other peaks corresponding to $HNEt_2 \cdot HCl$ were also seen. This is consistent with the expected reaction scheme for ammonolysis of the silicon reagent, Fig. 6.2. The IR spectrum of the Tb:SiN_x after pyrolysis at 800 ^oC, Fig. 6.8(b), was similar to that of the ceramic SiN_x product, Fig. 6.5, except the presence of a small peak at 1400 cm^{-1} that was attributed to (υ_{C-N}).

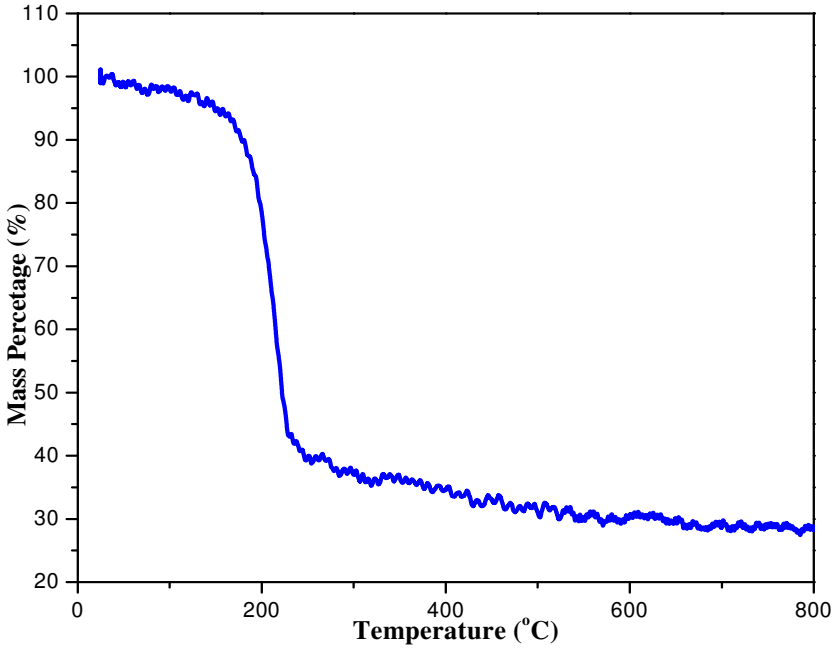

Fig. 6.7 Thermogravimetric analysis of the Tb:SiN_x xerogel under N_2 flow.

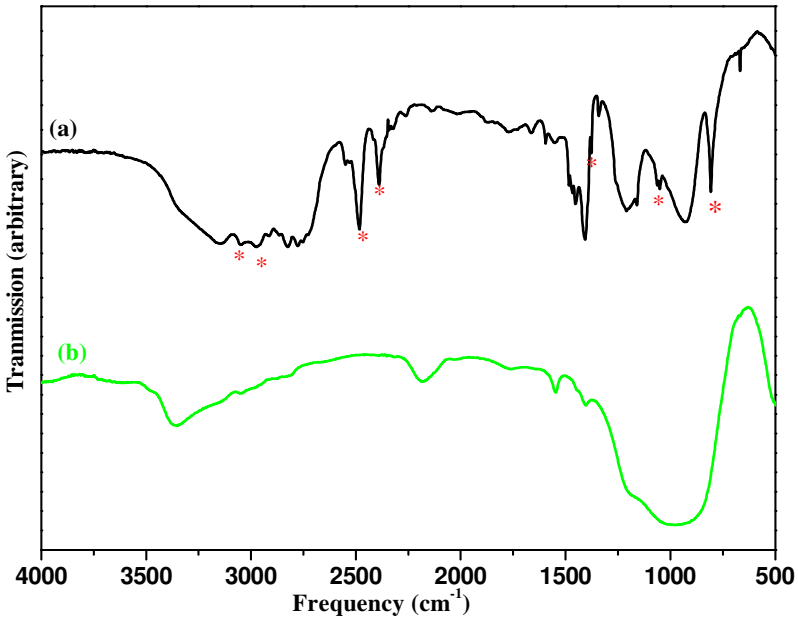

Fig. 6.8 IR spectra of a typical Tb:SiN_x xerogel as obtained (a) and after pyrolysis at 800 °C (b). Peaks due to the $HNEt_2$·HCl by-product in the top spectrum are marked with asterisks.

TGA of the terbium doped silicon nitride material after firing in NH_3 at 800 ^oC showed that when heated under N_2 it underwent no further mass loss. The microanalysis of that material showed a nitrogen content of 28.75 %, hydrogen of 1.54 % and small carbon content of 0.21 %. The decrease in nitrogen content raises some concern that small amounts of oxygen might be incorporated into the lattice and be preferentially coordinated to the oxophilic Tb^{3+} ions, see comments in the photoluminescence study (section 6.3.3).

The topographies of the fired samples have been investigated using SEM and TEM. SEM showed large spherical particles with diameters of ~0.5-1.5 μm with powdery material, Fig. 6.9. This spherical morphology is similar to that often obtained when SiO_2 is grown under basic conditions (the Stöber process).[25] EDX showed the spherical and powdery material to have similar Tb concentrations. The EDX probe in the SEM used does not detect N due to absorption from the BN window but a strong nitrogen signal was observed in the EDX when measured in the TEM.

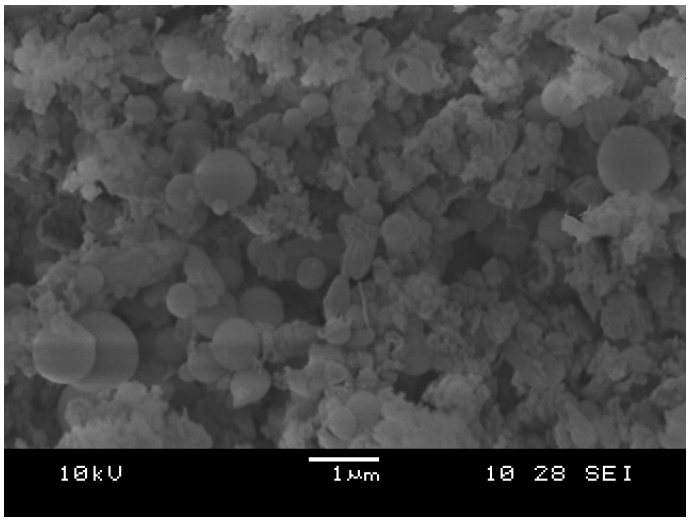

Fig. 6.9 SEM image of Tb:SiN_x containing 3.55 atomic% Tb. The SEM shows the mixture of spherical and powdery particles.

TEM images of the fired samples, Fig. 6.10, showed the sample to be of homogenous density and amorphous. No nanoparticles were observed as might be expected if phase segregation was occurring and the more sinterable TbN component was beginning to crystallise.

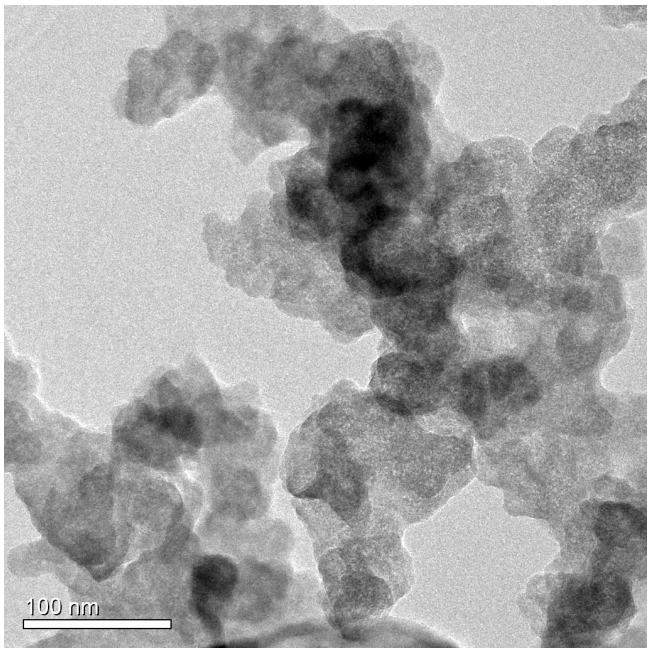

Fig. 6.10 TEM image of Tb:SiN_x containing 3.55 atomic% Tb.

6.3.3 Photoluminescence of Tb:SiN_x

The photoluminescence of the terbium doped silicon nitride samples has been checked first using UV irradiation with a 240 nm lamp. These fired samples were found to emit high intensity green light, Fig. 6.11.

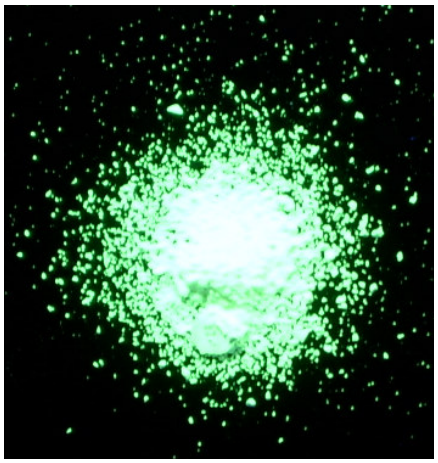

Fig. 6.11 Green emitted from fired Tb:SiN_x sample.

The room temperature photoluminescence (PL) spectra of the terbium doped silicon nitride solids have been recorded see Fig. 6.12. It showed the four characteristic intense PL peaks associated with the Tb^{3+} ion. A small degree of Stark splitting is observed on the $^5D_4 \rightarrow {}^7F_5$ line but the overall line widths are relatively narrow, suggesting that Tb^{3+} ions are all in similar high symmetry environments.

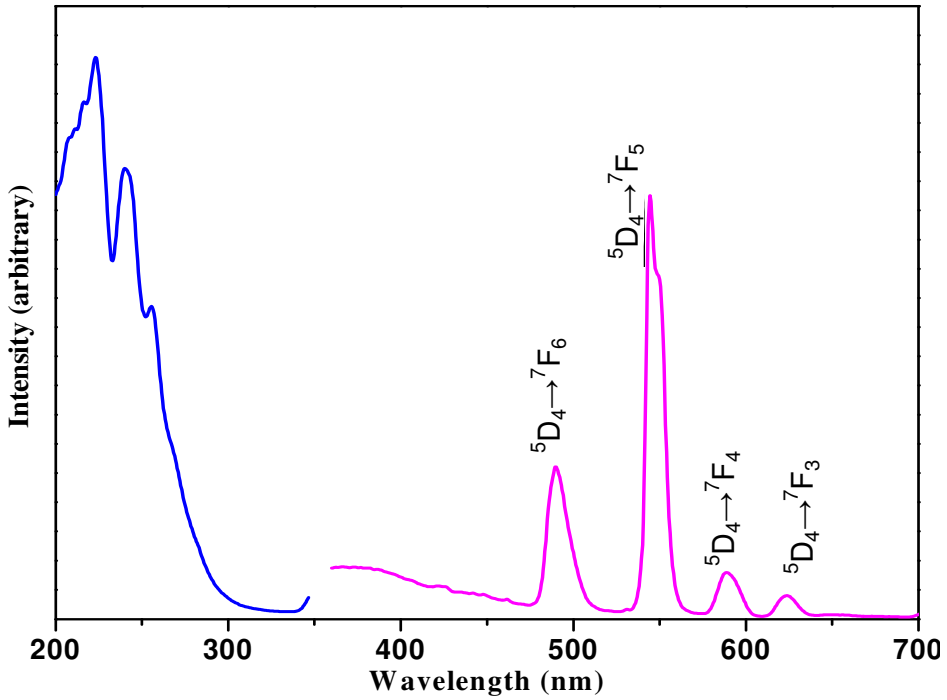

Fig. 6.12 Photoluminescence excitation (left, using 545 nm emission) and emission (right, 242 nm excitation) spectra for Tb:SiN_x containing 3.55 atomic% Tb. The sample was diluted with powdered NaCl for this measurement.

Emission intensity varies with dopant ion concentration, so samples were produced with 0.03 to 0.06g [$Tb(N(SiMe_3)_2)_3$]. The variation in intensity of the emission from these phosphors with the Tb concentration is shown in Fig. 6.13. The $^5D_4 \rightarrow {}^7F_6$ line was used so that undiluted samples could be studied (the $^5D_4 \rightarrow {}^7F_5$ was off-scale with all slit combinations). The intensity of emission is seen to increase with composition until it reaches a maximum at around 3.5 atomic% (the most intense sample was produced using 0.05 g [$Tb(Si(NMe_2)_3)_3$] with 0.5 cm^3 [$SiCl(NEt_2)_3$]. At higher concentrations quenching was observed to cause a reduction in the photoluminescence intensity.

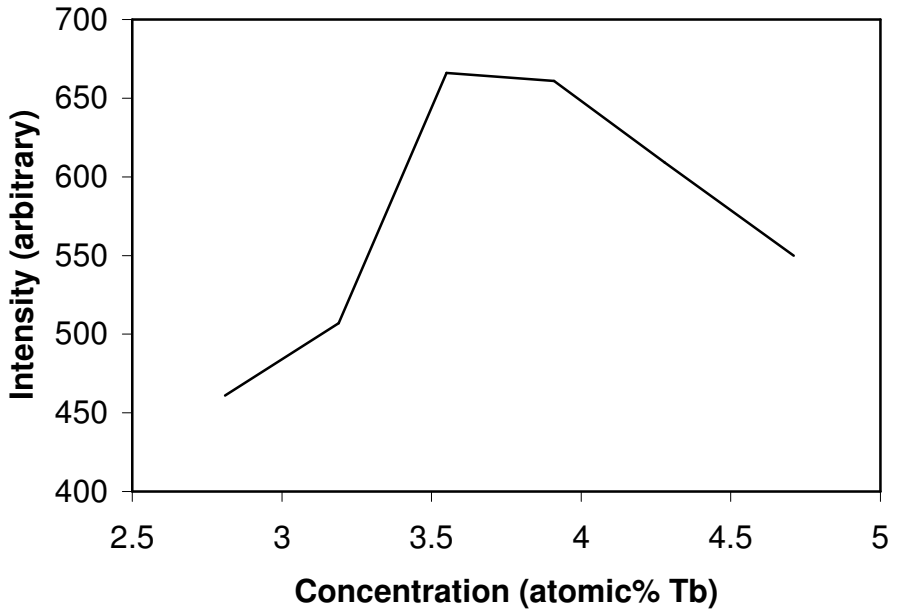

Fig. 6.13 The variation in photoluminescence intensity related to the Tb^{3+} ion concentrations.

A comparison of the positions of these characteristic lines, associated with Tb^{3+} ions, with those found in other Tb^{3+}-doped materials is summarised in Table 6.1. The results showed similar positions to those found in other nitride materials doped with Tb^{3+} and also to Tb^{3+} doped SiO_2. No significant shift in the positions due to the nitride lattice is observed and the peak positions are even comparable with those observed for the $Tb^{3+}_{(aq)}$ ion.[26] This is not uncommon with rare earth ions since the *f*-electrons are relatively well shielded from the host lattice.

For the samples described above the anhydrous grade ammonia was passed through a 70 cm column of dried molecular sieves to remove trace water, but to check the effect of moisture a sample was fired under undried ammonia. The PL spectrum of this 3.55 atomic% Tb sample showed a 26% weaker $^5D_4 \rightarrow {}^7F_6$ line than the sample heated under dried NH_3. This suggests that a higher oxygen content reduces the efficiency of the phosphors and that Tb is mainly N-coordinated in these materials. This conclusion is supported by the previous observation that Tb^{3+} photoluminescence in SiO_2 films is much weaker than similar concentrations in SiN_x films.[5]

Table 6.1 PL peak positions and linewidths compared with related Tb^{3+} phosphors.

Environment of Tb^{3+} ion	$^5D_4 \rightarrow {}^7F_6$ / nm	$^5D_4 \rightarrow {}^7F_5$ / nm	FWHM of $^5D_4 \rightarrow {}^7F_5$ / nm	$^5D_4 \rightarrow {}^7F_4$ / nm	$^5D_4 \rightarrow {}^7F_3$ / nm
SiN_x powder (this work)	491	545	11	591	625
SiN_x film[5,6]	491-494	547	12-20	590-593	623-625
SiO_2 film[4,5]	487-491	541-547	15-16	588-590	620-623
c- BN powder[7]	486	543	12	588	623
AlN film[8,11,12]	490-492	541-554	9-12	587-589	625-627
AlN powder[10]	484	542	15	585	621
GaN film[12]	487	541	6	583	623
GaN powder[13]	480	550	9	580	620

The excitation spectrum has maxima at 224, 242 and 257 nm but with strong excitation at all wavelengths up to ~270 nm. The sample couples well with a standard 240 nm UV lamp (Fig. 6.11). One feature of nitride phosphors that is useful for solid state lighting is that the excitation range can often extend into the near UV or the blue region of the visible spectrum, allowing coupling to GaN based LEDs. These phosphors will not be useful for these applications. However, the range of wavelengths in which excitation occurs is comparable to Tb^{3+} implanted SiN_x films[5,6] that have been investigated as the basis of Si-based emitters with tunnelling electrons causing electroluminescence. Hence the further development of sol-gel SiN_x films doped with Tb that behaves similarly to the powders described in this chapter would be of interest.

6.4 Conclusion

Tb-doped silicon nitride phosphors have been prepared using a sol-gel type route. $[SiCl(NEt_2)_3]$ is an effective starting material for producing phosphors in powdered form with the $[Tb(Si(NMe_2)_3)_3]$ precursor since the rapid precipitation of the former with ammonia can immobilise Tb ions in the nitride lattice. Chemical compositions of the fired precipitate under ammonia were characterised using infrared spectroscopy, combustion microanalysis and thermogravimetric analysis techniques. For phosphor morphology studies, SEM and TEM

The characteristic emission peaks of the Tb^{3+} ions have been measured using a photoluminescence spectrometer. The frequencies of the Tb^{3+} emission lines are similar to those seen in oxides, so there is no shift due to the different electronegativity of the lattice ions, but in line with results from ion implantation the SiN_x lattice appears to yield a higher emission intensity than equivalent SiO_2 systems. Furthermore the quenching concentration of this phosphor has been examined using different Tb^{3+} ion concentrations. The emission intensity reached its maximum at around 3.5 atomic %.

Sol-gel approaches are versatile in the range of product morphologies that they can be used to access. Hence homogeneous SiN_x films could be produced relatively cheaply with good control over the content of the luminescent ion.

6.5 References

[1] R.-J. Xie, N. Hirosaki, *Sci. Tech. Adv. Mater.*, **8,** 2007, 588.

[2] C. Feldmann, T. Jüstel, C. R. Ronda, P. J. Schmidt, *Adv. Inorg. Mater.*, **13,** 2003, 511.

[3] R. Mueller-Mach, G. Mueller, M. R. Krames, H. A. Höppe, F. Stadler, W. Schnick, T. Juestel, P. Schmidt, *Phys. Stat. Sol.*, **202,** 2005, 1727.

[4] H. Amekura, A. Eckau, R. Carius, Ch. Buchal, *J. Appl. Phys.*, **84,**1998, 3867.

[5] Z. Yuan, D. Li, M. Wang, P. Chen, D. Gong, L. Wang, D. Yang, *J. Appl. Phys.*, **100,** 2006, 083106; Z. Yuan, D. Li, M. Wang, D. Gong, P. Cheng, P. Chen, D. Yang, *Mater. Sci. Eng. B*, **146,** 2008, 126.

[6] M. J. V. Bell, L. A. O. Nunes, A.R. Zanatta, *J. Appl. Phys.*, **86,** 1999, 338.

[7] E. M. Shishonok, S. V. Leonchik and J. W. Steeds, *Phys. Stat. Sol.*, **244,** 2007, 2172.

[8] R. Weingärtner, O. Erlenbach, A. Winnacker, A. Welte, I. Brauer, H. Mendel, H. P. Strunk, C. T. M. Ribeiro, A. R. Zanatta, *Opt. Mater.*, **28,** 2006, 790.

[9] N. Hirosaki, R.-J. Xie, K. Inoue, T. Sekiguchi, B. Dierre, K. Tamura, *Appl. Phys. Lett.*, **91,** 2007, 061101.

[10] B. Han, K. C. Mishra, M. Raukas, K. Klinedinst, J. Tao, J. B. Talbot, *J. Electrochem. Soc.*, **154,** 2007, J262.

[11] F. S. Liu, W. J. Wa, Q. L. Liu, J. K. Liang, J. Luo, L. T. Yang, G. B. Song, Y. Zhang, G. H. Rao, *Appl. Surf. Sci.,* **245,** 2005, 391.

[12] H. Mendel, S. B. Aldabergenova, R. Weingärtner, G. Frank, H. P. Strunk, A. A. Andreev, *Opt. Mater.*, **28,** 2006, 794.

[13] A. Podhorodecki, M. Nyk, J. Misiewicz , W. Strek, *J. Lumin.*, **126,** 2007, 219.

[14] A. A. Ismail, M. Abboudi, P. Holloway, H. El-Shall, *Mater. Res. Bull.*, **42,** 2007, 137; S. Lepoutre, D. Boyer, R. Mahiou, *Opt. Mater.*, **28,** 2006, 592.

[15] B. M. Gray, S. Hassan. A. L. Hector, A. Kalaji, B. Mazumder, *Chem. Mater.,* **21,** 2009, 4210.

[16] J. Löffelholz, J. Engering, M. Jansen, *Z. Anorg. Allg. Chem.*, **626,** 2000, 963.

[17] Cheng, S. M. Kelly, F. Lefebvre, S. Clark, R. Supplit, J. S. Bradley, *J. Mater. Chem.*, **15,** 2005, 772; S. Kaskel, G. Chaplais, K. Schlichte, *Chem. Mater.*, **17,** 2005, 181.

[18] F. Cheng, S. M. Kelly, S. Clark, N. A. Young, S. J. Archibald, J. S. Bradley, *Chem. Mater.*, **17,** 2005, 5594.

[19] D. V. Baxter, M. H. Chisholm, G. J. Gamma, V. F. DiStasi, A. L. Hector, I. P. Parkin, *Chem. Mater.*, **8,** 1996, 1222.

[20] R. Rovai, C. W. Lehmann, J. S. Bradley, *Angew. Chem. Intl. Ed.*, **38,** 1999, 2036; F. Cheng, S. J. Archibald, S. Clark, B. Toury, S. M. Kelly, J. S. Bradley, *Chem. Mater.*, **15,** 2003, 4651; C. Balan, K. W. Völger, E. Kroke, R. Riedel, *Macromolecules*, **33,** 2000, 3304.

[21] S. Hassan, A. L. Hector, J. R. Hyde, A. Kalaji, D. C. Smith, *Chem. Commun.*, 2008, 5304.

[22] D. C. Bradley, J. S. Ghotra, F. A. Hart, *J. Chem. Soc., Dalton Trans.*, 1973, 1021.

[23] D. C. Bradley, J. S. Ghotra, F. A. Hart, *J. C. S. Chem. Comm.,***193,** 1972, 349.

[24] F. Cheng, S. Clark, S. M. Kelly, J. S. Bradley, *J. Am. Ceram. Soc.*, **87,** 2004, 1413.

[25] U. Schubert, N. Hüsing, "Synthesis of Inorganic Materials," Wiley-VCH, Weinheim, 2000.

[26] L. Rebohle, J. von Borany, W. Skorupa, I. E. Tyschenko, H. Fröb, K. Leo, *Appl. Phys. Lett.*, **71,** 1997, 2809.

CONCLUSION

Sol-gel methods are useful in materials synthesis. They attract considerable attention due their low cost, simplicity, low temperature processing and the ability of tailoring pore size by modification of reaction parameters.[1] Furthermore different morphologies such as films, fibres, dense monolith, mesoporous structures and nanostructured materials can be produced with large area coverage and homogeneous dispersion.[2] This method has traditionally been used for synthesis of oxide materials. However, to a limited extent these methods have been successfully expanded to nitride materials using amide precursors. Due to their high sensitivity to moisture and oxygen, air free environments are required.

Silicon nitride has many superior properties of good resistance to thermal and chemical attack, high-temperature strength, good oxidation resistance and good dielectric character.[3,4] These properties suggest silicon nitride for use in several fields such as optical[5] and microelectronic applications.[6] It has been used for protective coatings, as a gate insulator[7], diffusion masks[8] and environment filters.[9] A main object of this thesis was to make different forms of silicon nitride employing several sol-gel techniques.

Amorphous silicon nitride thin films have a wide range of applications including hydrogen passivation and antireflection coatings for crystalline solar cells.[10,11] Two general strategies are employed for preparation: physical vapour deposition (PVD)[12] or chemical vapour deposition (CVD).[13] In the former silicon is reactive sputtered in nitrogen using radio-frequency glow discharge to ionise gases required to deposit on cold or heated substrate. For the latter a mixture of SiH_4 and NH_3 gases are pyrolytically decomposed on substrate at high temperature. Recently hydrogenated amorphous silicon nitride alloy films (a-SiN:H) were synthesised using hot wire chemical vapour deposition (HWCVD).[14] It has been used as protective coating for moisture resistance in LED application and as a biosensor material for bio-devices.[15]

In chapter three, silicon nitride films were prepared using TMAS as the precursor. 0.8 molar equivalents of NH_3 were condensed into 0.5 g of TMAS solution (in THF). Triflic acid was added to the sol to catalyse condensation. The effects of different condition: rate of dipping, firing temperatures and various substrates, on the final

morphology of the films have been studied using SEM. Slow withdrawal of substrate resulted in less cracking of the surface. For thicker layers, more cycles were applied. The substrates were fired at 500, 700 or 1000 ^{o}C with programmed heating under a flow of ammonia. Films with reduced carbon content were achieved at 1000 ^{o}C. Among the substrates used, a Si wafer showed a smooth relatively crack free film. Furthermore, XPS showed that films deposited on Si wafers and fired at 1000 ^{o}C contained a significant amount of nitrogen with lower oxygen levels compared with other substrates.

For ordered macroporous nitride material production, atomic layer deposition (ALD) was previously employed through arrays of close-packed silica spheres.[16] Lately self-assembled block-copolymer (BC) monolayers have successfully been used as templates for fabrication of densely packed nanoporous arrays and ultrathin highly porous membranes by combination of BC lithography and standard microtechnology approaches.[17] The final products were extremely promising for integration in biomolecular ultrafiltration, biosensing and controlled drug delivery devices. Furthermore, silicon nitride has been successful as a catalyst support and silicon imidonitride compositions are also effective solid base catalysts. The presence of significant number of NH and NH_2 groups are responsible for catalyst activity.[18] Hence the formation of porous silicon nitrides is of significant interest.

Through chapter four, silicon nitride aerogels were produced using sol-gel methods followed by supercritical drying. 0.5 g of TMAS solution in THF was reacted with two equivalents of dry ammonia and left to warm overnight. A gel was formed 40 mins after triflic acid addition. Different drying techniques: supercritical fluid, autoclave and ambient drying, were applied separately. The effect of these methods on the final composition, surface area, pore size distribution and morphologies were studied using IR, microanalysis, nitrogen adsorption isotherm, SEM and TEM. Gels produced from the supercritical fluid drying method had a high nitrogen percentage. They also showed a high surface area with pore size distribution range from 65 to 130 nm. SEM demonstrates an open porous structure that was confirmed with TEM, which showed a network structure with pores connected together through thin walls. Although the bomb aerogel has a high surface area with similar pore network, more shrinkage was observed and high carbon and hydrogen contents were obtained. Ambient pressure drying resulted in loss of the porosity.

Chapter five examined the preparation of ordered macroporous SiN_x thin films using crosslinked polystyrene sphere arrays as templates. The template tiles were coated with TMAS (0.5 g) solution in 6 ml solvent, left to dry then pyrolysed at the required temperature under flow of dry ammonia. Several solvents, coating methods and firing temperatures have been employed. The morphologies of the final templated films under these conditions were studied using SEM. Of the various solvents used to produce solutions for filling the polystyrene arrays, hexane caused the least interference with the array structure and yielded the best results. Dip-coating the array into a precursor solution and annealing at 500 ^{o}C with a structured heating rate in ammonia removed the polystyrene template and resulted in a well ordered macroporous structure with the porosity extending throughout the structure. Increasing pyrolysis temperature to 600 ^{o}C did not improve the porous structure but caused a remarkable distortion and further cracking of the templated structure.

Since the sol-gel method offers an effective means of adding elements into an Si-N matrix, and combining the low reactivity of these materials with other functional properties by doping in different elements has great potential, silicon nitride materials doped with lanthanide elements have been fabricated in chapter six. $[SiCl(NEt_2)_3]$ is an effective starting material for producing phosphors in powdered form with the $[Tb(Si(NMe_2)_3)_3]$ precursor. The rapid precipitation of the former with ammonia can immobilise Tb ions in the nitride lattice. A mixture of $[Tb(N(SiMe_3)_2)_3]$ (various amounts in 10 mL THF) and $[SiCl(NEt_2)_3]$ (0.5 mL / 0.53 g in 10 mL THF) solutions was ammonolysed with stirring for 1 hr. The resultant precipitate was collected by filtration and dried *in vacuo*, then heated to 800 °C at 10 ^{o}/min under flowing dry ammonia and held at this temperature for 2 hr. before cooling down. The effect of concentration was studied using 0.03, 0.035, 0.04, 0.045, 0.05, 0.055, 0.06 or 0.065 g of $[Tb(N(SiMe_3)_2)_3]$. The final ceramic phosphor was examined by IR spectroscopy, microanalysis and TEM. The photoluminescence spectra were collected on NaCl-diluted phosphor samples. The SEM and TEM showed that Tb^{3+} ions are spread evenly through the solid. The photoluminescence properties of the phosphor material have been investigated initially under a 240 nm UV lamp. It has bright green emission. The photoluminescence measurements showed that doped terbium into SiN_x matrix didn't change the frequencies of the Tb^{+} characteristic emission peaks but yield a higher emission intensity than equivalent SiO_2 systems. Furthermore the quenching

concentration of this phosphor has been examined using different Tb^{3+} ion concentrations. The emission intensity reached its maximum at around 3.5 atomic %.

The work in this thesis demonstrates that non-oxide sol-gel methods can produce new forms of nitride materials in directly analogous forms to those produced in oxides. There is significant future potential to expand the range of nitride materials formed, e.g. to metal nitrides, other main group nitrides and mixed anion materials. A series of potential applications can also be addressed using these techniques.

7.1 References

[1] A.L.Hector, *Chem. Soc. Rev.,* **36,** 2007, 1745.

[2] A. L. Hector, *Chem. Soc. Rev.,* **36,** 2007, 1745. B. Mazumder, A. L. Hector, *J. Mater. Chem.*, **19,** 2009, 4673.

[3] A. Liu, M. Cohen, *Phys. Rev.,* **B 41**, 1990, 727.

[4] J. Kim, K. Chung, *J. Appl. Phys.,* **83**, 1998, 5831.

[5] M. Arienzo, W. A. Orrarienzo, *Preparation and Properties of Silicon Nitride Based Materials,* Materials Science Forum Vol.**47**, Eds. D. A. Bonnell, T. Y. Tien (Trans Tech Publications, Zürich, 1989).

[6] T. P. Ma, IEEE Trans. Electron Devices, **45**, 1998, 680.

[7] S. K. Patra, G. Mohan Rao, *Mater. Sci. and Engin. B,* **90***,* 2002, 90.

[8] G. C. Han, P. Luo, K. B. Li, Z. Y. Liu, Y. H. Wu, *Appl. Phys.,* **A 74,** 2002, 243.

[9] K.P. Pluckett, M. Quinlan, L. Garrido, L. Genova, *Mater. Sci. Eng. A,* **489,** 2008, 337.

[10] N. Matsuki, Y. Abiko, K. Miyazaki, M. Kobayashi, H. Fujioka, H. Koinum, *Thin Solid Films,* **486,** 2005, 210.

[11] W. M. M. Kessels, J. Hong, F. J. H. Van Assche, J. D. Moschner, T. Lauinger, W. J. Soppe, A. W. Weeber, D. C. Scram, M. C. M. Van de Sanden, *J. Vac. Sci. Technol. B,* **20,** 2002, 1704.

[12] H. F. Sterling, R. C. G. Swann, *Solid State Electron.,* **8,** 1965, 653.

[13] V.Y. Doo, D. R. Nichols, G. A. Silvey, *J. Electrochem. Soc.,* **113,** 1966, 1279.

[14] B. P. Swain, B. S. Swain, N. M. Hwang, *Appl. Surf. Sci.,* **225,** 2008, 2557.

[15] J. Gustavsson, G. Altankov, A. Errachid, J. Samitier, J. A. Planell, E. Engel, *Adv. Sci. Technol.,* **53,** 2006, 122.

[16] Y. Xia, B. Gates, Y. Yin, Y. Lu, *Adv. Mater.,* **12,** 2000, 693.

[17] A-M Popa, P. Niedermann, H. Heinzelmann, J. A. Hubbell, R. Pugin, **20,** 2009, 485303.

[18] D. Hullmann, G. Wendt, U. Singliar, G. Ziegenbalg, *Appl. Catal. A: Gen.* **225**, 2002, 261.